

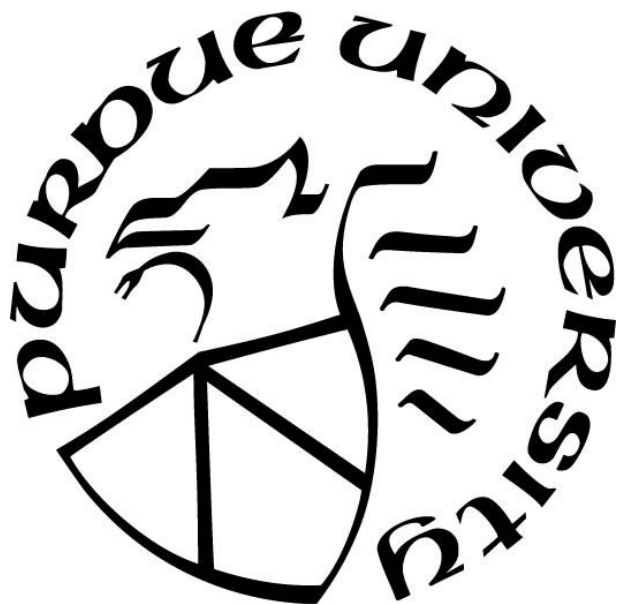
**NITROGEN TETROXIDE TO MIXED OXIDES OF NITROGEN:  
HISTORY, USAGE, SYNTHESIS, AND COMPOSITION  
DETERMINATION**

by  
**Andrew Head**

**A Thesis**

*Submitted to the Faculty of Purdue University  
In Partial Fulfillment of the Requirements for the degree of*

**Master of Science in Aeronautics and Astronautics**



School of Aeronautics and Astronautics  
West Lafayette, Indiana  
December 2021

**THE PURDUE UNIVERSITY GRADUATE SCHOOL  
STATEMENT OF COMMITTEE APPROVAL**

**Dr. Timothee Pourpoint, Co-Chair**

School of Aeronautics and Astronautics

**Dr. Carson D Slabaugh, Co-Chair**

School of Aeronautics and Astronautics

**Dr. Alexey Shashurin**

School of Aeronautics and Astronautics

**Approved by:**

Dr. Gregory Blaisdell

*Dedicated to my mother and father, Yu-Jiuan Chen and Stephen Head,  
for their unwavering belief in me.*

## ACKNOWLEDGMENTS

Throughout the writing of this dissertation I have received a great deal of support and guidance.

I would first like to express my deepest appreciation to my supervisor, Professor Timothee Pourpoint, for his patient support, advice, and mentorship. Thank you for all of the opportunities given to further my research. It was an honor and a privilege to be on your team.

I would also like to extend my deepest gratitude to my committee, which include Professor Carson Slabaugh and Professor Alexey Shashurin. Thank you for your time, expertise, and contributions to this research.

I would like to extend my sincere thanks to several colleagues and consultants for their peer reviews of the report that preceded this dissertation. They include Dr. Alicia Benhidjeb-Carayon, Dr. Robert Orth, and Christopher Burnside. Your insightful feedback sharpened the report and brought my work to a higher level.

I would like to give a special thanks to my colleague, Yash Pande, who was a mentor, associate, and friend for much of the original report. Your continual encouragement and support was always appreciated. I would also like to give a special thanks to my colleague, Caglar Yilmaz, who provided guidance outside of our project. Thank you for your sincere interest in our well-being and our progress as graduate students and research assistants.

I would also like to thank my other colleagues who worked on other portions of the original MON project, which my report stemmed from. This includes Jason Gabl, Taylor Groom, Robert Kitching, Jeremy Marcum, Philip Piper, Benjamin Updike, and Ben Whitehead. Some of the information on MON is sourced from their work, and I am truly grateful for those contributions.

I am also grateful to my partner, Ashley Baldwin, for her patience and encouragement. Thank you for always pushing me to follow my passions and achieve my full potential.

Finally, I am deeply indebted to my parents for their unwavering support and belief in me. I could not have completed this dissertation, and Masters program, without you.

# TABLE OF CONTENTS

LIST OF TABLES .....	7
LIST OF FIGURES .....	8
ABSTRACT .....	10
1. INTRODUCTION .....	12
2. THE HISTORY OF $N_2O_4$ AND MON PROPELLANTS .....	16
2.1 The Niche for $N_2O_4$ .....	17
2.2 Freezing Point Reduction.....	20
2.3 Stress Corrosion Mitigation .....	26
2.4 Summary of $N_2O_4$ and MON Progression .....	34
3. PRESENT AND FUTURE USAGE OF $N_2O_4$ AND MON PROPELLANTS .....	38
3.1 Reaction Control Systems (RCS) and Auxiliary Thrusters .....	39
3.2 Abort Engines .....	41
3.3 Liquid Apogee Engines (LAE) and In-Space Primary Propulsion.....	42
3.4 Launch Vehicle and Missile Stages .....	47
3.5 Future Plans involving $N_2O_4$ and MON Propellants.....	50
3.5.1 Mission One.....	50
3.5.2 Mission Two .....	51
3.5.3 Mission Three .....	52
4. MON SYNTHESIS .....	54
4.1 Synthesis Test Stand and Procedure .....	54
4.2 Determining MON Composition via The $N_2O_3$ Oxidation Method .....	58
4.3 Water Contamination .....	60
5. MON COMPOSITION DETERMINATION.....	67
5.1 Subscript Notation .....	67
5.2 Stoichiometric Equations .....	68
5.3 MIL-SPEC Equation Derivation.....	70
5.3.1 Recap of the MIL-SPEC Equation .....	70
5.3.2 Deriving the Number: 187.5 .....	71
5.3.3 Accounting for the $O_2$ dissolved in $N_2O_4$ .....	72

5.3.4	Solving for <b><i>mO<sub>2g</sub>, 3</i></b> , the Gaseous O <sub>2</sub> in Headspace after Oxidation .....	73
5.3.5	Deriving the Number: 0.003857 .....	76
5.3.6	Final Compilation of Results .....	77
5.4	Solubility Factor Derivation .....	78
6.	SOLUBILITY FACTOR DETERMINATION .....	83
6.1	MIL-SPEC Solubility Factor .....	83
6.2	Option 1: <b><i>moxidl, 3 = mMON, 2</i></b> .....	83
6.3	Option 2: <b><i>moxidl, 3 = moxid, 3</i></b> .....	86
6.4	Option 3: <b><i>mN204l, 3 = mN204, 3</i></b> .....	87
6.5	Option 4: Solving the Oxidation Method System.....	89
6.5.1	Stoichiometric Relations.....	90
6.5.2	Phase Relations .....	94
7.	EXPERIMENTAL DATA AND ANALYSIS .....	99
8.	DISCUSSION AND CONCLUSIONS .....	104
	REFERENCES .....	108

## LIST OF TABLES

Table 1. MON Synthesis and NO Content Data .....	61
Table 2. MON Synthesis and NO Content Data with Water Contamination Estimates.....	64
Table 3. MON Synthesis and NO Content Data with Water Contamination Estimates after Adjustments to Reduce Water Contamination.....	66

## LIST OF FIGURES

Figure 1. From left to right: Luigi Crocco [13], Valentin Petrovich Glushko [14], Robert Esnault-Pelterie [15].....	17
Figure 2. Titan-II ICBM silo test launch, Vandenberg Air Force Base [19].....	19
Figure 3. Titan II LR87-5 [20].....	20
Figure 4. Surveyor Vernier Propulsion System, with emphasis on Oxidizer Tanks [22].....	22
Figure 5. Transit Thermal Performance of Vernier Engine Tanks [21] .....	23
Figure 6. AQM-37A target missile loaded onto the wing of an A-6E Intruder aircraft [25].....	24
Figure 7. Sandpiper Target Missile Diagram [24] .....	25
Figure 8. Lunar Module Diagram [29] .....	27
Figure 9. Failed Apollo tank after being pressurized with N <sub>2</sub> O <sub>4</sub> for 34 hours [4].....	28
Figure 10. Failed Apollo tank after being pressurized with N <sub>2</sub> O <sub>4</sub> for 34 hours [4].....	28
Figure 11. Stress-corrosion cracks from Apollo tank tests (x500) [4].....	29
Figure 12. Minuteman III [31].....	30
Figure 13. Minuteman III Payload Bus with PSRE [34] .....	31
Figure 14. Space Shuttle Orbital Maneuvering System (OMS) [38].....	33
Figure 15. Space Shuttle Orbital Maneuvering System (OMS) Pod Schematic [39].....	34
Figure 16. The History of N <sub>2</sub> O <sub>4</sub> and MON Propellants [16] .....	35
Figure 17. Chemical Composition and Physical Properties [42].....	37
Figure 18. List of Rocket Engines for Orbital Launch Vehicles [43].....	38
Figure 19. R-D4 Engines on Apollo Lunar Module [48].....	39
Figure 20. 200N Aft Thruster Cluster for ATV [49] .....	40
Figure 21. Draco Engine Nozzles on Dragon Qualification Unit [53] .....	41
Figure 22. SuperDraco Engines firing during Crew Dragon Tests [54].....	42
Figure 23. Artist's Rendering of AJ10 Engine firing on Orion at Earth's Moon [59] .....	43
Figure 24. KTDU-80 Base Set of the Soyuz TM [64].....	44
Figure 25. Docking of Cygnus Spacecraft at the International Space Station.....	45
Figure 26. Artist's Rendering of LEROS 1b Engine firing on Juno at Jupiter [73] .....	46
Figure 27. Artist's Rendering of S400 Engine firing on the Trace Gas Orbiter at Mars[75] .....	47

Figure 28. Artist’s Rendering of S5.92 Engine firing on Fregat Upper Stage [77] .....	48
Figure 29. Proton First Stage firing during Launch [83] .....	49
Figure 30. Astrobotic Peregrine Lander [98] .....	51
Figure 31. Masten XL1 [102] .....	52
Figure 32. Astrobotic Griffin Lander [106] .....	53
Figure 33. Schematic of MON Synthesis Test Stand .....	55
Figure 34. Small-scale MON synthesis stand at the Zucrow Laboratories.....	56
Figure 35. A Sample of Synthesized MON-5 .....	57
Figure 36. Oxidation Progression from MON to N <sub>2</sub> O <sub>4</sub> .....	60
Figure 37. Phases, Processes, and Subscript Notation.....	68
Figure 38. Relationship between numbers of moles across two processes.....	70
Figure 39. Phase Relations in N <sub>2</sub> O <sub>3</sub> Oxidation Method Sample.....	95
Figure 40. MON Composition via Mass Method vs. MON Composition via Oxidation Method .....	100
Figure 41. Solubility Factor vs. MON Composition.....	102
Figure 42. Expected Solubility Factor Trend Curves vs. MON Composition up to MON-40 ...	103
Figure 43. MIL-SPEC Equation Breakdown and Explanation.....	104

## ABSTRACT

Since as early as the 1920s, dinitrogen tetroxide ( $N_2O_4$ ) has been regarded as a promising oxidizer in rocket propulsion systems. In more recent times, its predecessor, mixed oxides of nitrogen (MON), remains a top contender among oxidizers, due to its unique characteristics such as low freezing temperature and compatibility with common spacecraft materials. Today, these  $N_2O_4$ -based oxidizers are the preferred choice in many upper stages, launch escape systems, reaction control systems, liquid apogee engines, and in-space primary propulsion systems.  $N_2O_4$ -based oxidizers are a key factor in rocket propulsion, and thoroughly understanding their history, development, characteristics, synthesis, and composition analysis are crucial for space exploration today and into the future.

To fully understand and predict the physical properties of a MON sample, it is important to measure and quantify its chemical composition. The recommended method for MON composition analysis, as prescribed by the Department of Defense's Defense Specification (MIL-SPEC) document on  $N_2O_4$ , involves the oxidation of NO and dinitrogen trioxide ( $N_2O_3$ ) in the MON sample to determine their amounts. An equation unofficially called the "MIL-SPEC equation" is then used to determine the amount of NO needed to mix with  $N_2O_4$  to synthesize that particular MON sample. However, no explanation is given as to how the equation was derived, or its significance.

This thesis aims to collect and organize key information on the synthesis, handling, and composition analysis of MON propellant. First, the history of development of  $N_2O_4$ -based oxidizers was researched, and current and future uses of  $N_2O_4$  and MON propellants were identified. Then a method for synthesis and composition analysis was devised and tested. Water contamination was expected of skewing the results, so the process of water contamination was examined analytically. Then a detailed derivation of the MIL-SPEC equation was conducted, to fully understand its mechanics. An attempt was then made to reverse-engineer an unexplained numerical value in the equation, labeled by the author as the "solubility factor". Several derivations were provided with varying degrees of complexity, producing alternative solubility factors of varying accuracies. Finally, experimental data was applied to these derived, hypothetical solubility

factors and the MIL-SPEC solubility factor, with the intent of determining whether improvements could be made to the MON composition determination process.

The results suggest that the MIL-SPEC equation is sufficient for providing a relatively accurate measurement of the composition of a MON sample, while also being easy to implement, both in taking the necessary measurements and in conducting the numerical calculation. However, some minor adjustments to the equation could produce consistently more accurate composition measurements without adding any more difficulty or complication.

# 1. INTRODUCTION

Throughout the history of rocket propulsion, one of the most commonly used and studied oxidizers is dinitrogen tetroxide (NTO,  $N_2O_4$ ).  $N_2O_4$  was reportedly prepared as early as the 1700s [1], and its oxidizer derivatives have since gone on to become the preferred oxidizer for many rocket propulsion systems such as those on the Titan II and the Apollo Lunar Module [9]. These systems span a large range of sizes, from small attitude control thrusters to large launch motors.  $N_2O_4$ -based oxidizers are used in combination with either monomethylhydrazine (MMH) or Aerozine-50 (50% unsymmetrical dimethylhydrazine (UDMH), 50% hydrazine) as the fuel.[3] Although large rockets and missiles have more recently moved away from  $N_2O_4$ -based oxidizers, these oxidizers are still the preferred choice in many upper stages, launch escape systems, reaction control systems, liquid apogee engines, and in-space primary propulsion systems.  $N_2O_4$ -based oxidizers are a key factor in rocket propulsion, and thoroughly understanding their history, development, characteristics, synthesis, and composition analysis are crucial for space exploration today and into the future.

$N_2O_4$  is a red-brown liquid at standard temperature and pressure (STP), and is a yellowish liquid at temperatures below  $0^\circ\text{C}$ . However, it freezes at approximately  $-10^\circ\text{C}$  ( $14^\circ\text{F}$ ) when under atmospheric pressure, and corrodes many spacecraft materials, including titanium and titanium-aluminum alloys [4]. These attributes rule out  $N_2O_4$  for planetary landers and deep space propulsion system. However, the high freezing temperature and corrosive nature of  $N_2O_4$  can be alleviated by introducing nitric oxide (NO) to the  $N_2O_4$ , which decreases the freezing point of  $N_2O_4$  and inhibits some of its corrosive tendencies [4]. The resulting green mixture of  $N_2O_4$  and NO is referred to as mixed oxides of nitrogen (MON) and is denoted as “MON-X,” where X refers to the mass fraction of NO added into the NO-  $N_2O_4$  system. For example, a mixture that is 75 %  $N_2O_4$  and 25% NO by weight would be referred to as MON-25.

Mixing  $N_2O_4$  and NO produces MON propellant, a complicated mixture that incorporates a long series of equilibrium reactions occurring simultaneously, resulting in the presence of not only  $N_2O_4$  and NO, but also dinitrogen trioxide ( $N_2O_3$ ), nitrous oxide ( $N_2O$ ), and nitrogen dioxide ( $NO_2$ ) [5]. In fact, it is the blue liquid  $N_2O_3$  which mixes with the yellowish orange  $N_2O_4$  (at temperatures

below 0°C) to give MON its characteristic greenish hue [4]. Additionally, Martens, Owens, and Cooks report the potential for pure oxygen (O<sub>2</sub>) to be formed due to decomposition of NO<sub>2</sub> into NO and O<sub>2</sub> [6]. Mueller reports that the liquid portion of the MON mixture consists only of N<sub>2</sub>O<sub>4</sub> and N<sub>2</sub>O<sub>3</sub>, while the headspace consists of NO, NO<sub>2</sub>, N<sub>2</sub>O<sub>3</sub>, and N<sub>2</sub>O<sub>4</sub> [5].

It is common for lower NO concentrations to be used, typically MON-1 and MON-3, but higher concentrations (up to MON-25) have also been used for propulsion systems [7], and even higher concentrations (up to MON-40) have been synthesized and studied [8], [9]. MON-25 and MON-30 have freezing points of -55°C and -80°C respectively [10], and thus have been used for extreme-temperature applications such as Martian and lunar landers, as well as deep space probes. If either MON-25 or MON-30 is implemented, then on-board oxidizer tank heaters would not be necessary (or would require less power than with lower MON grades), saving mass that can be used to carry more payload to the intended destination, or more payload back to Earth on a return trip.

In order to provide accurate control of a vehicle's flight path, propulsion systems require the delivery of precise amounts of liquid propellants. Such precision is only possible with detailed knowledge of the flow characteristics of the liquid propellant. These flow characteristics include thermal conductivity, viscosity, density, and vapor pressure. However, despite MON being an attractive oxidizer for propulsion systems, much of the available physical property data is either outdated, poorly documented, reported without any measurement uncertainties, or extrapolated from previous results. MON physical property data has often been extracted from papers published prior to 1970, and thus were collected using smaller sample sizes than are common in the scientific community today. At times, it is unclear whether the values given are experimental, extrapolated from experimental data, or estimated from thermodynamic models. Some papers neglect to mention units [11], [12], are not publicly available [5], or have mentions of NO contamination [12]. For a process as precision-based and as costly as space propulsion, the lack of clarity involving physical property data is of concern.

The physical properties of a MON sample are dependent on the NO content of the sample during the synthesis process, which will be referred to as its MON composition. A clear example of this is the freezing point, which has a clear relation with NO content. In order to accurately document the physical properties of a MON sample, or accurately predict how a MON sample will react in

a propulsion system, it is also vitally important to know the precise MON composition of the sample.

Unfortunately, however, the difference in equilibrium compositions between the liquid and vapor portions of MON implies that filling a test apparatus with MON from the liquid fraction of a bulk supply tank will result in a different MON composition than would a mass equivalent loading pulled from the headspace of the same vessel. In either case, the MON composition in the test apparatus would vary from the MON composition in the bulk vessel. This can become especially problematic if the MON composition changes by an unknown amount when it is loaded into another tank or even a spacecraft. Such a change could alter the physical properties of the propellant and lead to unexpected results. Thus, it is advantageous to measure and validate the composition of the MON after every transfer to a new container, such as when being loaded to a propulsion system, even if the MON composition in the bulk vessel is already known.

As mentioned earlier, the liquid portion of the MON mixture consists only of  $\text{N}_2\text{O}_4$  and  $\text{N}_2\text{O}_3$ , so measuring the NO content present in the liquid MON after synthesis is meaningless, as there is none. It is actually the amount of NO that is used during the synthesis process that determines the numerical value of “X” in the "MON-X" designation. Therefore, when measuring the MON composition of a loaded, altered sample, one must reverse-engineer the amount of NO that would have been used during synthesis.

In the last few decades,  $\text{N}_2\text{O}_4$  and MON have seen less usage in large launch vehicles and missiles, and more usage in reaction control systems (RCS), auxiliary thrusters, liquid apogee engines (LAE), and in-space primary propulsion. Such systems involve minute burns of propellant in order to conduct delicate maneuvers, often times while in space or in transit. More accuracy regarding propellant physical properties is required in order to ensure that the expected maneuvers match the outcomes during live missions. Thus, it is crucial that  $\text{N}_2\text{O}_4$  and MON are thoroughly understood across the span of MON compositions, and in a variety of extreme space-relevant conditions.

In light of the unique uses of  $\text{N}_2\text{O}_4$  and MON, and because of the uncertainty involving the data of many MON physical properties, there is an increasing interest in validating these values by using modern techniques and standards. As a result, several teams of students at Purdue University, led by Professor Timothee Pourpoint, were tasked by NASA to measure the physical properties of

MON. In addition to that goal, the teams set out to determine an accurate way to synthesize MON propellant in a laboratory setting and measure its composition.

The following thesis is a wholistic study on  $N_2O_4$  and MON. Following this introduction chapter, Chapter 2 summarizes the long and unique history of  $N_2O_4$  and MON development, isolating the steps towards freezing point reduction from the steps towards stress corrosion mitigation. Chapter 3 introduces a number of notable rocket engines and systems that currently use  $N_2O_4$  and MON, as well as several future plans involving those propellants. Chapter 4 discusses MON synthesis, including the MON synthesis test stand and procedure devised by Purdue University students, the  $N_2O_3$  oxidation method for MON composition analysis, and the potential issues connected to water contamination. Chapter 5 is an analysis of the  $N_2O_3$  oxidation method for MON composition determination, and a derivation of its central equation. Chapter 6 is a detailed breakdown of the solubility factor of the MIL-SPEC equation, including its derivation and potential alternative equations, as well as an analytical breakdown of the synthesis and oxidation method system and its application to the experimental data. Chapter 7 discusses the experimental data from tests on  $N_2O_4$  and MON, comparing different types of composition analysis and alternative values of the solubility factor. Finally, Chapter 8 is a discussion of the previous chapters, including further improvements of the  $N_2O_3$  oxidation method. This research was conducted to further advance the understanding and knowledge regarding  $N_2O_4$  and MON propellant, to aid in the utilization of this unique oxidizer for future missions to the moon, Mars, and beyond.

## 2. THE HISTORY OF N<sub>2</sub>O<sub>4</sub> AND MON PROPELLANTS

From the early days of rocket science up until the end of the Space Race, nitrogen tetroxide (N<sub>2</sub>O<sub>4</sub>) has stood on the forefront of space propulsion. More recently its successor, mixed oxides of nitrogen (MON), has continued this tradition. The historical context surrounding N<sub>2</sub>O<sub>4</sub> and MON is important in understanding the crucial roles that the propellants play in the quest to explore space, today and into the future.

Since as early as the 1920s, N<sub>2</sub>O<sub>4</sub> has been regarded as a promising oxidizer in rocket propulsion systems. This is due to N<sub>2</sub>O<sub>4</sub>'s ability to be stored indefinitely at room temperature, unlike liquid oxygen which boils at temperatures above  $-183^{\circ}\text{C}$  ( $-297^{\circ}\text{F}$ ).

In 1929, Luigi Crocco of Italy was one of the earliest rocket scientists to break away from the liquid oxygen oxidizer, when he began work on a highly sophisticated motor design which ran on gasoline and N<sub>2</sub>O<sub>4</sub> [2]. Valentin Petrovich Glushko of Russia also came to a similar conclusion when he performed his first firings of a toluene-N<sub>2</sub>O<sub>4</sub> propulsion system in 1930 [2]. Shortly afterwards in 1931, Robert Esnault-Pelterie of France became the third experimenter to independently use N<sub>2</sub>O<sub>4</sub> as an oxidizer, this time with benzene as a fuel [2]. Thus, within three years, three separate teams throughout Eurasia (their leaders shown in Figure 1) came to the same conclusion to use N<sub>2</sub>O<sub>4</sub> as an oxidizer, in order to avoid the complications surrounding liquid oxygen.



Figure 1. From left to right: Luigi Crocco [13], Valentin Petrovich Glushko [14], Robert Esnault-Pelterie [15]

Around this time, in March 1931, Friedrich Wilhelm Sander of Germany began firing a motor with a unique oxidizer called red fuming nitric acid (RFNA) [2]. This was a mixture of nitric acid ( $\text{HNO}_3$ ) and 5 to 20 percent  $\text{N}_2\text{O}_4$ .

Between 1950 and 1954, research conducted by the United States Navy's United States Naval Ordnance Test Station (NOTS) and the Jet Propulsion Laboratory (JPL) investigated the  $\text{N}_2\text{O}_4$ -NO system in detail [2]. Interest in  $\text{N}_2\text{O}_4$  continued to rise in the late 1950s and early 1960s, when  $\text{N}_2\text{O}_4$  was found to be less corrosive, more stable, and higher performing than nitric acid [16]. This led to  $\text{N}_2\text{O}_4$  becoming the storable oxidizer of choice for rockets in both the United States and the USSR [2].

## 2.1 The Niche for $\text{N}_2\text{O}_4$

In 1955, the Glenn L. Martin Company began development of the Titan I. The Titan I was an intercontinental ballistic missile designed to launch from underground missile silos, allowing for

the United States to respond to an enemy's nuclear first strike with a second strike response of its own. The Air Force received delivery of its first Titan in 1958, and the first Titan I squadron was placed on operational alert in 1962 [17].

The Titan I's first stage initially used the LR87-3 engine, while the second stage used the LR91-3. Both engines burned liquid oxygen and RP-1 (a highly refined form of kerosene, similar to jet fuel). Liquid oxygen cannot be stored at room temperature, and proved to be dangerous to use in enclosed spaces such as a missile silo. Liquid oxygen also could not be stored in oxidizer tanks for long periods, and even resulted in the explosive destruction of several Titan I and Atlas rockets, along with their respective silos. As a result, the missiles could not be filled with the oxidizer in advance. The liquid oxygen would need to be cooled cryogenically outside of the missile when not in use, and then loaded immediately before launching. The missiles also had to be raised out of their silos when loading the oxidizer [18]. These steps added significant delays and hindered the responsiveness of the Titan I fleet.

In response to these shortcomings, the Martin Company quickly designed the Titan II (Figure 2). The first and second stages of the Titan II used the updated LR87-5 (Figure 3) and LR91-5 engines, which were similar to the LR87-3 and LR91-3 except modified to burn  $N_2O_4$  and Aerozine 50 (a 50:50 mix by weight of hydrazine and unsymmetrical dimethylhydrazine, also known as UDMH) instead of liquid oxygen and RP-1. Since  $N_2O_4$  and Aerozine 50 are hypergolic propellants, there was no longer a need for an independent ignition system. But more importantly,  $N_2O_4$  and Aerozine 50 could be stored at room temperature, allowing the Titan II missiles to be kept fully fueled at all times, and ready to launch on short notice, within 60 seconds and directly from within its silo [18]. As a result of the new propellant design, the updated engines had less modes of failure, were easier to maintain, had reduced risk of accidents, and were lighter and simpler [17].



Figure 2. Titan-II ICBM silo test launch, Vandenberg Air Force Base [19]

The new propellant design also resulted in significant performance improvements, with the Titan II first stage delivering 430,000 pounds of thrust (versus the 300,000 pounds of thrust of the Titan I first stage), and the Titan II second stage delivering 100,000 pounds of thrust (versus the 80,000 pounds of thrust of the Titan I second stage) [17]. The Titan II was also capable of delivering a larger payload, and had a longer range of 9,000 miles (versus the 6,300 miles of the Titan I) [17]. Development of the Titan II took place in parallel with the Titan I program, with the goal of rapidly replacing the Titan I fleet. The Titan II rocket began operations in 1963, while the last Titan I was removed from alert in 1965 [17].



Figure 3. Titan II LR87-5 [20]

## 2.2 Freezing Point Reduction

During the 1960's, the widespread usage of  $N_2O_4$  caused a large push to understand its thermal-physical properties and compatibility with various containment materials.

In 1960, NASA set out to demonstrate the feasibility of a soft landing on the Moon as a precursor to the Apollo program. NASA did so by initiating the Surveyor program, which aimed to send the first American spacecraft to the surface of an extraterrestrial body via soft landing, and survey the portion of the moon where manned spacecraft were likely to land. The spacecraft would also need to survive the first lunar day and a portion of the lunar night [21].

The requirements of the mission imposed unique constraints on the thermal control system and propulsion system that had not been addressed in American spacecraft at the time. First, the spacecraft would need to survive the 66 hour cislunar transit phase. The expected temperature range was complicated by multiple maneuvers, radiant and convective heating interactions between the spacecraft and its multiple types of engines, and changes in vehicle configuration (e.g. deployment of landing gear and the antenna). Second, in the 1960's, the thermal characteristics of the lunar surface were not fully defined. The Surveyor spacecraft would have to survive the wide range of lunar surface temperatures that occurred between day and night conditions, taking into account varying sun angles and altering shadow patterns [21].

The mission profile required that the Surveyor spacecraft be launched toward the moon on an Atlas-Centaur rocket, at which point its vernier propulsion system of three vernier engines (Figure 4) would perform a midcourse correction maneuver. The vernier engines and a solid retrorocket were then used during terminal lunar descent. The solid retrorocket slowed the spacecraft velocity by nearly 95% and then was jettisoned, while the vernier engines continued firing, completing the rest of the soft landing. The vernier engines used were the Thiokol Rocket Motors Division (RMD) TD-339 [22].

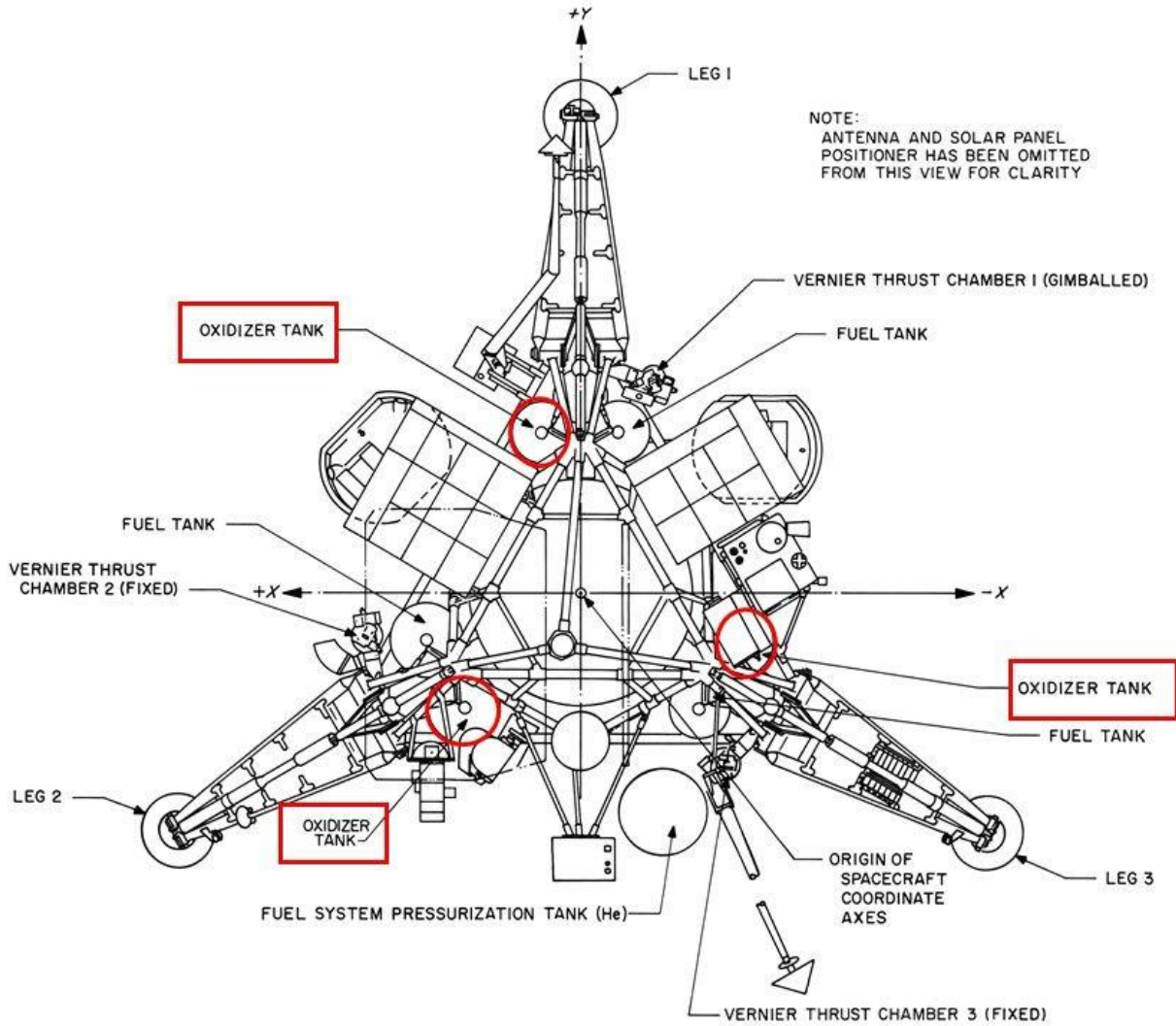


Figure 4. Surveyor Vernier Propulsion System, with emphasis on Oxidizer Tanks [22]

Although the lunar surface temperature approached  $-250^{\circ}\text{F}$  ( $-157^{\circ}\text{C}$ ) at night, that was not required of the vernier propulsion system, which would only operate during the cislunar transit and landing procedures. It was found that most of the subsystems could operate within a temperature range of  $0$  to  $125^{\circ}\text{F}$  ( $-18$  to  $52^{\circ}\text{C}$ ) with little decrease in performance or reliability [21]. The freezing point of pure  $\text{N}_2\text{O}_4$  was  $11.84^{\circ}\text{F}$  ( $-11.2^{\circ}\text{C}$ ), which would have excluded the vernier propulsion system from this category of  $0$ -to- $125^{\circ}\text{F}$  operational subsystems. However, by adding 10%  $\text{NO}$  by weight, the freezing point of the  $\text{N}_2\text{O}_4$  oxidizer could be reduced to  $-9.7^{\circ}\text{F}$  ( $-23.2^{\circ}\text{C}$ ) [16], extending its operational temperature range beyond the  $0$ -to- $125^{\circ}\text{F}$  criteria. As a result, the vernier propulsion

system chose to utilize MON-10. Figure 5 shows the behavior of the oxidizer and fuel tanks for two typical Surveyor spacecraft (Surveyor I and Surveyor III) during transit. As mission time increases, the temperatures drop, such that the final temperature of the Surveyor III became relatively close to the freezing temperature of pure  $N_2O_4$ , even with passive thermal controls. This diagram illustrates the need for freezing point reduction of the oxidizer.

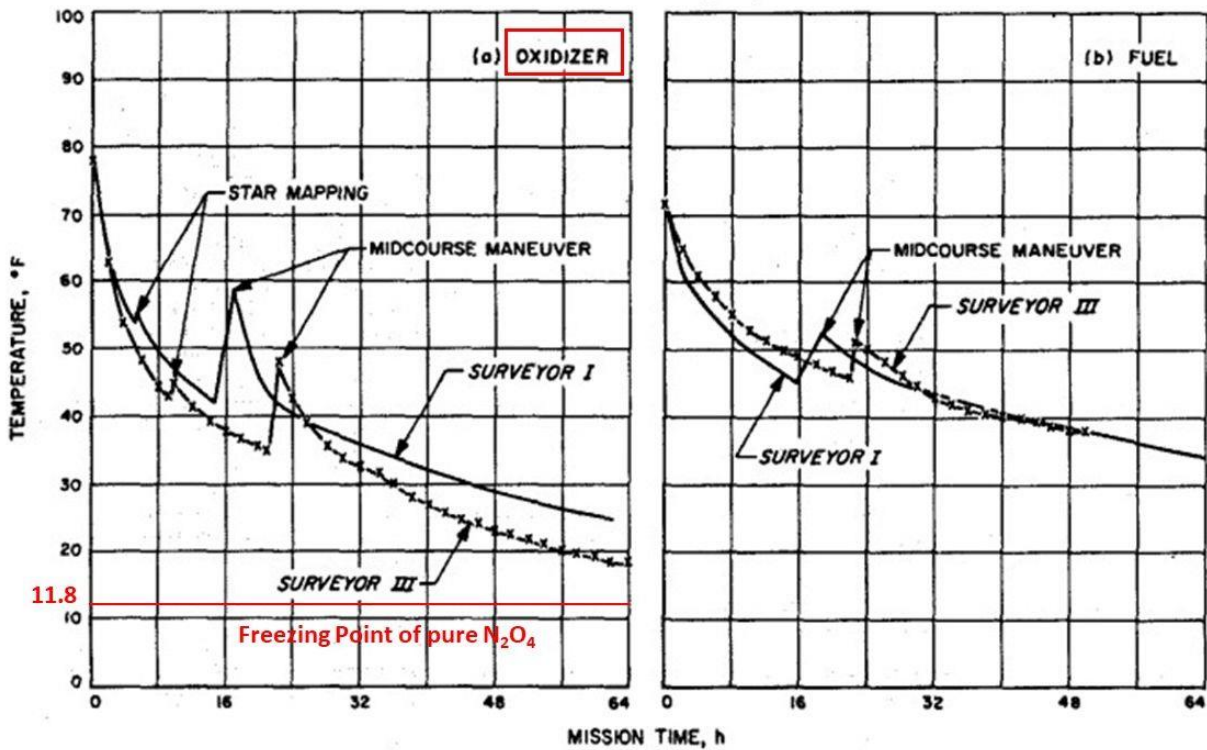


Figure 5. Transit Thermal Performance of Vernier Engine Tanks [21]

Meanwhile, also in the early 1960s, the Air Force developed the Beechcraft AQM-37 Jayhawk (Figure 6), an air-launched supersonic target drone capable of simulating inbound ICBM warhead packages and enemy aircraft for fleet shoot-down exercises. In 1967, an Air Force Required Action Directive [23] indicated that improved rocket-powered target missiles were needed to simulate the flight performance of the best aircraft a potential enemy might produce in the next decade [24]. Such an aircraft could be capable of maximum altitudes as high as 100,000 feet, with flight speeds up to Mach 5. To meet a variety of mission profiles, an extremely flexible propulsion system was required. This system would need thrust variation and extended burn times, with added traits of

being cost effective, easily handled, stored under a wide range of conditions, require minimum checkout and maintenance, and produce maximum safety and reliability [24].



Figure 6. AQM-37A target missile loaded onto the wing of an A-6E Intruder aircraft [25]

The Sandpiper program set out to investigate an alternate propulsion scheme for the AQM-37 missile, which would be called the Sandpiper target missile, and later the HAST (High Altitude Supersonic Target). This vehicle was designed to be aircraft launched and fly horizontally for ranges over 100 miles and at several altitudes and Mach numbers up to Mach 5 [26].

A review of existing propulsion systems revealed that such technology was not available, although hybrid propulsion was the most promising option for accomplishing these goals. The resulting hybrid propulsion design was an engine which burned solid fuel consisting of 10% powdered magnesium dispersed in 90% polymethylmethacrylate (Plexiglas), and an oxidizer of MON-25. Reports stated that the NO addition provided storability in the liquid state over a temperature range of  $-54^{\circ}\text{C}$  ( $-65^{\circ}\text{F}$ ) to  $74^{\circ}\text{C}$  ( $165^{\circ}\text{F}$ ). The propellants were commended for being nonexplosive,

nonhypergolic, and readily available at moderate cost [24]. Figure 7 shows a schematic of the Sandpiper target missile, with indication of a “nitrogen tetroxide + nitric oxide” propellant tank.

The Sandpiper program eventually chose IRFNA (Inhibited Red Fuming Nitric Acid) as its oxidizer [26], but the program still marked one of the first instances of using NO contents as high as 25% to reduce the freezing point of  $N_2O_4$ .

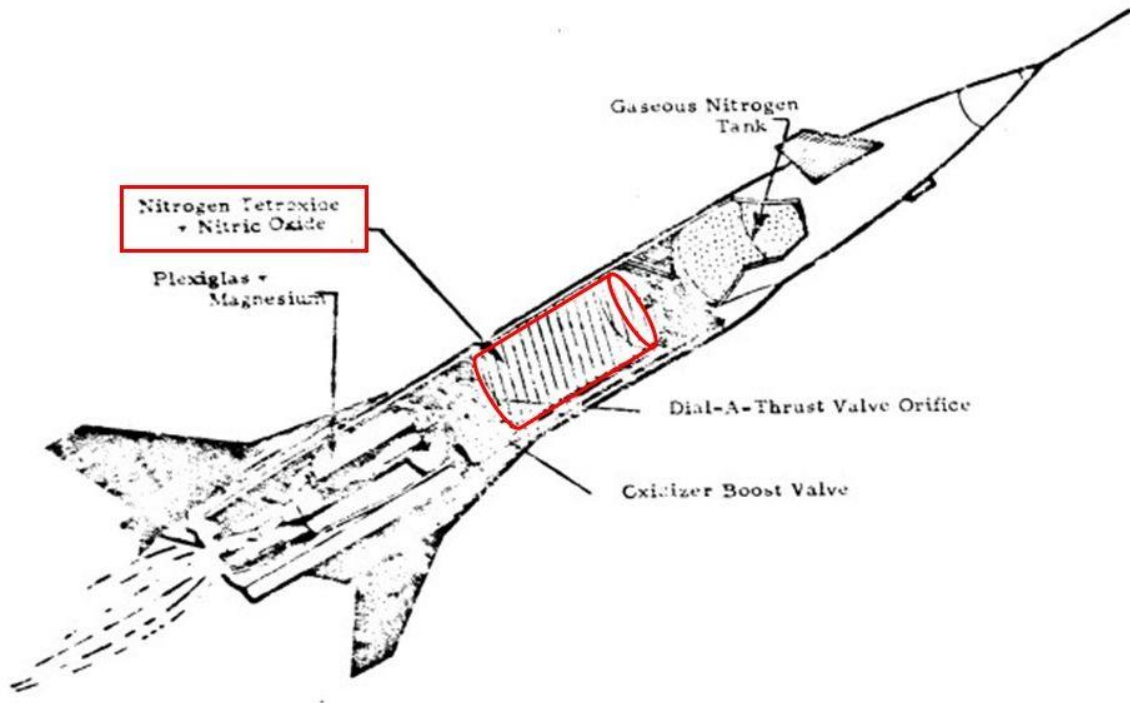


Figure 7. Sandpiper Target Missile Diagram [24]

The increasing demand for an  $N_2O_4$  variant that could withstand extreme temperatures led to the development of the MIL-SPEC document MIL-P-27408, which detailed specifications for “mixed oxides of nitrogen” for the first time, in 1964 [27]. The updated MIL-P-27408A listed the requirements for MON-10 and MON-25 in 1971 [28].

### 2.3 Stress Corrosion Mitigation

The other concern about  $N_2O_4$  systems was material compatibility. Initially, aerospace  $N_2O_4$  systems were constructed out of aluminum and stainless steel. However, those materials resulted in significant corrosion and flow decay that led engineers to seek more compatible alternatives. The titanium alloy, Ti-6Al-4V, was eventually chosen because it not only exhibited corrosion resistance to  $N_2O_4$  but also possessed a high strength-to-weight ratio. As a result,  $N_2O_4$  and Ti-6Al-4V are often in contact, causing their compatibility to be of considerable interest.

From 1960 to 1963, several studies were done by Allied Chemical Corp and the North American Aviation Inc. to test the compatibility of  $N_2O_4$  with Ti-6Al-4V [4]. Those studies concluded that the two were fully compatible.

Meanwhile, the Apollo program was in full swing. At the time, one of the most desirable rocket propellant combinations was Aerozine 50 and  $N_2O_4$ . This hypergolic system was implemented throughout the main propulsion and reaction control systems (RCS) of the Apollo design, namely in the lunar module descent and ascent stages (see Figure 8), the lunar module RCS, the Saturn booster attitude control, and the Lunar Orbiter Vehicle attitude control. It was thus a critical part of the Apollo design, which was the first major program to implement the Ti-6Al-4V- $N_2O_4$  combination during the 1960's. [4]

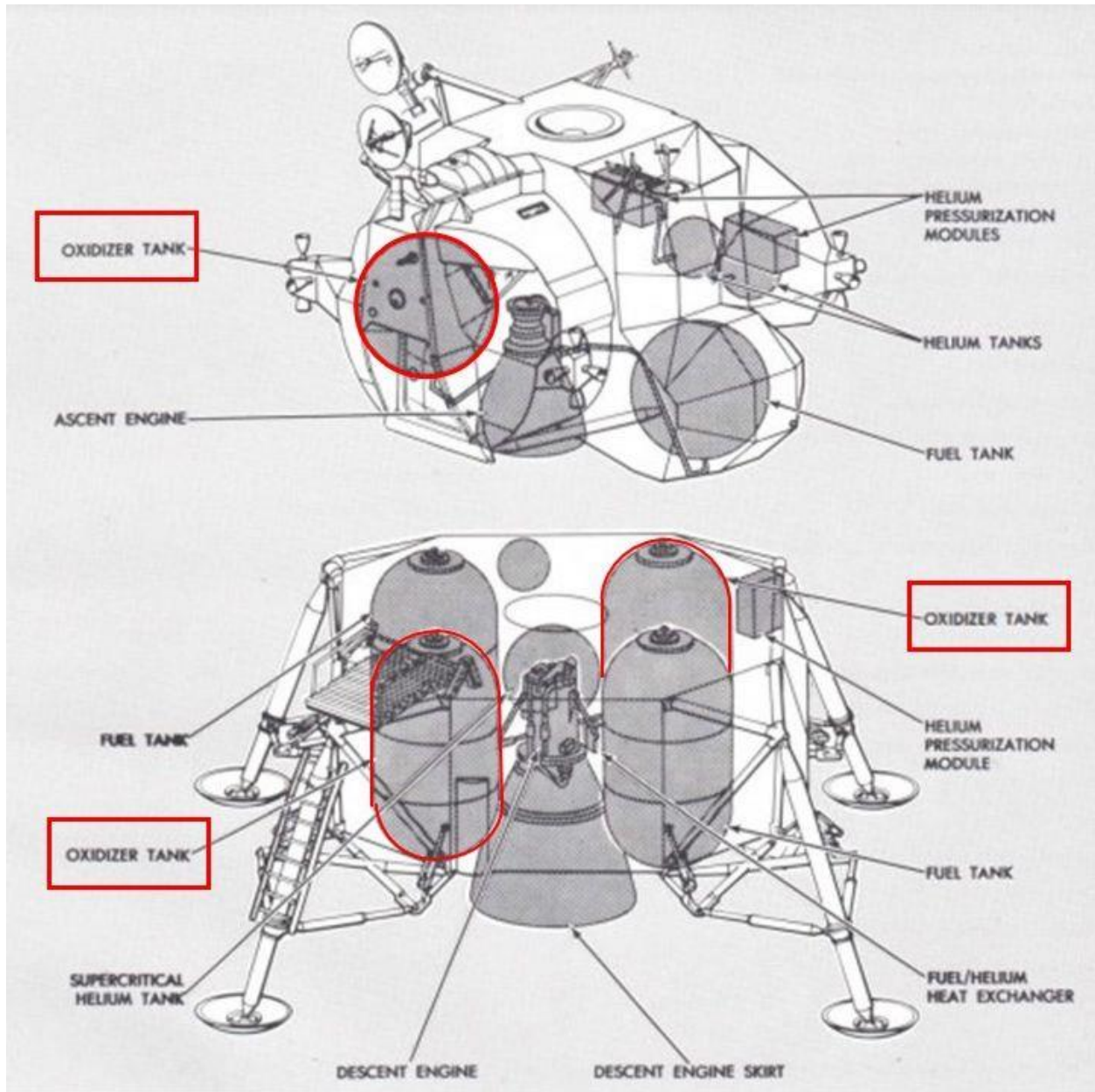


Figure 8. Lunar Module Diagram [29]

Initially, NASA compatibility testing of  $N_2O_4$  in pressurized titanium alloy tanks produced positive results. However, during testing in 1965, NASA encountered its first failure of a titanium alloy tank containing  $N_2O_4$ , caused by stress corrosion cracking. Subsequent tests also resulted in the same mode of failure. Figure 9, Figure 10, and Figure 11 show images of failed Apollo tanks after being pressurized with  $N_2O_4$  at  $40.6^\circ\text{C}$  ( $105^\circ\text{F}$ ) for 34 hours.

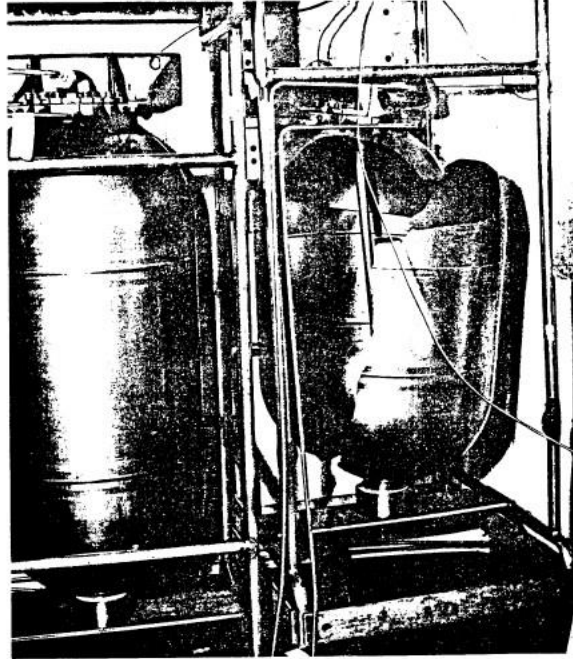


Figure 9. Failed Apollo tank after being pressurized with  $N_2O_4$  for 34 hours [4]

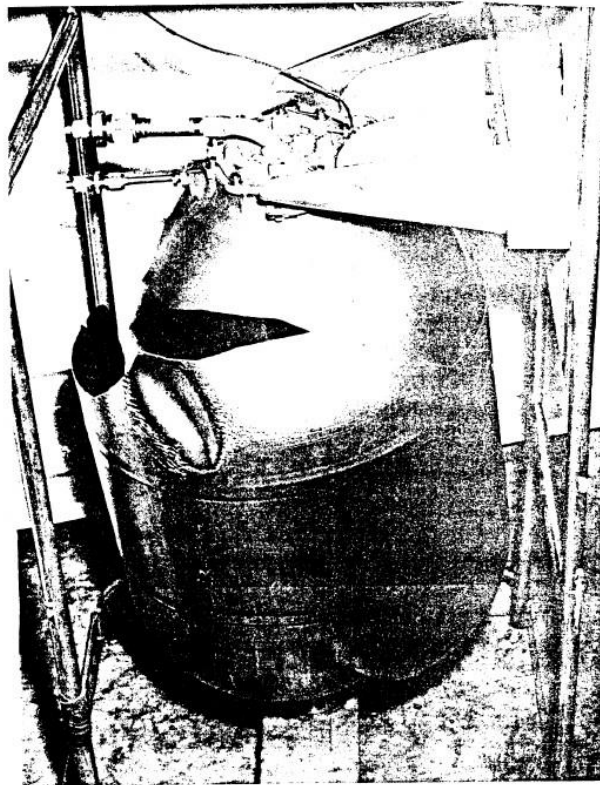


Figure 10. Failed Apollo tank after being pressurized with  $N_2O_4$  for 34 hours [4]

By then, much of the Apollo hardware had already been constructed out of the titanium alloy, and the program could not afford the delays and expenses of switching to a different material. This forced NASA to address the  $N_2O_4$ -titanium compatibility issue head on, prompting NASA and its contractors to conduct nearly twenty separate studies to determine the cause of the stress corrosion cracking, and to identify a solution that could be applicable to the Apollo program.

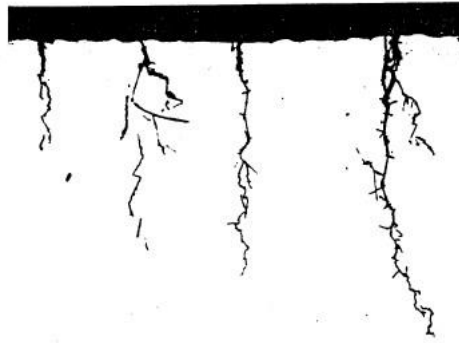


Figure 11. Stress-corrosion cracks from Apollo tank tests (x500) [4]

Eventually, Bell Aerosystems Company cooled down the  $N_2O_4$  samples to  $0^{\circ}F$  ( $-17.8^{\circ}C$ ) and found that some  $N_2O_4$  samples turned yellow while others turned green. The yellow oxidizers were pure  $N_2O_4$ , which is commonly reddish brown at room temperature, but which transitions to yellow when cooled. The green oxidizers, however, were a mixture of bluish  $N_2O_3$  and yellowish  $N_2O_4$ . The  $N_2O_3$  is created when nitric oxide (NO) and  $N_2O_4$  react with one another. The reddish brown  $N_2O_4$  samples were causing the stress corrosion during tests, while the green  $N_2O_4$  samples were not [4].

Thus it was discovered that prior to June of 1964, manufactured  $N_2O_4$  contained trace quantities of NO. Unbeknownst at the time, this presence of NO had prevented stress corrosion cracking from taking place, and was the reason that NASA's original  $N_2O_4$ -titanium tests had been successful. An NO content as low as 0.25% by weight was capable of preventing such corrosion [4]. However, in June of 1964, an additional step was added to  $N_2O_4$  processing which purified the  $N_2O_4$ , removing the trace NO. This resulted in the first tank failures in January of 1965. At the time, military specification of  $N_2O_4$  did not require NO analysis, so this effect was not suspected [4].

In light of this discovery regarding NO content, NASA created distinct terminology for red  $N_2O_4$  and green  $N_2O_4$ . Further tests found that “Red Reactive  $N_2O_4$ ” (or “RR  $N_2O_4$ ”) cracked 30 out of 30 titanium-aluminum specimens during testing, while “Green 8  $N_2O_4$ ” (or “G8  $N_2O_4$ ”) ( $N_2O_4$  with 0.8% NO) was found to not crack 10 specimens under identical conditions [30]. Later tests involving “Green 4  $N_2O_4$ ” (or “G4  $N_2O_4$ ”) ( $N_2O_4$  with 0.4% NO) confirmed its compatibility with Ti-6Al-4V, resulting in a 0.4%-0.8% NO content range for  $N_2O_4$  used in Apollo applications [4].

Meanwhile, during the 1960s, the Air Force and Boeing Aerospace were developing the LGM-30 Minuteman III (Figure 12), a land-based, long-range, solid-fuel, three-stage intercontinental ballistic missile that would replace the Titan II as the backbone of America’s strategic nuclear deterrent force.



Figure 12. Minuteman III [31]

The Minuteman III was the first deployed ICBM with a Multiple Independently targeted Reentry Vehicle (MIRV): a fourth stage exoatmospheric ballistic missile payload containing several warheads on a Payload Bus (Figure 13), each capable of striking a different target with a high degree of accuracy. The Payload Bus utilized the Propulsion System Rocket Engine (PSRE): a post-boost propulsion system (PBPS) powered by hydrazine and  $N_2O_4$  [32]. These hypergolic propellants provided good specific impulse, rapid restart capabilities, and thrust metering/impulse cycling required for precise angular positioning and range maneuvering necessary for deploying multiple warheads. And, like the Titan II, these propellants were storable (non-cryogenic and non-degrading), meaning that the missiles could be preloaded and ready to launch in a moment's notice [33].

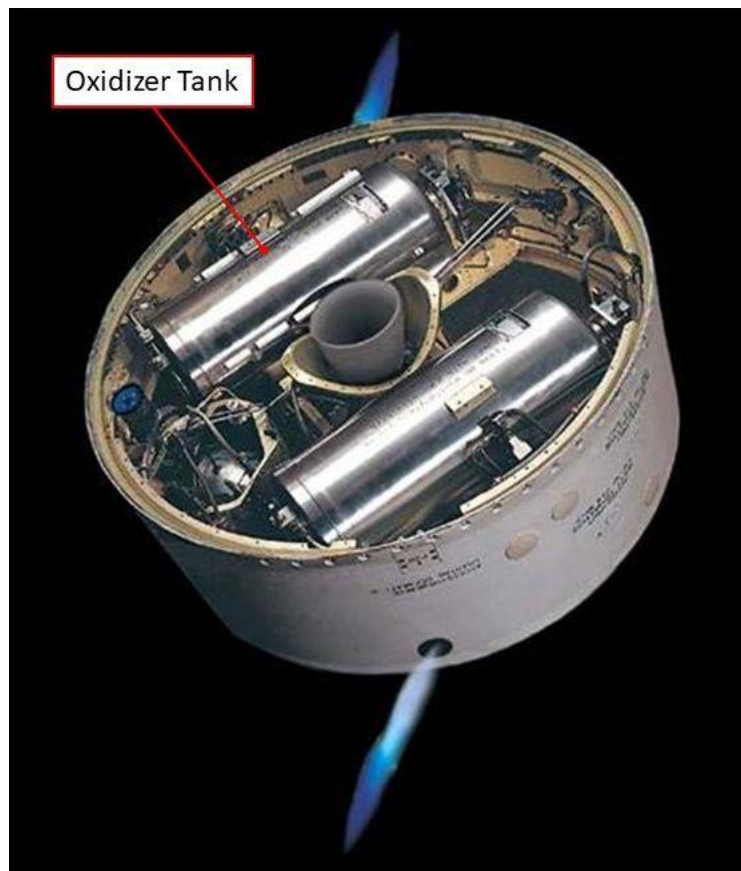


Figure 13. Minuteman III Payload Bus with PSRE [34]

During development in 1965, the Air Force was concerned about possible corrosion problems within the PBPS. As a result, the contractor, Autonetics Division, North American Rockwell, created a propellant specification for  $N_2O_4$  which included acceptable ranges for NO and chloride content. This specification, called “Minuteman Grade”  $N_2O_4$ , was designed to prevent corrosion attack on the steel bellows in the PBPS tanks. Soon afterwards, in 1970, the chemical requirements for procuring  $N_2O_4$  and MON-1 were added to the MIL-SPEC document for nitrogen tetroxide, in Specification MIL-P-26539C. While NASA still called the propellant “green  $N_2O_4$ ”, the Air Force had already begun to call it MON-1 [16].

NASA later determined that some of the NO content in MON propellant was lost through venting [35]. This finding became critically important in the late 1960’s and early 1970’s as NASA was completing its design of the Space Shuttle orbiter. This revolutionary spacecraft would utilize the Space Shuttle Orbital Maneuvering System (OMS) (Figure 14), a pair of aft-mounted hypergolic AJ10-190 rocket engines that allowed the Space Shuttle orbiter to perform various orbital maneuvers, including orbital injection after main engine cutoff, orbital corrections during flight, and the final deorbit burn for reentry [36]. The Space Shuttle also used a reaction control system (RCS) that provided small amounts of thrust for attitude control. Both the OMS and RCS were housed in two pods mounted on the orbiter’s aft fuselage [37]. The OMS and RCS both burned monomethylhydrazine (MMH) and an  $N_2O_4$  -based oxidizer, although the NO content of the oxidizer was briefly in question.

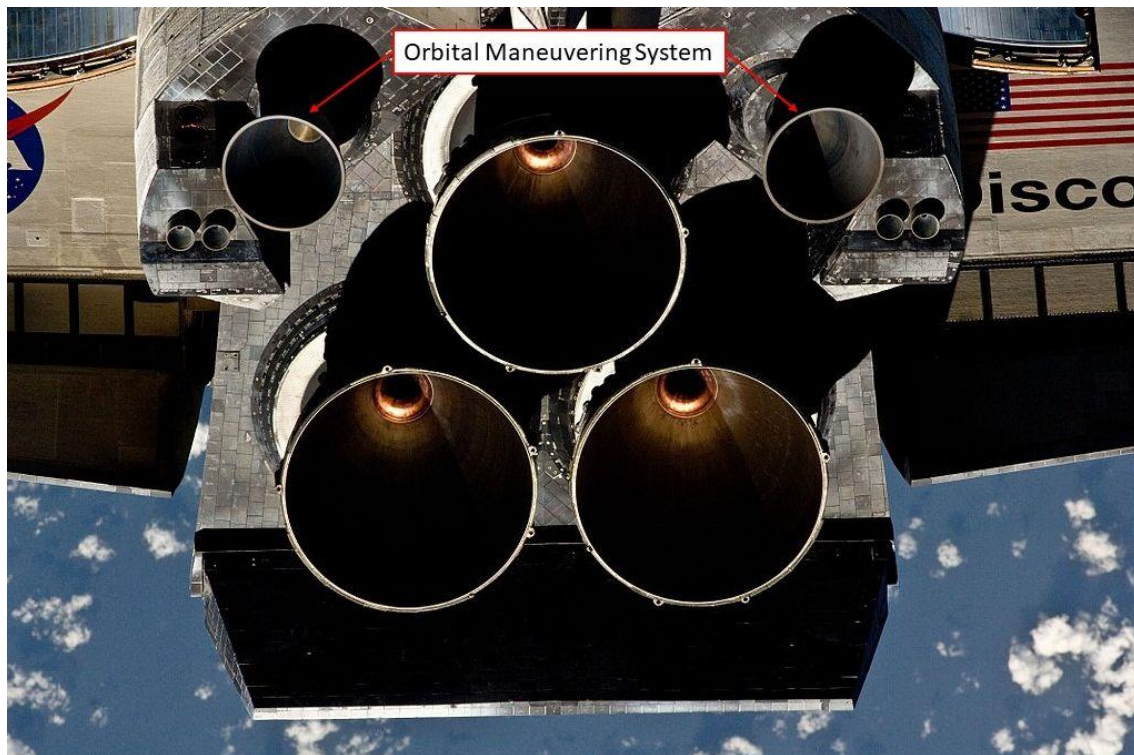


Figure 14. Space Shuttle Orbital Maneuvering System (OMS) [38]

At the time, NASA found that, in order to prevent stress corrosion in the Ti-6Al-4V alloy, green  $N_2O_4$  required an NO content greater than 0.5%. To ensure that this minimum NO content was met at all times, even after venting, the NO content during production was increased from 1% to 3%, and so MON-3 became the standard for  $N_2O_4$ -based oxidizers, starting with the Space Shuttle [16], [35].

In 1976, the chemical requirements for procuring MON-3 were incorporated into the MIL-SPEC document for nitrogen tetroxide, MIL-P-26539C, via Amendment 2. The slight addition of NO did not change the thermal-physical properties of  $N_2O_4$  from an applicational perspective, so the properties for  $N_2O_4$ , MON-1, and MON-3 are listed as identical [16]. Thus, MON-1 and MON-3 were intended to replicate the thermal-physical properties of  $N_2O_4$  while specifically preventing corrosion. As stated earlier, NASA continued to call the propellant “green  $N_2O_4$ ” or  $N_2O_4$ , while the Air Force and MIL-SPEC documents had begun to call the propellant MON-3. This is evidenced by the NASA schematic of an OMS pod in Figure 15, which labeled the oxidizer tank as “Nitrogen Tetroxide ( $N_2O_4$ ) Tank”.

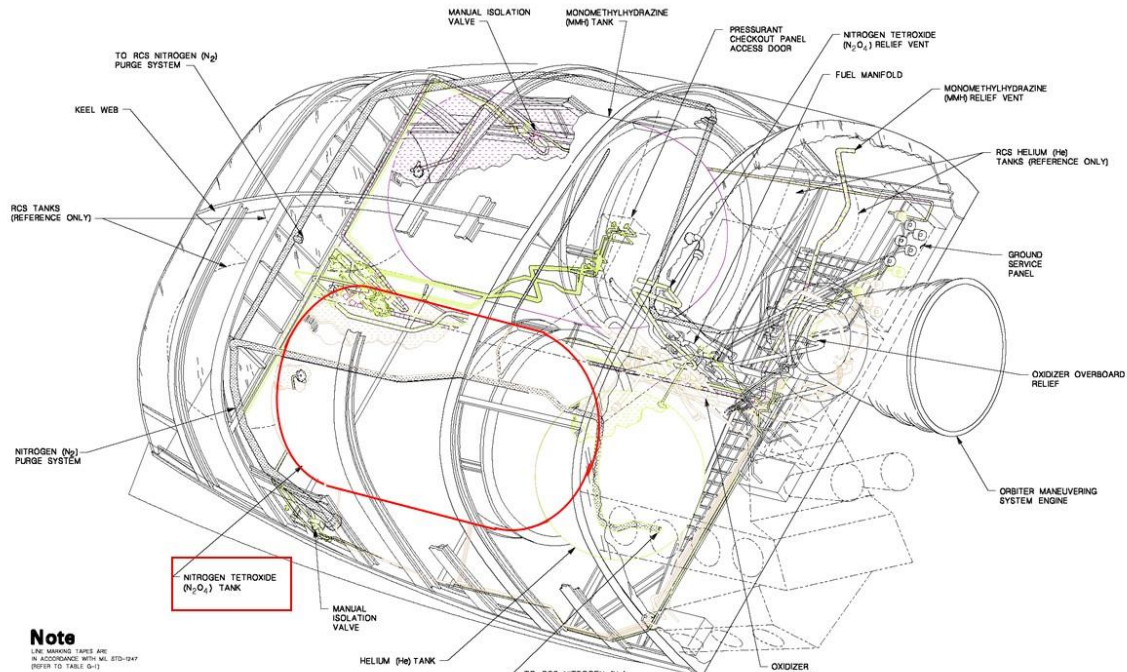


Figure 15. Space Shuttle Orbital Maneuvering System (OMS) Pod Schematic [39]

## 2.4 Summary of $N_2O_4$ and MON Progression

The need to prevent stress corrosion cracking and propellant freezing led to the widespread adoption of mixed oxides of nitrogen (MON) propellants in place of  $N_2O_4$ . For these reasons, today most NASA applications use MON rather than  $N_2O_4$ . The military specifications for MON propellant (MIL-P-27408) were updated in MIL-P-27408A in 1971 [40], and then discontinued in 1989, with future acquisition for MON being referred to MIL-P-26539D, the military specification document for nitrogen tetroxide [41]. This is the MIL-SPEC document variation that is commonly referred to today.

Figure 16 shows the progression of  $N_2O_4$  development over time, and for a variety of reasons. The progression begins in the top left corner, with pure red-brown  $N_2O_4$ . The arrows pointing downwards show that a need for freezing point reduction during the Surveyor and Sandpiper programs required large additions of NO, resulting in the usage of MON-10 and MON-25. The arrows pointing to the right show that a need for stress corrosion mitigation during the Apollo, Titan III, and Space Shuttle programs required smaller additions of NO, resulting in the usage of MON-1 and MON-3. The arrow pointing diagonally to the right and downwards shows that a need

for stress corrosion mitigation during the Minuteman III program also resulted in a controlled chloride specification.

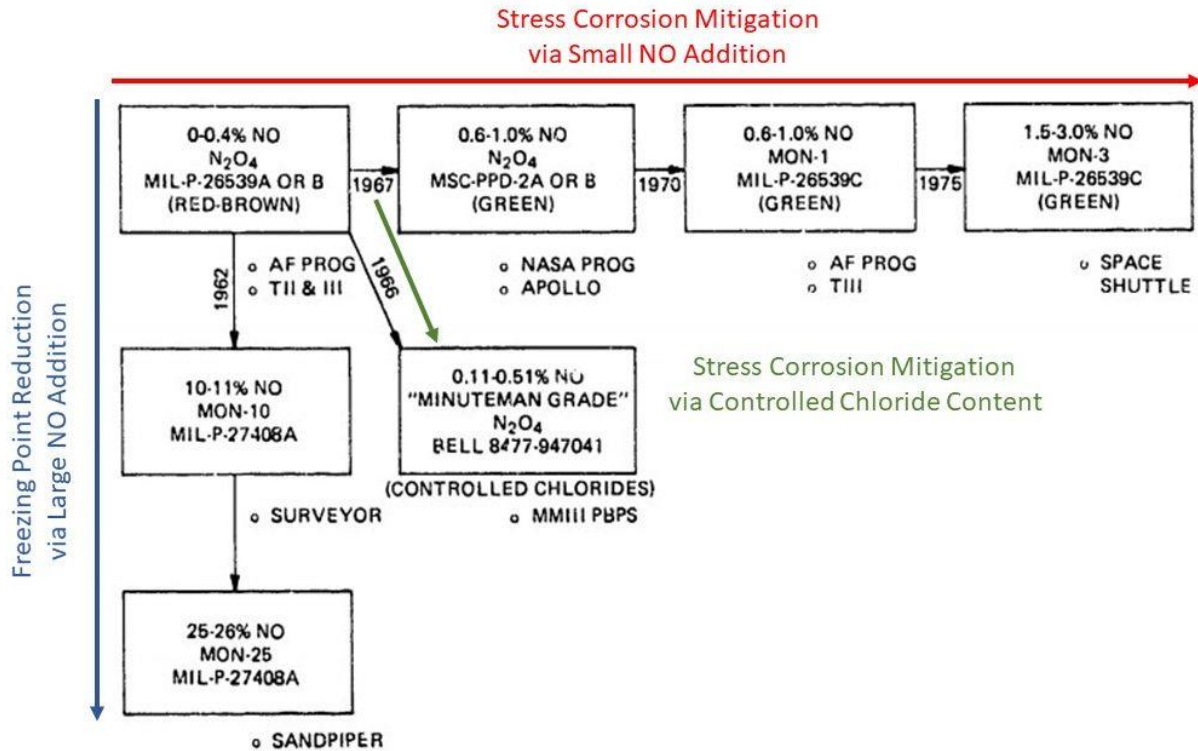


Figure 16. The History of N<sub>2</sub>O<sub>4</sub> and MON Propellants [16]

NO weight contents used by NASA range from a minimum of 1% (MON-1) to a maximum of 25% (MON-25) [7]. Figure 17 shows the military specification for common N<sub>2</sub>O<sub>4</sub> and MON Propellants. Records dating back to 1928 show that concentrations of up to 38.7% and 39.47% have been achieved at pressures of 43 atm [8], [9]. In fact, 39.47% is the highest NO weight percent possible for MON. At that concentration, all of the NO would react with all of the N<sub>2</sub>O<sub>4</sub> to create a sample of pure N<sub>2</sub>O<sub>3</sub>. Increasing the NO content during synthesis beyond 39.47% would result in unreacted NO, creating a mixture of N<sub>2</sub>O<sub>3</sub> and NO that would no longer be referred to as MON.

The chemical compositions and physical properties of N<sub>2</sub>O<sub>4</sub> and common MON propellants are listed in Figure 17, taken from the latest (as of this writing) MIL-SPEC document for N<sub>2</sub>O<sub>4</sub> (MIL-PRF-26539G w/Amendment 1, dated April 19, 2017). Notably, the Minuteman Grade, which often

existed on tables between Red-Brown  $\text{N}_2\text{O}_4$  (also known as NTO) and MON-1 during the 1970s [16], is no longer listed.

Composition	NTO (Red-Brown)	MON-1 (Green)	MON-3 (Green)	MON-10 (Green)	MON-15 (Green)	MON-25 (Green)	Test Paragraph
N <sub>2</sub> O <sub>4</sub> assay % wt, MIN	99.5	---	---	---	---	---	4.3.3
NO content %wt, MAX %wt, MIN	11	1.0 0.6	3.0 2.5	11.0 10.0	16.0 15.0	26.0 25.0	4.3.2
N <sub>2</sub> O <sub>4</sub> + NO %wt, MIN	---	99.5	99.5	99.5	99.5	99.5	4.3.3
Water equivalent %wt, MAX	0.17	0.17	0.17	0.17	0.17	0.17	4.3.4
Chloride content %wt, MAX <sup>12</sup>	0.040	0.040	0.040	0.040	0.040	0.040	4.3.5
Nonvolatile residue mg/L, MAX	---	10.0	10.0	10.0	10.0	10.0	4.3.6
Iron content ppm wt, MAX	---	0.5	0.5	0.5	0.5	0.5	4.3.7
Particulate mg/L, MAX	10.0	10.0	10.0	10.0	10.0	10.0	4.3.8
<p>NOTES</p> <p>11. The NO content shall be limited to that which does not change the specified red-brown color of the propellant (3.4)</p> <p>12. The chloride test need not be performed on any propellant type if the material was manufactured by the ammonia oxidation process</p>							

Figure 17. Chemical Composition and Physical Properties [42]

### 3. PRESENT AND FUTURE USAGE OF N<sub>2</sub>O<sub>4</sub> AND MON PROPELLANTS

Given the unique properties of N<sub>2</sub>O<sub>4</sub>, MON, and HNO<sub>3</sub>, they continue to play an important role in propulsion systems today. In fact, of the 107 liquid fuel rocket engines used for orbital launch vehicles listed on Wikipedia at the time of writing, 39 of them use (or have used) N<sub>2</sub>O<sub>4</sub>, MON, or HNO<sub>3</sub> as their oxidizer (while 64 engines have burned liquid oxygen, and 4 engines have burned other oxidizers) [43].

V · T · E		Rocket engines and solid motors for orbital launch vehicles	[hide]
Comparison of orbital rocket engines			
Liquid fuel	<b>Cryogenic (hydrolox)</b> (LH <sub>2</sub> / LOX)	China (YF-73 · YF-75 · YF-75D · YF-77) · Europe (HM7B · <i>Vinci</i> · Vulcain) · India (CE-7.5 · CE-20) · Japan (LE-5 · LE-7 · LE-9) · Russia (KVD-1 (RD-56) · RD-0120 · <i>RD-0146</i> ) · USA ( <i>BE-3U</i> · <i>BE-7</i> · J-2 · RL10 · RS-25 · RS-68)	
	<b>Cryogenic (methalox)</b> (CH <sub>4</sub> / LOX)	China ( <i>JD-1</i> · <i>TQ-11</i> · <i>TQ-12</i> ) · USA ( <i>BE-4</i> · <i>Raptor</i> ) · Europe ( <i>Prometheus</i> · Italy (with Russia) ( <i>M-10</i> ))	
	<b>Semi-cryogenic (kerolox)</b> (RP-1 / LOX)	China (YF-100 · YF-115) · India ( <i>SCE-200</i> ) · Russia (NK-15 · NK-33, 44 · RD-58 · RD-0105, 0109 · RD-0107, 0108, 0110 · RD-0110R · RD-0124 · RD-107, 108, 117, 118 · RD-120 · RD-170, 171 · RD-180 · RD-191, 151, 181 · <i>RD-193</i> · S1.5400) · Spain (TEPREL) · Ukraine (RD-8 · <i>RD-801</i> · <i>RD-810</i> ) · USA (F-1 · H-1 · Kestrel · LR-79 · LR-89 · LR-105 · LR70-NA, S-3D · Merlin · RS-27 · RS-27A · RS-56 · S-3D · Rutherford · XLR50)	
	<b>Storable (hypergolic)</b> (UDMH, UH 25, Aerozine or MMH reacting with NTO N <sub>2</sub> O <sub>4</sub> , MON or HNO <sub>3</sub> )	China (YF-1, 2, 3 · YF-20, 21, 22, 24, 25 · YF-23 · YF-40 · YF-50D) · Europe (Aestus · Astris · Vexin · Viking) · India (PS4 · Vikas) · Israel (LK-4) · North Korea (Paektusan LRE along other LREs) · Russia (17D61 · RD-0202 to 0206, 0208 to 0213 · RD-0207, 0214 · RD-0216, 0217, 0235 · RD-0233, 0234 · RD-0236 · RD-0237 · RD-0243 to 0245 · RD-0255 to 0257 · RD-215, 216 · RD-250 to 252, 261, 262 · RD-253, 275 · RD-263, 268, 273 · <i>RD-270</i> · RD-854, 861 · RD-855 · RD-856 · RD-864, 869 · S5.92 · S5.98M) · Ukraine (RD-843) · USA (AJ10 · LR-87 · LR-91 · TR-201 · XLR81*)	
	<b>Other propellants</b>	Europe (Gamma) · Russia (RD-109, 119 · RD-211 to 214) · USA (Curie · XLR81*)	
* Different versions of the engine use different propellant combinations.			
Solid fuel	China (FG-02 · FG-36 · FG-46 · FG-47 · SpaB-65 · SpaB-140C) · Europe (Mage 1 · P-4 · P-6 · PAP · P80 · P120 · P230 · Topaze · Waxwing · Zefiro 9 · Zefiro 23 · Zefiro 40) · India (S7 · S9 · S12 · S139 · S200) · Israel (LK-1 · RSA-3) · Japan (KM-V1 · KM-V2b · M-14 · M-24 · M-34 · M-34c · SRB-A) · USA (AJ-60A · Algol · Castor 30 · GEM · Orbus-6 · Orbus-21 · Orion · Space Shuttle SRB · Star 37 · Star 48 · UA120 · SRMU · X-248 · X-254)		
Engines under development are in <i>italics</i> .			

Figure 18. List of Rocket Engines for Orbital Launch Vehicles [43]

Several notable N<sub>2</sub>O<sub>4</sub>-based rocket engines in current or recent operation are listed below and organized by type. It should be noted that several engine oxidizers are publicly stated as “N<sub>2</sub>O<sub>4</sub>” or “dinitrogen tetroxide” despite them having 1%-3% NO content to prevent corrosion, and thus are technically MON-1 or MON-3. Other engine oxidizers are publicly stated as “MON” without disclosing the exact NO content. Also, this is not an exhaustive list, as there are many other N<sub>2</sub>O<sub>4</sub>-based rocket engines.

### 3.1 Reaction Control Systems (RCS) and Auxiliary Thrusters

The R-4D is a hypergolic rocket engine, originally designed by Marquardt Corporation for use as an RCS thruster on both the Apollo Service Module and the Lunar Module. Today, modern versions of the R-4D are manufactured by Aerojet Rocketdyne in the United States.[44] These engines burn  $N_2O_4$  and MMH. The R-4D variants have been used on a variety of US Navy satellites, the Japan Aerospace Exploration Agency (JAXA) H-II Transfer Vehicle (HTV) and the European Space Agency (ESA) Automated Transfer Vehicle (ATV).[45] R-4D engines will provide auxiliary thruster capability to the upcoming Orion spacecraft.[46], [47]

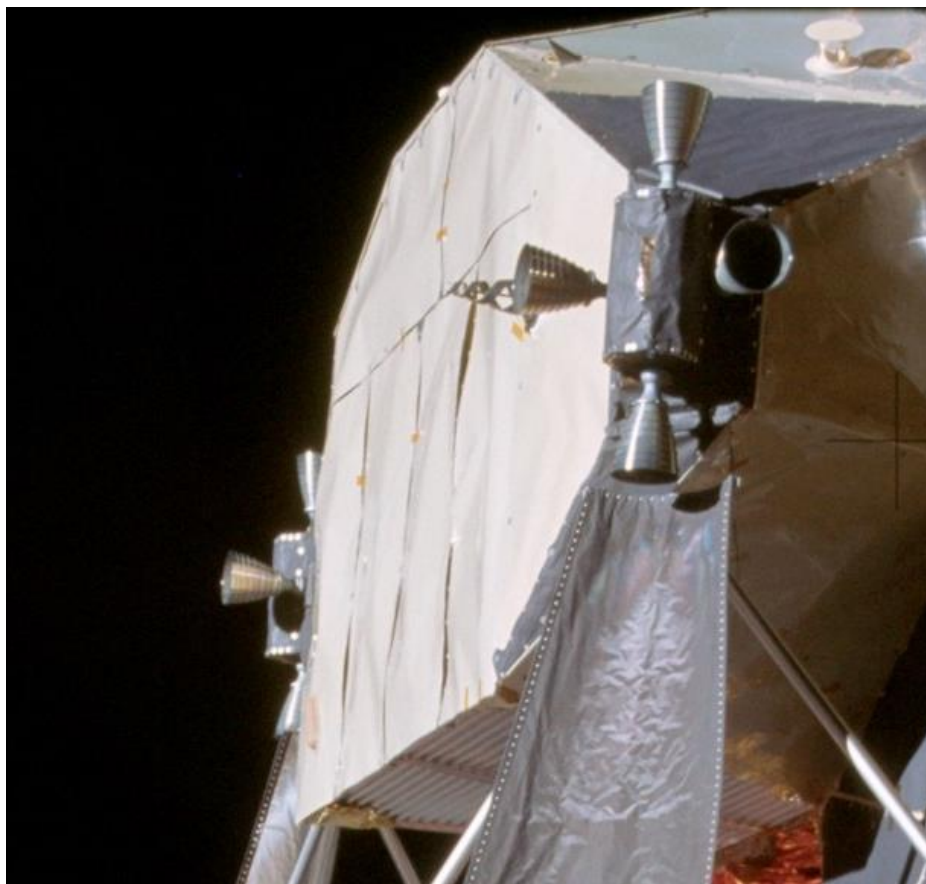


Figure 19. R-D4 Engines on Apollo Lunar Module [48]

The 200N bipropellant thruster is a hypergolic rocket engine manufactured by ArianeGroup in Europe. This engine is qualified to burn MON-3 and MMH, and has demonstrated the ability to burn  $N_2O_4$  and unsymmetrical dimethylhydrazine (UDMH).[49] The 200N was used on the system

bus section of ESA's Automated Transfer Vehicle (ATV), providing attitude control and braking capability.[50] More recently, the 200N has been selected for the RCS of the upcoming Orion European Service Module.[47], [49]

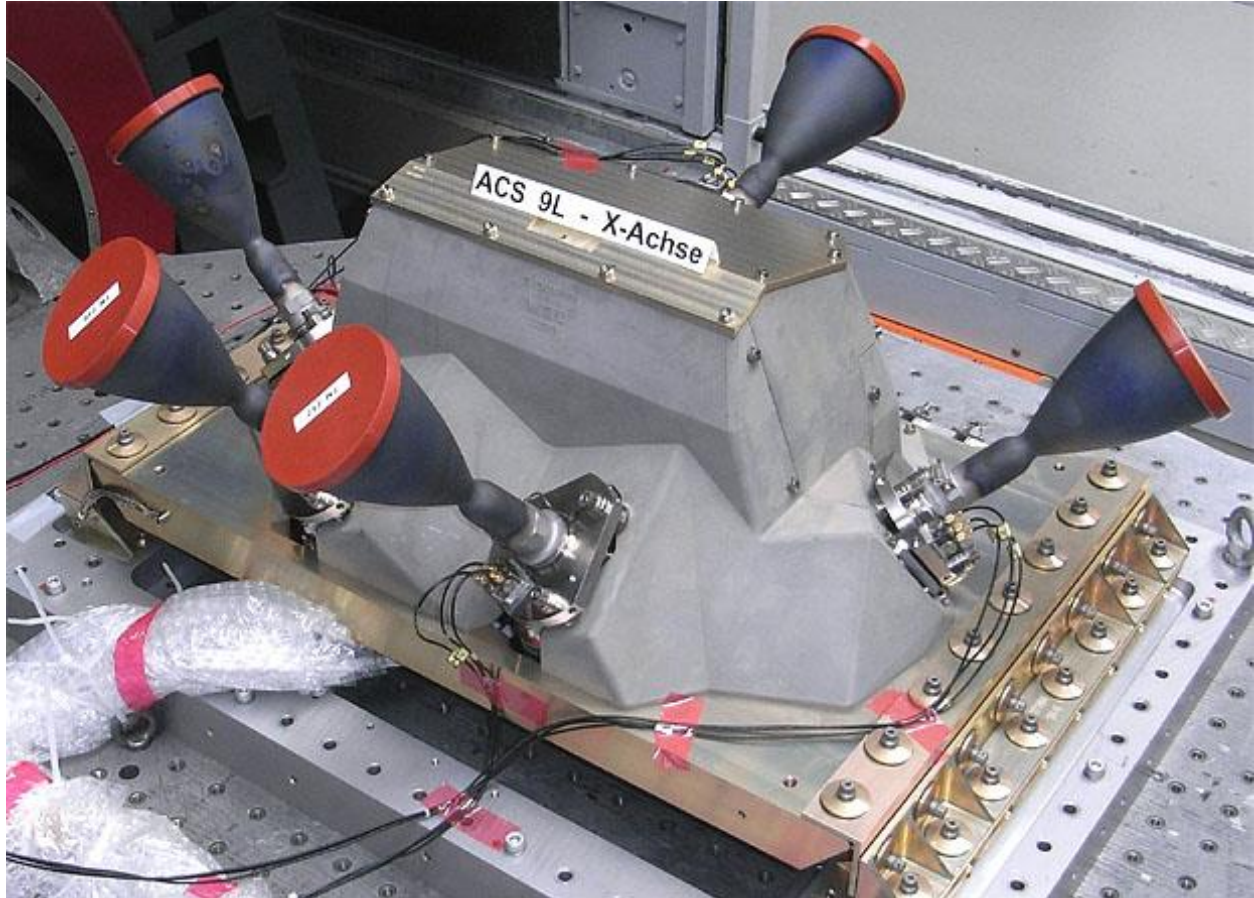


Figure 20. 200N Aft Thruster Cluster for ATV [49]

Draco is a hypergolic rocket engine manufactured by SpaceX in the United States. This engine burns  $N_2O_4$  and MMH. Sixteen Draco engines provide RCS capability for the Dragon 1 and Dragon 2 spacecraft, including both Dragon 2 variants: the currently-operating Cargo Dragon and Crew Dragon [51]. As of the current writing, there have been twenty-three successful Dragon launches out of twenty-four attempts [52].



Figure 21. Draco Engine Nozzles on Dragon Qualification Unit [53]

### 3.2 Abort Engines

SuperDraco is a hypergolic rocket engine manufactured by SpaceX in the United States. This engine burns  $N_2O_4$  and MMH. Eight Draco engines are used on the launch escape system of the Crew Dragon, which can propel the Dragon spacecraft half a mile away from the launch vehicle in less than eight seconds. Despite the similarity in name, the SuperDraco can exert 73 kN of thrust, which is nearly 200 times more than the 400 N of thrust of the Draco [51].



Figure 22. SuperDraco Engines firing during Crew Dragon Tests [54]

### 3.3 Liquid Apogee Engines (LAE) and In-Space Primary Propulsion

The AJ10 is a hypergolic rocket engine family manufactured by Aerojet Rocketdyne in the United States. These engines burn  $N_2O_4$  and Aerozine. Variants of the AJ10 were used to propel the upper stages of several launch vehicles, including the Delta II and the Titan III. The AJ10 was also used in the main propulsion system of spacecraft such as the Apollo command and service module (CSM) and the Space Shuttle orbiter. For the Apollo CSM, the AJ10 was used in its service propulsion system (SPS), which placed the spacecraft into and out of lunar orbit and performed corrections. For the Space Shuttle orbiter, two AJ10 engines were used to perform orbital injection, corrections, and deorbit burns [55]. Today, a single AJ10 is planned to be used on the upcoming Orion spacecraft's European Service Module (ESM), to perform orbital transfers [56], [57]. However, the AJ10 will only be utilized for the first five or so Orion missions, and NASA is seeking bids to develop a new engine with more modern levels of performance [58].

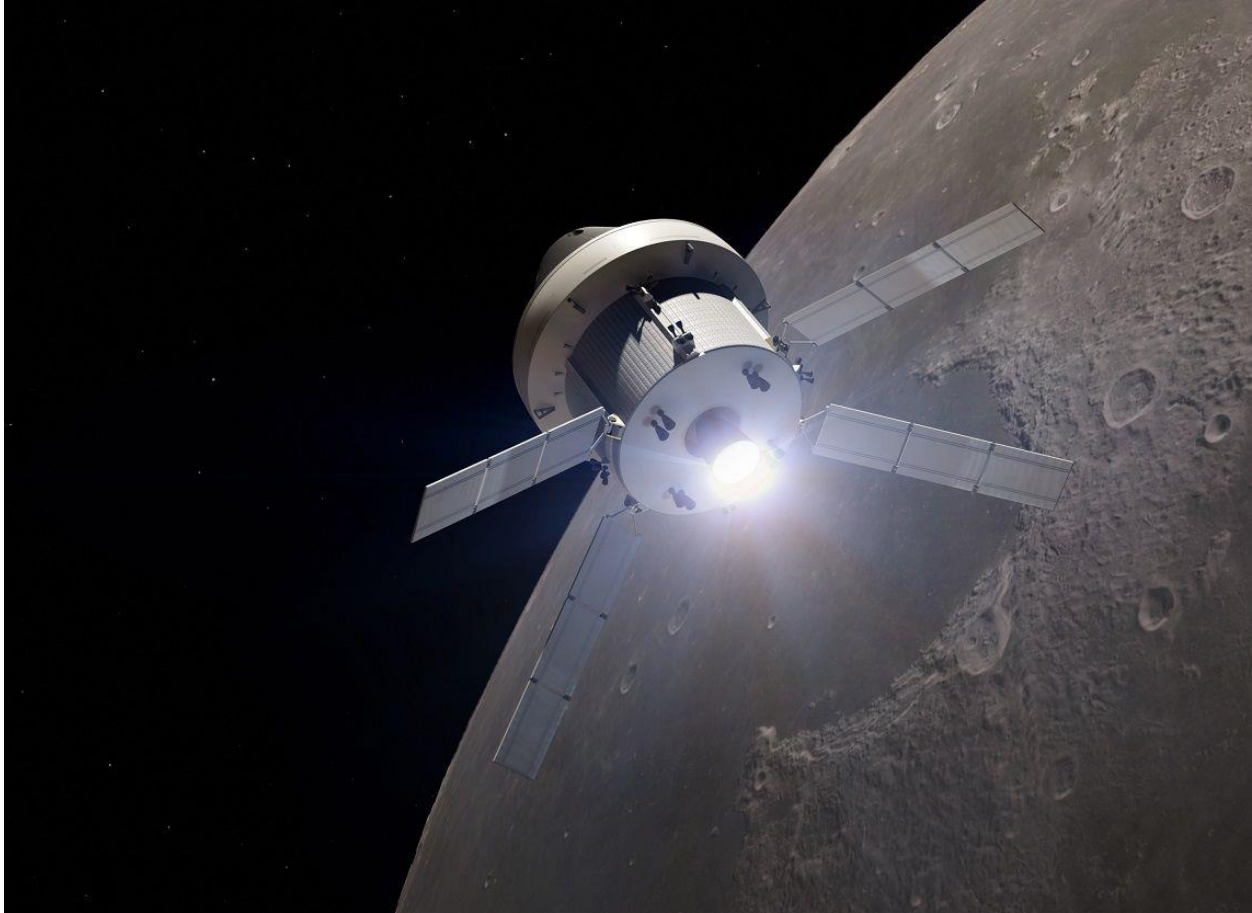


Figure 23. Artist's Rendering of AJ10 Engine firing on Orion at Earth's Moon [59]

The KTDU-80 is an integrated propulsion system manufactured by the A.M. Isayev Chemical Engineering Design Bureau in Russia. This propulsion system burns  $N_2O_4$  and UDMH. The KTDU-80 integrates three different engines: the S5.80 for the main propulsion system, the 11D428 for the RCS, and the S5.142 for attitude control, all of which are fed with a common supply of pressurized propellant [60]. The KTDU-80 first flew on the Soyuz-TM in 1986, and its variants have been incorporated into all of the Soyuz spacecraft since then (the Soyuz-TMA, Soyuz TMA-M, and the Soyuz MS) [61], [62]. Its predecessor system, the KTDU-426, also used three different engines that were fed by a common supply of  $N_2O_4$  and UDMH [63]. These integrated propulsion systems had several key advantages. First, they allowed for the RCS to be used as backup of the main propulsion system, removing the need for a separate backup thruster. Second, these integrated systems implemented more extensive redundancy while keeping the mass down. Third,

all propellant reserves could be consolidated and shared amongst the three types of thrusters, reducing mass further [63].

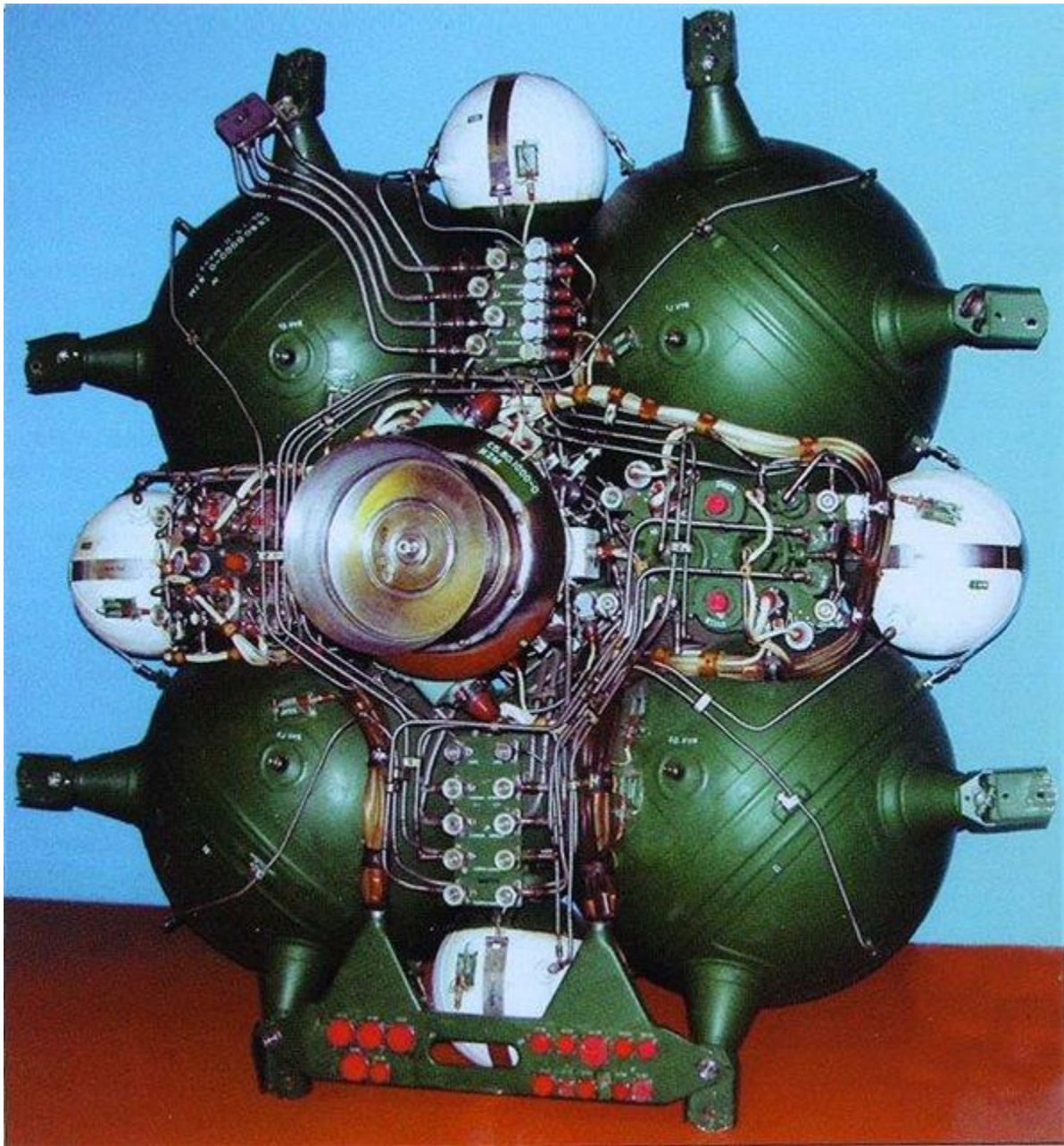


Figure 24. KTDU-80 Base Set of the Soyuz TM [64]

The BT-4 is a hypergolic rocket engine family manufactured by IHI Aerospace in Japan. These engines typically burn various combinations of  $N_2O_4$ /MON-3 and hydrazine/MMH.[65] The BT-4 is used as a liquid apogee engine for geostationary communications satellites, as the orbital maneuvering engine on the Cygnus spacecraft and the H-II transfer vehicle (HTV), and as a thruster on the Antares Bi-propellant Third Stage (BTS).[66]–[68] In 2010, the BT-4 achieved its 100th-unit foreign engine export since it started selling abroad in 1999.[69]



Figure 25. Docking of Cygnus Spacecraft at the International Space Station with BT-4 Nozzle Visible [70]

LEROS is a family of hypergolic rocket engines manufactured by Nammo [71] in the United Kingdom. These engines burn MON and either hydrazine or MMH. LEROS engines are used as primary apogee engines for telecommunications satellites as well as deep space missions. The family (Figure 26) includes LEROS 1b, LEROS 1c, LEROS 2b, and LEROS 4. NASA missions that used LEROS engines include NEAR Shoemaker, Mars Global Surveyor, MESSENGER, and

Juno. Other spacecraft that used the LEROS include GEO 1 and GEO 2 of the Space-Based Infrared System (SBIRS) for the United States Space Force, and the Beresheet lunar lander built by Israel's SpaceIL. As of 2011, more than 70 LEROS 1 series engines had been flown successfully [72].



Figure 26. Artist's Rendering of LEROS 1b Engine firing on Juno at Jupiter [73]

The S400 is a family of hypergolic rocket engines manufactured by ArianeGroup in Europe. These engines burn MON and MMH. The S400 engines are used as primary apogee engines for telecommunication satellites and deep space missions. The family includes S400-12 and S400-15. Notable ESA missions that used the S400 include Venus Express, ExoMars Trace Gas Orbiter (TGO), and Jupiter Icy Moons Explorer (JUICE). The S400 engines have consistently won several contracts per year since 1989 [74].

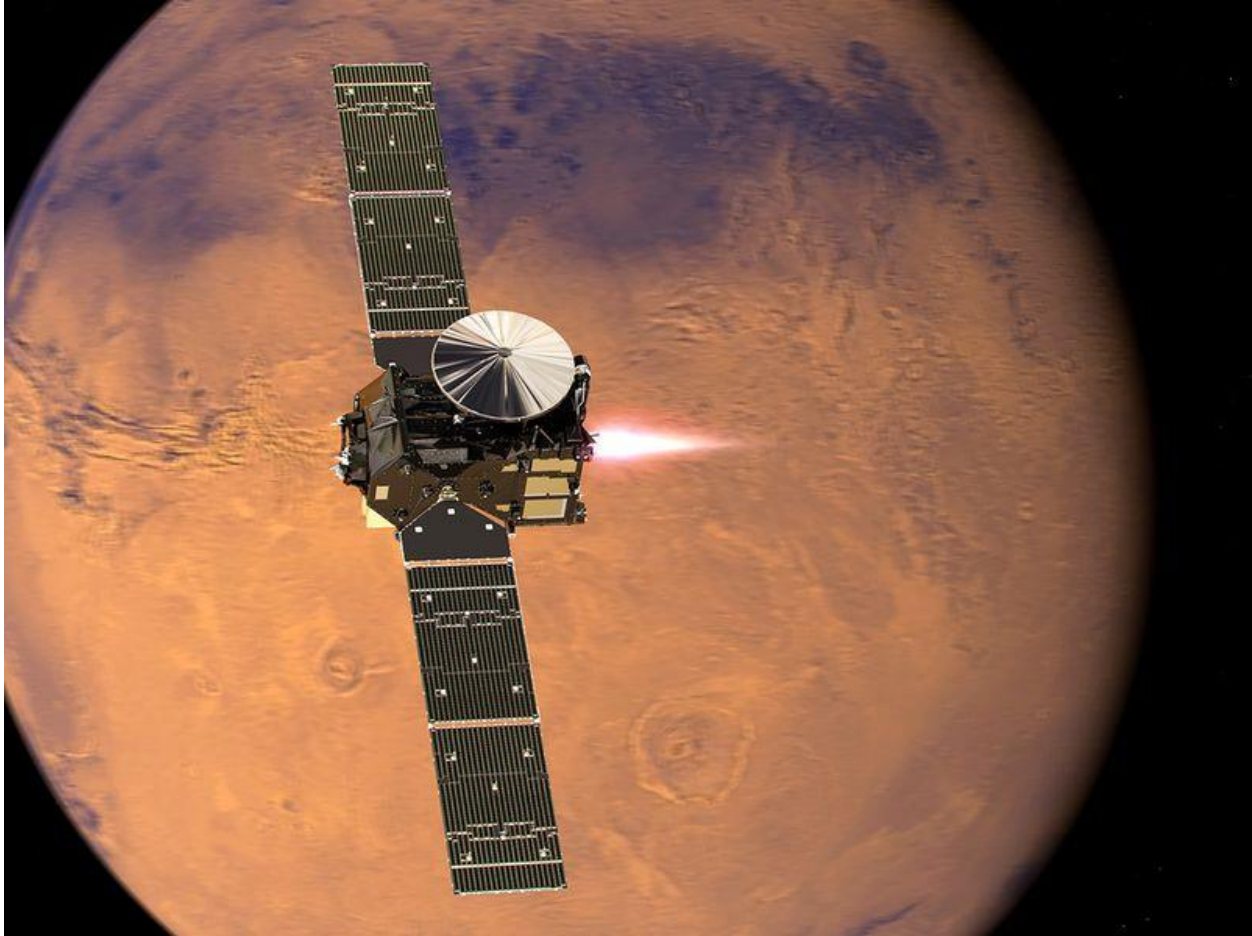


Figure 27. Artist's Rendering of S400 Engine firing on the Trace Gas Orbiter at Mars[75]

### **3.4 Launch Vehicle and Missile Stages**

The S5.92 is a hypergolic rocket engine manufactured by the A.M. Isayev Chemical Engineering Design Bureau (also known as KB KhimMash) in Russia. This engine burns  $N_2O_4$  and UDMH. The S5.92 is currently used on Fregat, the upper stage of the Soyuz and Zenit launch vehicles. After its latest launch on April 25, 2021, the success rate of Fregat was 97.8% (87 successful launches and 2 failures). Fregat has successfully delivered more than 300 payloads to space and is the only upper stage in the world that can place its payload into 3 or more different orbits in a single launch [76].

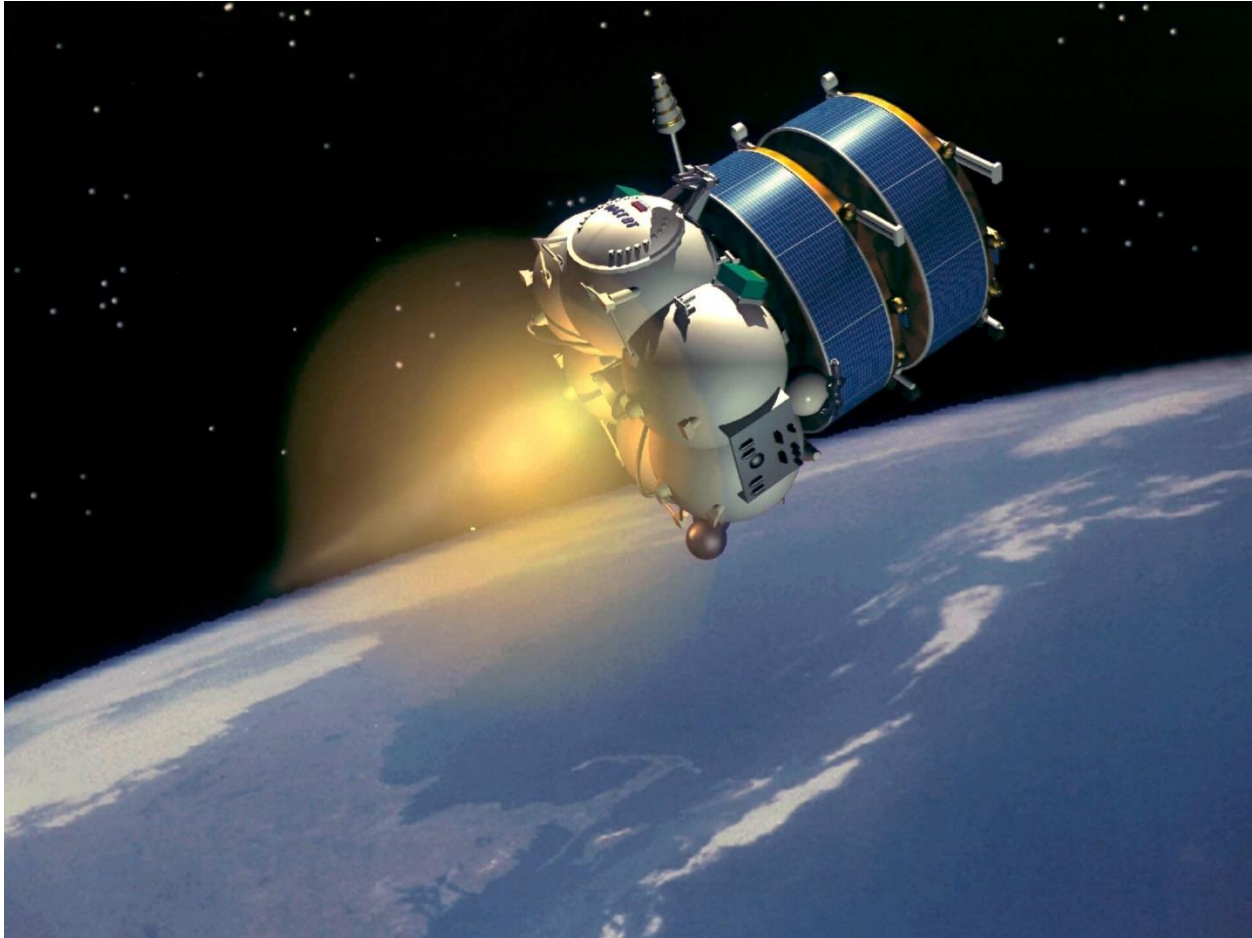


Figure 28. Artist's Rendering of S5.92 Engine firing on Fregat Upper Stage [77]

Proton is an expendable launch system manufactured at the Khrunichev State Research and Production Space Center factory and Chemical Automatics Design Bureau in Russia. The first, second, and third stages burn  $N_2O_4$  and UDMH (while the fourth stage burns liquid oxygen and RP-1).[78] Proton was initially intended as a "super heavy ICBM", but was hugely oversized for that purpose and was eventually converted into a space launch vehicle.[79] Proton launched the first uncrewed Soviet circumlunar flights in the 1960's, and was intended to launch the crewed Soviet circumlunar flights until that program was cancelled in light of the successful Apollo 8 mission.[80] Proton launched the Salyut space stations, the Mir core segment and expansion modules, and both the Zarya and Zvezda modules of the ISS.[78] Proton continued to launch commercial satellites until 2019, and continues to launch numerous Roscosmos and Russian

government payloads, with missions scheduled into 2023.[81] However, the Proton is intended to be phased out and eventually replaced by the Angara launch system, to avoid dealing with the highly toxic UDMH and  $N_2O_4$ . [82]



Figure 29. Proton First Stage firing during Launch [83]

It is important to note that the trend for large rocket engines among western space launch agencies has been away from hypergolic propellants (such as  $N_2O_4$ ) and towards non-hypergolic, cryogenic or semi-cryogenic propellants. These propellant combinations are usually liquid oxygen (LOX) as the oxidizer with either hydrogen ( $LH_2$ ), methane ( $CH_4$ ) or RP-1 as the fuel. Despite the need for cryogenic storage and propellant-loading right before launch, these non-hypergolic propellants yield higher performance than their hypergolic counterparts, and do not involve the risks of handling toxic chemicals.

Examples of this include the Ariane and Titan rocket families.

Ariane 1 through 4 used hypergolic propellants in their first and second stages, all of which burned  $N_2O_4$ . These earlier Ariane versions have since been retired and replaced by Ariane 5, which substituted the two hypergolic lower stages of the previous designs with a single  $LH_2/LOX$  core stage.[84] Ariane 6, which is currently in development and scheduled to replace Ariane 5, employs two stages that burn  $LH_2$  and  $LOX$ . [85]

Likewise, Titan II, III, and IV used hypergolic propellants in their first and second stages, all of which burned  $N_2O_4$ . The Titan II ICBM was eventually replaced by the LGM-30 Minuteman missile, which had three solid-fuel stages.[86] Most of the decommissioned Titan II ICBMs were refurbished and used for Air Force space launch vehicles.[87] The Titan II and Titan III launch vehicles were eventually phased out and replaced by the Atlas rocket family and the Delta IV.[88] The Atlas V and the Delta IV Heavy are still in operation today, and both employ first and second stages that burn  $LOX$  as their oxidizers.[89], [90]

Despite the lack of hypergolic propellants in large rockets, they are still used in upper stages when multiple burn-coast periods are required, and in launch escape systems such as the SpaceX Crew Dragon. Hypergolic propellants also continue to play a major role in RCS, liquid apogee engines, and in-space primary propulsion systems.

### **3.5 Future Plans involving $N_2O_4$ and MON Propellants**

It is no coincidence that  $N_2O_4$  and MON, oxidizers with deep roots in lunar lander history, continue to sit on the forefront of lunar exploration today. Some of the more notable future missions involving  $N_2O_4$ -based oxidizers are those of Astrobotic Technology, an American private company that develops space robotics technology for lunar and planetary missions.

#### **3.5.1 Mission One**

Mission One is Astrobotic's first lunar lander mission, in which their Peregrine lander (Figure 30) will deliver payloads to the lunar surface. Peregrine's propulsion system features five thrusters manufactured by Frontier Aerospace in America. These hypergolic rocket engines burn MON-25 and MMH, and would conduct the trans-lunar injection, trajectory corrections, lunar orbit

insertion, and powered soft-landing descent.[91], [92] For attitude control, the spacecraft uses twelve thruster that also burn MON-25 and MMH.[92]

In July 2021, the United Launch Alliance (ULA) is expected to launch Astrobotic's Peregrine aboard a Vulcan Centaur launch vehicle.[93] The Peregrine lander will carry 14 commercial payloads and 14 NASA-sponsored payloads (a \$79.5 million NASA contract)[94], for a total of 28 payloads.[95] These payloads include lunar rovers, instruments, and time capsules.[96] Peregrine will carry a maximum payload mass of 90 kg (200 lb) during Mission One.[97]

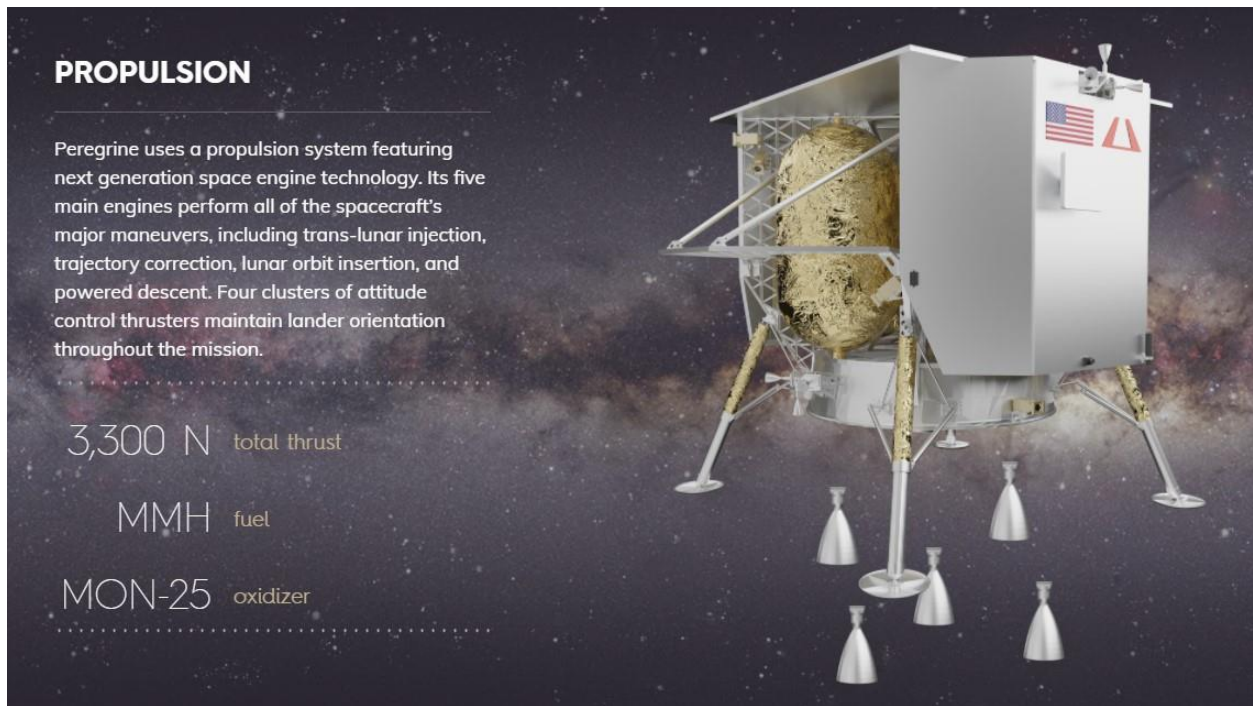


Figure 30. Astrobotic Peregrine Lander [98]

### 3.5.2 Mission Two

In 2019, Astrobotic and Carnegie Mellon University were awarded a \$5.6 million NASA contract to develop an autonomous lunar rover, which will land on the moon in 2022.[99] The rover, called MoonRanger, will land via Masten Space System's XL1 lander.[100] This lander (Figure 31) will burn Masten Space System's MXP-351, a 'green' hypergolic propellant combination that is both non-toxic and storable at room temperature.[101] Although it is unknown whether the oxidizer is N<sub>2</sub>O<sub>4</sub>-based, Mission Two has been included in this list for reference and completeness.

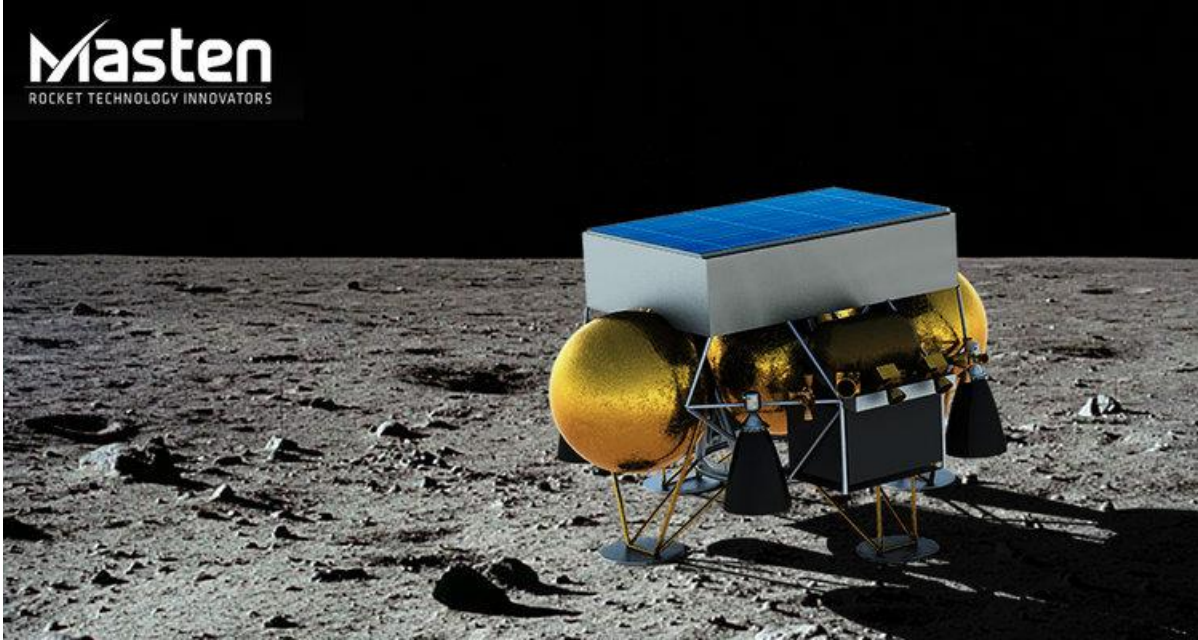


Figure 31. Masten XL1 [102]

### 3.5.3 Mission Three

For Astrobotic's third lunar lander mission, their Griffin lander (Figure 32) will deliver NASA's Volatiles Investigating Polar Exploration Rover (VIPER) rover to the lunar surface in 2023 (a \$199.5 million NASA contract).[103] Griffin's propulsion system features five F500E engines manufactured by Frontier Aerospace, and twelve altitude control thrusters manufactured by Agile Space Industries.[104] While Peregrine is planned to have a maximum surface payload of 100 kg, Griffin would have a surface payload of 500 kg.[97] Although an early description of the Griffin lander on the Astrobotic's website stated that it used MON-3 as an oxidizer[105], that figure has since been changed, with no oxidizer specified.[106]

## PROPULSION

Griffin uses a propulsion system featuring next generation space engine technology. Its seven main engines perform all of the spacecraft's major maneuvers, including trans-lunar injection, trajectory correction, lunar orbit insertion, and powered descent. Four clusters of attitude control thrusters maintain lander orientation throughout the mission.



Figure 32. Astrobotic Griffin Lander [106]

## 4. MON SYNTHESIS

In the last few decades, MON have seen less usage in large launch vehicles and missiles, and more usage in propulsion systems which involve minute burns of propellant to conduct delicate maneuvers. More accuracy regarding propellant physical properties, and how they relate to NO content, is required to ensure that the intended maneuvers match the outcomes during live missions.

In order to accurately document the physical properties of a MON sample, it is vitally important to know its precise MON composition (NO content by weight during synthesis). Teams of students at Purdue University were able to measure MON composition by designing and building a test stand that can synthesize MON samples and then perform the  $N_2O_3$  oxidation method for MON composition analysis. The follow chapter lays the foundation for that work, and explains the resulting test stand.

### 4.1 Synthesis Test Stand and Procedure

A group of students at Purdue University, under the guidance of Professor Pourpoint, devised a test stand and procedure for MON synthesis as well as MON composition determination.

The project had several main objectives:

1. Create MON-X by mixing liquid  $N_2O_4$  with gaseous NO
2. Determine the MON composition of a sample to within  $\pm 0.1$  weight % NO
3. Measure the vapor pressure of MON-X at varying temperatures
4. Allow for gas and liquid withdrawal of MON-X

Some key requirements were that the test stand must fit in a specified fume hood, produce results with error in measurement of less than 0.5%, be relatively cost effective, and have a low lead time.

A schematic (Figure 33) shows that the MON synthesis test stand generally consists of a synthesis chamber, an  $NO_2$  tank, an NO tank, an oxygen tank, a nitrogen source, and a water tank connected to a fume hood vent. The red lines are designated for  $NO_2$  and  $N_2O_4$ , blue lines are designated for

NO, green lines are designated for MON (i.e. any combination of NO<sub>2</sub>, N<sub>2</sub>O<sub>4</sub>, N<sub>2</sub>O<sub>3</sub>, and NO), and purple lines are designated for nitrogen. The schematic also shows where key pressure transducers (labeled PT) and thermocouples (labeled TC) are located, to monitor the pressure and temperature for safety reasons and to enable the calculation of the mass of gases via the ideal gas law. A glass beaker was placed around the synthesis chamber and filled with ice and water, to maintain a temperature of roughly 0°C in order to liquify the gases inside the synthesis chamber. That glass beaker was placed on top of a stir plate, which rotated a stir bar placed inside the synthesis chamber, to promote homogenous mixing and expedite the synthesis and oxidation process. The constructed test stand is shown in Figure 34, without the beaker of ice. The synthesis chamber is filled with gaseous N<sub>2</sub>O<sub>4</sub> and NO<sub>2</sub>.

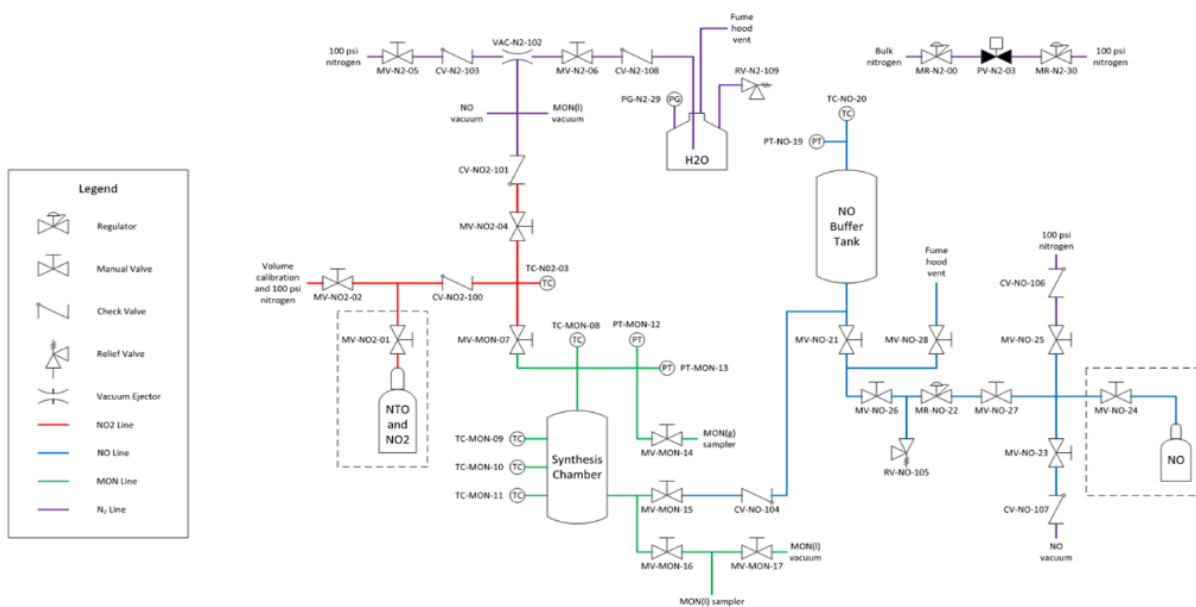


Figure 33. Schematic of MON Synthesis Test Stand

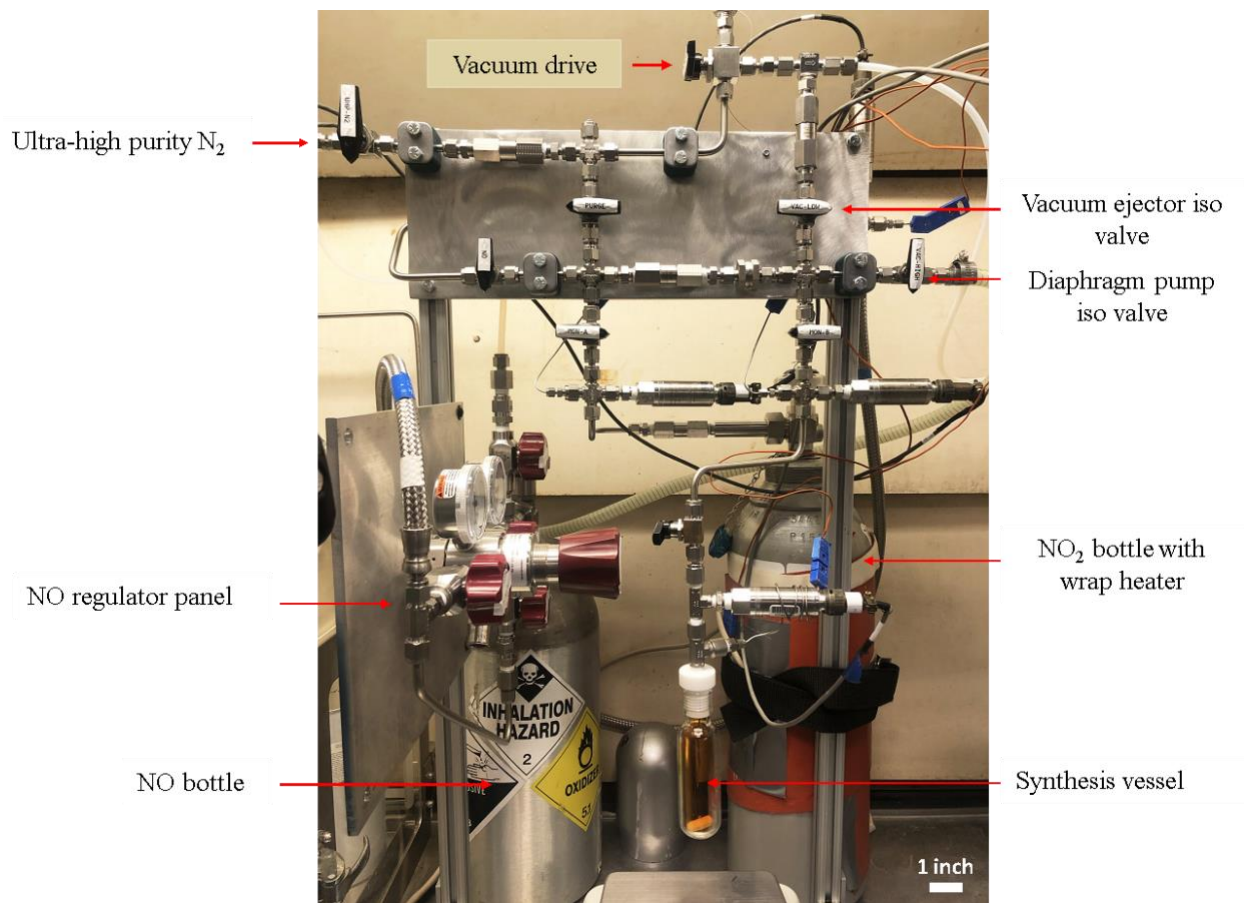


Figure 34. Small-scale MON synthesis stand at the Zucrow Laboratories

Figure 35 shows a sample of MON-5 after synthesis. The sample is a dark green color, characteristic of MON. The headspace is filled with gaseous  $N_2O_4$  and  $NO_2$ , hence the reddish brown hue. The beaker of ice and water ensures that the sample stays in the liquid phase.



Figure 35. A Sample of Synthesized MON-5

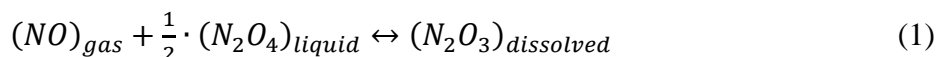
The general structure of the MON synthesis procedure is as follows:

First, the test stand is prepared by purging the necessary lines with nitrogen, NO, and then NO<sub>2</sub>. This is to ensure that there are no contaminants or unwanted gas in the lines prior to synthesis. The lines are filled with nominal amounts of the gases intended for them. The synthesis chamber is also weighed on a scale.

Next, gaseous NO<sub>2</sub> is added to the synthesis chamber. Due to the low temperature (roughly 0°C) caused by the presence of ice-water surrounding the synthesis chamber, the gaseous NO<sub>2</sub> will condense into an reddish-brown liquid mixture of NO<sub>2</sub> and N<sub>2</sub>O<sub>4</sub>. Then the synthesis chamber is

removed and weighed again. The difference between the first and second mass measurements of the synthesis chamber determines the mass of the NO<sub>2</sub> that was added to the synthesis chamber.

Next, gaseous NO is added to the chamber. The mass of NO added is initially estimated by using the synthesis chamber's temperature measurement, pressure measurement, known volume, and the ideal gas law. A stir bar placed at the bottom of the synthesis chamber is rotated for several minutes, promoting the gaseous NO to react with some of the liquid N<sub>2</sub>O<sub>4</sub> to create the blue liquid N<sub>2</sub>O<sub>3</sub>, via the stoichiometric equation below.



The blue N<sub>2</sub>O<sub>3</sub> mixes with the remaining reddish N<sub>2</sub>O<sub>4</sub> to create the characteristic dark green color associated with liquid MON. This continues until the calculated mass of NO added reaches the desired amount predetermined for that trial, at which point the MON has been fully synthesized. Finally, the lines are vented, a vacuum is pulled on the stand, and the system is purged with nitrogen. The synthesis chamber is then removed from the test stand and weighed on a scale. The difference between the second and third mass measurements of the synthesis chamber determines the actual mass of the NO that was added to the synthesis chamber (the ideal gas method is only used as a mid-procedure estimate, whereas the scale method is the final verdict of how much NO is added).

#### 4.2 Determining MON Composition via The N<sub>2</sub>O<sub>3</sub> Oxidation Method

MIL-PRF-26539G [1] is the Department of Defense performance specification for all types of dinitrogen tetroxide propellants. This document describes two methods used to determine the nitric oxide (NO) content in samples of mixed oxides of nitrogen (MON). One of these methods, which will be referred to as the N<sub>2</sub>O<sub>3</sub> oxidation method, consists of oxidizing the NO and dinitrogen trioxide (N<sub>2</sub>O<sub>3</sub>) to determine their amounts.

The N<sub>2</sub>O<sub>3</sub> oxidation method first requires that the MON sample and vessel are weighed. Then, oxygen is added to the sample vessel at 30 psi. The oxygen reacts with the N<sub>2</sub>O<sub>3</sub> and NO in the MON to create N<sub>2</sub>O<sub>4</sub>, via the stoichiometric equation below:



Once all the  $N_2O_3$  and  $NO$  have reacted, the sample vessel will not receive any more oxygen, stopping the incoming flow. A rotameter is used to determine whether the oxygen flow has stopped, at which point the reaction is complete. The liquid in the sample vessel is now fully  $N_2O_4$ , with minute amounts of dissolved oxygen. Thus, it has returned to a reddish-brown color.

The sample and vessel are weighed again, and the difference between the new mass and the previous mass is the mass of oxygen added to the vessel. The more oxygen that was added to the  $MON$  sample, the higher its  $N_2O_3$  and  $NO$  content had been, and thus the more  $NO$  was used to synthesize the  $MON$ .

The added oxygen mass can be used to calculate the original  $NO$  content of the  $MON$  sample via the following equation, which will be referred to as the MIL-SPEC equation:

$$NO, wt \% = \frac{[y - 0.003857(z - \frac{x+y}{1.49})]187.5}{x} - 0.15 \quad (4)$$

$x$  is the  $MON$  sample mass in grams,  $y$  is the mass of the oxygen added in grams, and  $z$  is the volume of the sample volume in milliliters.

Figure 36 shows the progression of the oxidation process with timestamps. At 0 minutes, the sample is  $MON-5.06$ . Note that the liquid is an opaque dark bluish green. As time progresses, oxygen reacts with the blue  $N_2O_3$  until it has all been consumed, leaving only reddish brown  $N_2O_4$  and trace amounts of oxygen. Note that the liquid is now translucent, and the stir bar is visible. This aligns with other experiments which have shown that  $N_2O_4$  is a translucent reddish brown at  $0^\circ C$ . [107]

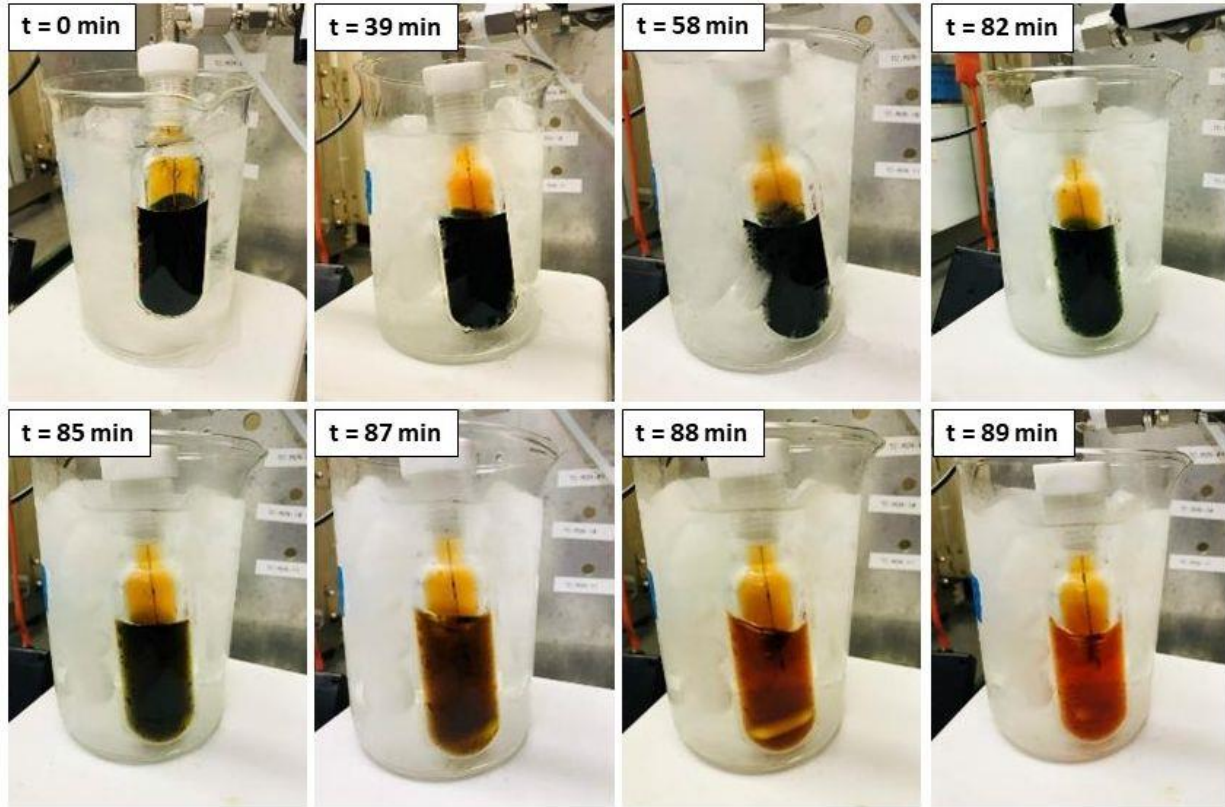


Figure 36. Oxidation Progression from MON to  $N_2O_4$

### 4.3 Water Contamination

The NO content in the MON samples can be measured in two different ways:

1. Scale Measurement Method: The mass of the synthesis chamber is measured before and after the addition of  $NO_2$ , and before and after the addition of NO. The difference between the measurements provides the masses of the  $NO_2$  ( $m_{NO_2}$ ) and NO ( $m_{NO}$ ) added. Then the NO content ( $NO$  wt. %) can be calculated via the equation below:

$$NO \text{ wt. \%} = \frac{m_{NO}}{m_{NO} + m_{NO_2}} \cdot 100\% \quad (5)$$

2. The  $N_2O_3$  Oxidation Method; The mass of the synthesis chamber is measured before and after the addition of oxygen. The difference between the measurements provides the mass of the oxygen ( $y$ ) added. Then the NO content can be calculated via the equation below:

$$NO \text{ wt. \%} = \frac{[y - 0.003857(z - \frac{x+y}{1.49})]187.5}{x} - 0.15 \quad (6)$$

$x$  is the MON sample mass in grams,  $y$  is the mass of the oxygen added in grams, and  $z$  is the volume of the sample volume in milliliters.

After several tests, a pattern emerged in which the  $N_2O_3$  oxidation method consistently produced a larger NO content than the scale measurement method. In Test #5, no amount of NO was added to the  $N_2O_4$ , and the  $N_2O_3$  oxidation method was conducted on pure  $N_2O_4$  (i.e. MON-0). Even that test found that there was 1.79% NO in the sample, signifying that something was crucially wrong with the implementation of the  $N_2O_3$  oxidation method. The relevant data is shown in Table 1.

Table 1. MON Synthesis and NO Content Data

Test #	NO Content			Error
	Target	Scale Measurement Method	$N_2O_3$ Oxidation Method	
4	5.00%	5.28%	5.78%	9.43%
5	0.00%	0.00%	1.33%	N/A
6	5.00%	4.74%	5.17%	9.04%

As a result of the data above, an effort was made to determine how the NO content measurements could have been skewed. The possibility of water contamination was then thoroughly investigated. If water were present in the system, it would react with  $NO_2$  to create nitric acid ( $HNO_3$ ) and NO, via the following stoichiometric equation:



The created NO would cause a higher NO content measurement during the N<sub>2</sub>O<sub>3</sub> oxidation method, relative to the scale measurement method, which would be unaffected by the presence of trace amounts of water.

The first step in understanding the NO content measurement discrepancies was to analytically calculate the potential mass of water in the system. Based on the stoichiometric equation above, there is a 3-to-1 ratio between the moles of NO<sub>2</sub> consumed during this reaction ( $n_{NO_2,cons}$ ) and the moles of water (H<sub>2</sub>O) in the system ( $n_{H_2O}$ ). There is a 2-to-1 ratio between the moles of HNO<sub>3</sub> produced by the reaction ( $n_{HNO_3}$ ) and the moles of water in the system ( $n_{H_2O}$ ). There is also a 1-to-1 ratio between the moles of NO produced by the reaction ( $n_{NO,prod}$ ) and the moles of water in the system ( $n_{H_2O}$ ). These relationships can be expressed in molar form:

$$n_{NO_2,cons} = 3 \cdot n_{H_2O} \quad (8)$$

$$n_{HNO_3} = 2 \cdot n_{H_2O} \quad (9)$$

$$n_{NO,prod} = n_{H_2O} \quad (10)$$

Next, by using the molecular weights of the molecules, the relationship between the masses and number of moles of the components can be identified:

$$m_{NO_2,cons} = n_{NO_2,cons} \left( 46 \frac{g}{mol} \right) \quad (11)$$

$$m_{HNO_3} = n_{HNO_3} \left( 63 \frac{g}{mol} \right) \quad (12)$$

$$m_{NO,prod} = n_{NO,prod} \left( 30 \frac{g}{mol} \right) \quad (13)$$

$$m_{H_2O} = n_{H_2O} \left( 18 \frac{g}{mol} \right) \quad (14)$$

By substituting Equations (8), (9), and (10) into Equations (11), (12), and (13) respectively, one can express the mass of the NO<sub>2</sub> consumed ( $m_{NO_2,cons}$ ), the mass of the HNO<sub>3</sub> produced ( $m_{HNO_3}$ ), and the mass of the NO produced ( $m_{NO,prod}$ ) as functions of the number of moles of water in the system ( $n_{H_2O}$ ), which can then be expressed as functions of the mass of the water in the system ( $m_{H_2O}$ ) by using the relationship in Equation (14):

$$m_{NO_2,cons} = 3 \cdot n_{H_2O} \left(46 \frac{g}{mol}\right) = 3 \cdot \left(\frac{m_{H_2O}}{18 \frac{g}{mol}}\right) \left(46 \frac{g}{mol}\right) = 7.667 \cdot m_{H_2O} \quad (15)$$

$$m_{HNO_3} = 2 \cdot n_{H_2O} \left(63 \frac{g}{mol}\right) = 2 \cdot \left(\frac{m_{H_2O}}{18 \frac{g}{mol}}\right) \left(63 \frac{g}{mol}\right) = 7 \cdot m_{H_2O} \quad (16)$$

$$m_{NO,prod} = n_{H_2O} \left(30 \frac{g}{mol}\right) = \left(\frac{m_{H_2O}}{18 \frac{g}{mol}}\right) \left(30 \frac{g}{mol}\right) = 1.667 \cdot m_{H_2O} \quad (17)$$

Next, it is important to specify the quantitative difference between the expected NO content and the measured NO content.

The expected NO content ( $NO\ wt_{.exp}$ ) is what the NO content would have been if all of the NO and NO<sub>2</sub> added had simply reacted to create MON. Note that, for simplicity of the derivation, it is not in units of percent here (for example, this value from Test #6 would be 0.0506). It can be expressed simply as the ratio of added NO mass ( $m_{NO,add}$ ) to the total added mass. These are all known quantities.

$$NO\ wt_{.exp} = \frac{m_{NO,add}}{m_{NO,add} + m_{NO_2,add}} \quad (18)$$

The measured NO content ( $NO\ wt_{.meas}$ ), on the other hand, is what the oxidation method and MIL-SPEC equation would produce. That value is also not in units of percent here (for example, this value from Test #6 would be 0.0517). It can be expressed simply as the ratio of actual NO mass ( $m_{NO,act}$ ) to the actual total mass in the synthesis chamber. This is the sum of the actual NO mass ( $m_{NO,act}$ ), actual NO<sub>2</sub> mass ( $m_{NO_2,act}$ ), and the HNO<sub>3</sub> mass ( $m_{HNO_3}$ ). There is no water mass in the denominator because it is completely consumed and converted into other substances.

$$NO\ wt_{.meas} = \frac{m_{NO,act}}{m_{NO,act} + m_{NO_2,act} + m_{HNO_3}} \quad (19)$$

The actual NO mass ( $m_{NO,act}$ ) in the numerator and denominator can be calculated by summing the NO mass added from the NO tank ( $m_{NO,add}$ ) and the NO mass produced by the presence of water via Reaction (7) ( $m_{NO,prod}$ ). The actual NO<sub>2</sub> mass ( $m_{NO_2,act}$ ) in the denominator can be calculated by subtracting the NO<sub>2</sub> mass consumed by Reaction (7) ( $m_{NO_2,cons}$ ) from the NO<sub>2</sub> mass added from the NO<sub>2</sub> tank ( $m_{NO_2,add}$ ):

$$NO\ wt.\_{meas} = \frac{m_{NO,add} + m_{NO,prod}}{(m_{NO,add} + m_{NO,prod}) + (m_{NO_2,add} - m_{NO_2,cons}) + m_{HNO_3}} \quad (20)$$

Substituting  $m_{NO,prod}$  from Equation (13),  $m_{NO_2,cons}$  from Equation (11), and  $m_{HNO_3}$  from Equation (12) into Equation (20) produces:

$$NO\ wt.\_{meas} = \frac{m_{NO,add} + 1.667 \cdot m_{H_2O}}{(m_{NO,add} + 1.667 \cdot m_{H_2O}) + (m_{NO_2,add} - 7.667 \cdot m_{H_2O}) + 7 \cdot m_{H_2O}} \quad (21)$$

Now all of the values are known except for  $m_{H_2O}$ . Both  $m_{NO_2,add}$  and  $m_{NO,add}$  were measured during the beginning of the MON synthesis process, and  $NO\ wt.\_{meas}$  was measured by the oxidation method and the MIL-SPEC equation. Solving for  $m_{H_2O}$  produces:

$$m_{H_2O} = \frac{m_{NO,add} [1 - NO\ wt.\_{meas}] - m_{NO,add} [NO\ wt.\_{meas}]}{NO\ wt.\_{meas} - 1.667} \quad (22)$$

Using this equation, the potential mass of water in the system ( $m_{H_2O}$ ) could be estimated. This estimation was used to examine whether water could have been a realistic source of error in the composition determination process. A raindrop has an estimated mass of 0.033 grams.[108] The conversion from grams of water to drops of water aided in the visualization of the potential mass of water. The relevant data is shown in Table 2, and the water contamination estimates are highlighted.

Table 2. MON Synthesis and NO Content Data with Water Contamination Estimates

Test #	NO Content			Error	Potential Water Contamination	
	Target	Scale Measurement Method	N <sub>2</sub> O <sub>3</sub> Oxidation Method		Mass (g)	Drops
4	5.00%	5.28%	5.78%	9.34%	0.09	3
5	0.00%	0.00%	1.33%	N/A	0.13	4
6	5.00%	4.74%	5.17%	9.04%	0.17	5

The results showed that approximately three to five drops of water could have been responsible for the inconsistent MON composition determinations. Based on the size of the test stand and the many tubes and valves that could hold trace amounts of water vapor, it was deemed plausible that such a small amount of water could be present in the test stand during either the synthesis or the composition determination procedure.

Several possible sources of water in the test stand were identified:

1. The ice bath containing the synthesis vessel could have produced humidity around its surface. The O-ring connecting the synthesis vessel to the test stand was several inches above the surface of the ice bath. Humidity from the ice bath could have transferred into the synthesis vessel through the O-ring.
2. Each time the synthesis vessel was weighed, it needed to be removed, placed on a scale, and then reattached. This process could lead to water contamination through the exposed tube leading to the test stand.
3. Vapor traveled through evacuation tubes into the test stand.

Minor adjustments were implemented, and extra care was given, to reduce the trace amounts of vapor that might enter the system and reduce any relevant human errors. These efforts resulted in noticeable improvements in the synthesis and composition determination.

The next trial, Test #7, was conducted on pure  $\text{N}_2\text{O}_4$  (i.e. MON-0), replicating the process done in Test #5. Although the  $\text{N}_2\text{O}_3$  oxidation method still detected an amount of  $\text{N}_2\text{O}_3$  in the sample (implying that NO was present during the synthesis process), that concentration was 0.75% in Test #7, a 44% improvement from the 1.33% concentration found in Test #5.

The trial after that, Test #8, was intended to create MON-10. The scale measurement method indicated that MON-11.03 had been synthesized. The  $\text{N}_2\text{O}_3$  oxidation method then determined that the composition was MON-10.70. This result is unique because, for the first time, the  $\text{N}_2\text{O}_3$  oxidation method had measured an NO composition that was lower than the NO composition measured by the scale measurement method, hence resulting in an error with a “negative” value (-2.98%) relative to the other results.

The unique results (highlighted in Table 3) implied that the effects of water contamination had been reduced, and that there were other, more dominant factors that skewed the newest results in other ways. However, the goal of reducing the magnitude of error between the scale measurement method and the N<sub>2</sub>O<sub>3</sub> oxidation method was successfully achieved.

Table 3. MON Synthesis and NO Content Data with Water Contamination Estimates after Adjustments to Reduce Water Contamination

Test #	NO Content			Error	Potential Water Contamination	
	Target	Scale Measurement Method	N <sub>2</sub> O <sub>3</sub> Oxidation Method		Mass (g)	Drops
4	5.00%	5.28%	5.78%	9.34%	0.09	3
5	0.00%	0.00%	1.33%	N/A	0.13	4
6	5.00%	4.74%	5.17%	9.04%	0.17	5
7	0.00%	0.00%	0.75%	N/A	0.09	3
8	10.00%	11.03%	10.70%	-2.98%	-0.08	-3

## 5. MON COMPOSITION DETERMINATION

The MIL-PRF-26539G document [7] does not explain how the MIL-SPEC equation was derived, how the coefficients were calculated, or what assumptions and physical property values were used (e.g. vapor pressures, Henry solubility constants, etc.). It also does not list any references. In addition, no current literature attempts to re-derive the equation, although many reports do rely on its assumed validity when determining the NO weight percent of MON samples.

Thus, the goal of this analysis was the re-derive the MIL-SPEC equation, assess its accuracy, and propose any improvements and amendments. In addition, we aimed to thoroughly understand the relationship between MON synthesis and the  $N_2O_3$  oxidation method, and produce an in-depth analytical system of equations to determine a variety of quantities at multiple stages of the processes.

### 5.1 Subscript Notation

When attempting to understand the MIL-SPEC equation, one must work backwards from the final oxidized sample, back to the raw reactants before they are mixed to create MON. Thus, there are two distinct processes to keep track of and distinguish from one another: MON synthesis, and the  $N_2O_3$  oxidation method on the products of said MON synthesis.

In order to track the steps, a subscript notion is used for all masses and numbers of moles that specifies the stage at which that value was present, which is displayed in Figure 37. Masses and numbers of moles that are reactants of the MON synthesis process will end with subscript 1, while masses and numbers of moles that are products of the MON synthesis process will end with subscript 2. Masses and numbers of moles that are reactants of the  $N_2O_3$  oxidation method will also end with subscript 2 (since many of them are products of the MON synthesis process), and masses and numbers of moles that are products of the  $N_2O_3$  oxidation method will end with subscript 3. Masses are denoted by  $m$  and the numbers of moles are denoted by  $n$ .

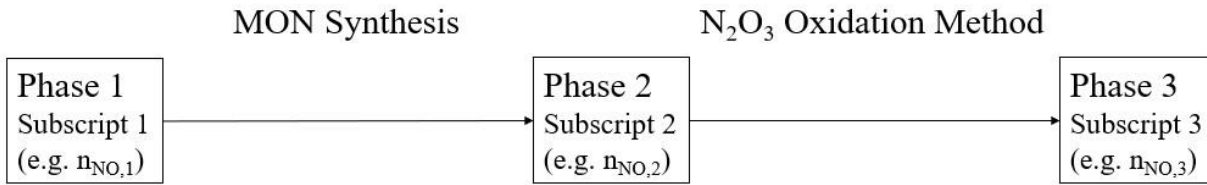
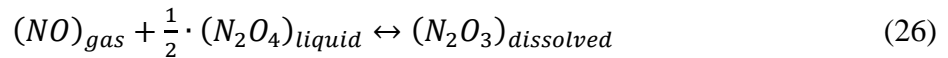
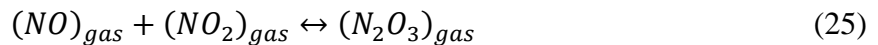


Figure 37. Phases, Processes, and Subscript Notation

## 5.2 Stoichiometric Equations

During MON synthesis, gaseous nitric oxide (NO) is added to dinitrogen tetroxide ( $N_2O_4$ ) and nitrogen dioxide ( $NO_2$ ), resulting in a mixture of the previously mentioned components and newly formed dinitrogen trioxide ( $N_2O_3$ ). This occurs based on the following five chemical reactions, which take place simultaneously in equilibrium: [5]



Reactions (25) and (26) are the only two reactions which involve the addition of NO and the formation of  $N_2O_3$ , and thus are the underpinnings of MON synthesis. The MON synthesis takes place at  $0^\circ\text{C}$ , forcing all the gaseous  $NO_2$  into the liquid  $N_2O_4$  via Reaction (23). Since there is a negligible amount of gaseous  $NO_2$  remaining, and because gaseous  $NO_2$  is one of the components necessary for  $N_2O_3$  formation via of Reaction (25), the contribution of Reaction (25) in the  $N_2O_3$  formation is also negligible and can be neglected. Therefore, we will consider Reaction (26) as the main driver in the  $N_2O_3$  formation.

Using the equilibrium constants for all five chemical reactions [5], we are able to confirm that liquid  $N_2O_4$  and dissolved  $N_2O_3$  are the main constituents of the MON sample at  $0^\circ\text{C}$ . From this

point on, Reaction (26) will be expressed without phase change notations, and all species will be multiplied by two to convert the fractions to whole numbers, as follows:



During the  $N_2O_3$  oxidation method, oxygen ( $O_2$ ) reacts with the  $N_2O_3$  that was produced during MON synthesis to produce additional  $N_2O_4$ . Thus, the stoichiometric equation for the  $N_2O_3$  oxidation method is:



Using Reactions (28) and (29), relationships between the numbers of moles of different species that participate in these reactions can be inferred. From Reaction (28) for MON synthesis:

$$n_{NO,1} = 2 \cdot n_{N_2O_4,reacted,1} = n_{N_2O_3,2} \quad (30)$$

The term “reacted” is used to distinguish  $n_{N_2O_4,reacted,1}$ , the smaller amount of  $N_2O_4$  that specifically reacts with the NO, from  $n_{N_2O_4,1}$ , the total  $N_2O_4$  used during synthesis.

Likewise, from Reaction (29) for the  $N_2O_3$  oxidation method:

$$n_{N_2O_3,2} = 2 \cdot n_{O_2,reacted,2} = n_{N_2O_4,created,3} \quad (31)$$

The term “reacted” is used to distinguish  $n_{O_2,reacted,2}$ , the smaller amount of  $O_2$  that specifically reacts with the  $N_2O_3$ , from  $n_{O_2,2}$ , the total  $O_2$  used during the oxidation method. The term “created” is used to distinguish  $n_{N_2O_4,created,3}$ , the smaller amount of  $N_2O_4$  that is specifically created during the oxidation method, from  $n_{N_2O_4,3}$ , the total  $N_2O_4$  in the sample vessel after the oxidation method.

Note that equations (30) ends with  $n_{N_2O_3,2}$ , while equation (31) begins with  $n_{N_2O_3,2}$ . Thus, all of the components in both equations are equal. By equating equations (30) and (31), they can be combined to show a comprehensive relationship between all of the listed numbers of moles reacting across the two processes:

$$n_{NO,1} = 2 \cdot n_{N_2O_4,reacted,1} = n_{N_2O_3,2} = 2 \cdot n_{O_2,reacted,2} = n_{N_2O_4,created,3} \quad (32)$$

Figure 38 below shows how this equation is justified, by relating the number of moles of different substances across the two processes.

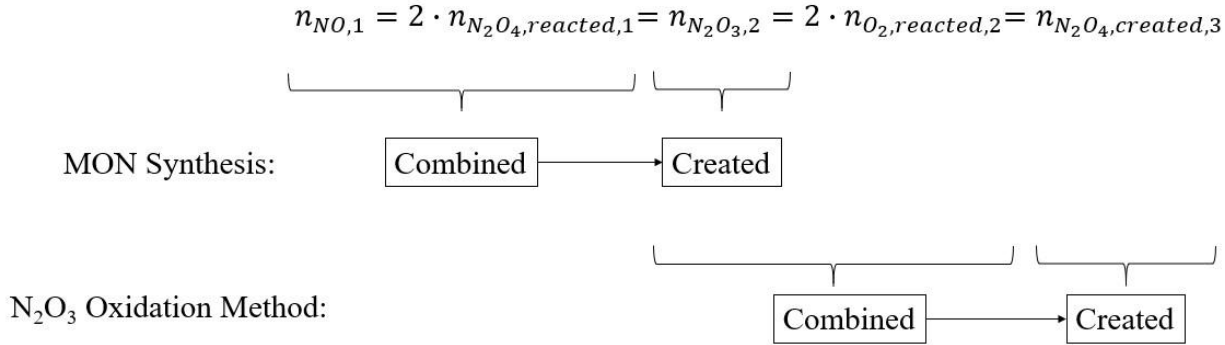


Figure 38. Relationship between numbers of moles across two processes

The numbers 1, 2, and 3 at the end of each subscript are used to denote where that value is present in the two processes. Also note that these are the number of moles that react with each other in a complete reaction, neglecting the constituents in the gas phase, which, although in small concentrations, are still present at 0°C.

To summarize, during MON synthesis,  $n_{NO,1}$  and  $2 \cdot n_{N_2O_4,reacted,1}$  are combined to create  $n_{N_2O_3,2}$ . Then during the N<sub>2</sub>O<sub>3</sub> oxidation method, the produced  $n_{N_2O_3,2}$  and newly added  $2 \cdot n_{O_2,reacted,2}$  is combined to create  $n_{N_2O_4,created,3}$ .

These reactions will be heavily referenced throughout the following derivations.

### 5.3 MIL-SPEC Equation Derivation

#### 5.3.1 Recap of the MIL-SPEC Equation

The original MIL-SPEC equation calculates the weight percentage of NO in MON:

$$NO \text{ wt. \%} = \frac{[y - 0.003857(z - \frac{x+y}{1.49})] \cdot 187.5}{x} - 0.15 \quad (44)$$

Each variable is described below, and will be assigned the new nomenclature:

$$x = \text{MON sample mass in grams} = m_{MON,2}$$

$$y = \text{total O}_2 \text{ mass added during N}_2\text{O}_3 \text{ oxidation method in grams} = m_{O_2,2}$$

$$z = \text{volume of sample bomb} = V_{vessel}$$

The MIL-SPEC equation can be written as:

$$NO \text{ wt. } \% = \frac{\left[ m_{O_2,2} - 0.003857 \left( V_{vessel} - \frac{m_{MON,2} + m_{O_2,2}}{1.49} \right) \right] \cdot 187.5}{m_{MON,2}} - 0.15 \quad (33)$$

### 5.3.2 Deriving the Number: 187.5

In order to derive this equation using the reactions and the resulting stoichiometric relationships, we begin with the equation for MON composition defined by the NO weight percent of the mixture:

$$NO \text{ wt. } \% = \frac{m_{NO,1}}{m_{MON,2}} \cdot 100\% \quad (34)$$

In which  $m_{NO,1}$  is the mass of NO used to produce the MON sample, and  $m_{MON,2}$  is the total mass of the MON sample produced.

Since the mass of the NO is unknown, this method relies on the oxidation of  $N_2O_3$  to  $N_2O_4$ , using  $O_2$ , to measure the unknown NO mass that was initially added.

Based on the molar relationships in Eq. (32), there are two moles of NO at the start of the MON synthesis process for every one mole of  $O_2$  in the  $N_2O_3$  oxidation method reaction:

$$n_{NO,1} = 2 \cdot n_{O_2,react,2} \quad (35)$$

This can be used to derive a relationship between the mass of initial NO and the mass of reacted  $O_2$ . Consider the masses of NO and  $O_2$ , written in terms of their molar mass and numbers of moles:

$$m_{NO,1} = M_{NO} \cdot n_{NO,1} \quad (36)$$

$$m_{O_2,react,2} = M_{O_2} \cdot n_{O_2,react,2} \quad (37)$$

Combining Eq. (35), (36), and (37), and solving for  $m_{NO,1}$ , produces:

$$m_{NO,1} = \frac{2M_{NO}}{M_{O_2}} \cdot m_{O_2,react,2} = a \cdot m_{O_2,react,2}, \text{ where } a = \frac{2M_{NO}}{M_{O_2}} = 1.875 \quad (38)$$

Converting the mass ratio equation to a mass percentage equation produces  $a \cdot 100$ , which is the 187.5 coefficient in the MIL-SPEC equation. The 187.5 coefficient converts the mass of reacted  $O_2$  to the mass of NO used to synthesize the MON sample.

Thus:

$$NO \text{ wt } \% = \frac{m_{NO,1}}{m_{MON,2}} \cdot 100 = a \cdot \frac{m_{O_2,react,2}}{m_{MON,2}} \times 100 = \frac{m_{O_2,react,2}}{m_{MON,2}} \cdot 187.5 \quad (39)$$

### 5.3.3 Accounting for the $O_2$ dissolved in $N_2O_4$

The total mass of  $O_2$  added to the MON sample can be broken down into reacted and unreacted components, where  $m_{O_2,unreact,2}$  is the mass of the  $O_2$  in the vessel that has not reacted with the  $N_2O_3$  in the MON.

$m_{O_2,unreact,2}$  can be further broken down into the gaseous  $O_2$  in the vessel headspace ( $m_{O_2(g),3}$ ) and the  $O_2$  that dissolves into the liquid  $N_2O_4$  that is produced from the excess  $O_2$  added during the  $N_2O_3$  oxidation method ( $m_{O_2(d),3}$ ). Thus, the total mass of  $O_2$  that the MON sample receives during the  $N_2O_3$  oxidation method can be written as:

$$m_{O_2,2} = m_{O_2,react,2} + m_{O_2,unreact,3} = m_{O_2,react,2} + m_{O_2(g),3} + m_{O_2(d),3} \quad (40)$$

Note that the masses of unreacted  $O_2$  ( $m_{O_2,unreact,3}$ ,  $m_{O_2(g),3}$ ,  $m_{O_2(d),3}$ ) all have the subscript 3. This is because these masses of  $O_2$  do not react during the  $N_2O_3$  oxidation process, are still present afterwards, and are thus considered as products of that process. Also note that  $m_{O_2,unreact,3}$  is the total mass of  $O_2$  after the  $N_2O_3$  oxidation method:

$$m_{O_2,unreact,3} = m_{O_2,3} = m_{O_2(g),3} + m_{O_2(d),3} \quad (41)$$

Using Eq. (40) to solve for the mass of the reacted O<sub>2</sub>, it can be expressed as:

$$m_{O_2,react,2} = m_{O_2,2} - m_{O_2(g),3} - m_{O_2(d),3} \quad (42)$$

Substituting  $m_{O_2,react,2}$  from Eq. (42) into Eq. (39) produces:

$$NO \text{ wt. } \% = \frac{m_{O_2,2} - m_{O_2(g),3} - m_{O_2(d),3}}{m_{MON,2}} \cdot 187.5 \quad (43)$$

Or:

$$NO \text{ wt. } \% = \frac{m_{O_2,2} - m_{O_2(g),3}}{m_{MON,2}} \cdot 187.5 - 187.5 \cdot \frac{m_{O_2(d),3}}{m_{MON,2}} \quad (44)$$

Then the derived equation begins to resemble the MIL-SPEC equation in Eq. (33):

$$NO \text{ wt. } \% = \frac{\left[ m_{O_2,2} - 0.003857 \left( V_{vessel} - \frac{m_{MON,2} + m_{O_2,2}}{1.49} \right) \right] \cdot 187.5}{m_{MON,2}} - 0.15 \quad (45)$$

$m_{O_2,2}$  and  $m_{MON,2}$  in Eq. (45) are known, and are represented by  $y$  and  $x$  respectively. Meanwhile,  $m_{O_2(g),3}$  and  $m_{O_2(d),3}$  are unknown. The next step is to express the variable  $m_{O_2(g),3}$ .

### 5.3.4 Solving for $m_{O_2(g),3}$ , the Gaseous O<sub>2</sub> in Headspace after Oxidation

$m_{O_2(g),3}$ , the mass of the gaseous O<sub>2</sub> in the headspace, can be found using the ideal gas equation as follows:

$$n_{O_2(g)} = \frac{P_{O_2(g)} V_{O_2(g)}}{R_u T_{O_2(g)}} \quad (46)$$

$$m_{O_2(g)} = \frac{P_{O_2(g)} V_{O_2(g)}}{R_u T_{O_2(g)}} M_{O_2} = \frac{P_{O_2(g)} V_{O_2(g)}}{R_{O_2} T_{O_2(g)}} \quad (47)$$

$V_{O_2(g)}$  is the volume of the gaseous O<sub>2</sub>, which is equivalent to the volume of the headspace:

$$V_{O_2(g)} = V_{headspace} = V_{vessel} - V_{liquid} \quad (48)$$

Substituting  $V_{O_2(g)}$  from Eq. (48) into Eq. (47) produces:

$$m_{O_2(g)} = \frac{P_{O_2(g)}(V_{vessel} - V_{liquid})}{R_{O_2} T_{O_2(g)}} \quad (49)$$

The next step is to express the only unknown variable on the right-hand side of the equation, which is  $V_{liquid}$ .

The volume of the liquid is found using Eq. (50):

$$V_{liquid} = \frac{m_{oxid(l),3}}{\rho_{oxid(l)}} \quad (50)$$

Where  $m_{oxid(l),3}$  is the mass of the liquid sample produced by the  $N_2O_3$  oxidation method.

The mass of the liquid sample produced after the  $N_2O_3$  oxidation method can be expressed as:

$$m_{oxid(l),3} = m_{N_2O_4(l),3} + m_{O_2(d),3} \quad (51)$$

Where  $m_{O_2(d),3}$  is the mass of gaseous oxygen that dissolves into the liquid  $N_2O_4$  during the  $N_2O_3$  oxidation method. Combining Eq. (50) and (51) produces:

$$V_{liquid} = \frac{m_{N_2O_4(l),3} + m_{O_2(d),3}}{\rho_{oxid(l)}} \quad (52)$$

$m_{O_2(d),3}$  is negligible compared to  $m_{N_2O_4(l),3}$  (typically less than 0.03%) such that the density of the liquid sample produced by the  $N_2O_3$  oxidation method is approximated to that of pure liquid  $N_2O_4$ . Therefore, the variable  $\rho_{oxid(l)}$  in the denominator can be replaced by  $\rho_{N_2O_4}$ :

$$V_{liquid} = \frac{m_{N_2O_4(l),3} + m_{O_2(d),3}}{\rho_{N_2O_4}} \quad (53)$$

Based on the structure of the MIL-SPEC equation, it can be inferred that the authors chose to neglect the mass of the gaseous component of  $N_2O_4$  in the sample vessel after the oxidation method, possibly to simplify to equation (deriving a similar equation without neglecting the mass of the gaseous  $N_2O_4$  will be explored in Section 6.5.2). But as explained earlier, it is a valid assumption that the gaseous component of  $N_2O_4$  in the sample vessel after the oxidation method is negligible compared to the liquid component of  $N_2O_4$ , such that:

$$m_{N_2O_4(l),3} = m_{N_2O_4,3} \quad (54)$$

Then Eq. (51) can be written as:

$$m_{oxid(l),3} = m_{N_2O_4,3} + m_{O_2(d),3} \quad (55)$$

$m_{oxid(l),3}$  can be further broken down and written as:

$$m_{oxid(l),3} = m_{N_2O_4,3} + m_{O_2(d),3} = m_{MON,2} + m_{O_2,react,2} + m_{O_2(d),3} \quad (56)$$

Where  $m_{MON,2}$  and  $m_{O_2,react,2}$  are the amounts of MON and O<sub>2</sub> that combine to create the final amount of N<sub>2</sub>O<sub>4</sub> after the N<sub>2</sub>O<sub>3</sub> oxidation method.

From Eq. (42), one can show that:

$$m_{O_2,react,2} + m_{O_2(d),3} = m_{O_2,2} - m_{O_2(g),3} \quad (57)$$

Entering  $m_{O_2,react,2} + m_{O_2(d),3}$  from Eq. (57) into Eq. (56) produces:

$$m_{oxid(l),3} = m_{N_2O_4,3} + m_{O_2(d),3} = m_{MON,2} + m_{O_2,2} - m_{O_2(g),3} \quad (58)$$

Entering this into the numerator of Eq. (53) produces:

$$V_{liquid} = \frac{m_{MON,2} + m_{O_2,2} - m_{O_2(g),3}}{\rho_{N_2O_4}} \quad (59)$$

The next step is to enter this expression for  $V_{liquid}$  back into the equation for  $m_{O_2(g),3}$ . Substituting  $V_{liquid}$  from Eq. (59) into Eq. (49) produces:

$$m_{O_2(g),3} = \frac{P_{O_2(g)}}{R_{O_2} T_{O_2(g)}} \left( V_{vessel} - \frac{m_{MON,2} + m_{O_2,2} - m_{O_2(g),3}}{\rho_{N_2O_4}} \right) \quad (60)$$

Simplifying and solving for  $m_{O_2(g),3}$  produces:

$$m_{O_2(g),3} = \frac{P_{O_2(g)}}{R_{O_2} T_{O_2(g)}} \left( V_{vessel} - \frac{m_{MON,2} + m_{O_2,2}}{\rho_{N_2O_4}} + \frac{m_{O_2(g),3}}{\rho_{N_2O_4}} \right) \quad (61)$$

$$m_{O_2(g),3} \left( 1 - \frac{P_{O_2(g)}}{R_{O_2} T_{O_2(g)} \rho_{N_2O_4}} \right) = \frac{P_{O_2(g)}}{R_{O_2} T_{O_2(g)}} \left( V_{vessel} - \frac{m_{MON,2} + m_{O_2,2}}{\rho_{N_2O_4}} \right) \quad (62)$$

Finally, the mass of the gaseous O<sub>2</sub> in the headspace can be expressed as:

$$m_{O_2(g),3} = \frac{\frac{P_{O_2(g)}}{R_{O_2} T_{O_2(g)}}}{1 - \frac{P_{O_2(g)}}{R_{O_2} T_{O_2(g)} \rho_{N_2O_4}}} \left( V_{vessel} - \frac{m_{MON,2} + m_{O_2,2}}{\rho_{N_2O_4}} \right) \quad (63)$$

$$m_{O_2(g),3} = \left( \frac{P_{O_2(g)} \rho_{N_2O_4}}{R_{O_2} T_{O_2(g)} \rho_{N_2O_4} - P_{O_2(g)}} \right) \left( V_{vessel} - \frac{m_{MON,2} + m_{O_2,2}}{\rho_{N_2O_4}} \right) \quad (64)$$

$$m_{O_2(g),3} = b \cdot \left( V_{vessel} - \frac{m_{MON,2} + m_{O_2,2}}{\rho_{N_2O_4}} \right) = b \cdot V_{headspace} \quad (65)$$

Where:

$$b = \frac{P_{O_2(g)} \rho_{N_2O_4}}{R_{O_2} T_{O_2(g)} \rho_{N_2O_4} - P_{O_2(g)}} \quad (66)$$

$b$  is the factor that converts a volume of headspace to the mass of gaseous O<sub>2</sub> in that headspace.

### 5.3.5 Deriving the Number: 0.003857

The next step is to calculate the value of the constant “ $b$ ”. This requires the values of the partial pressure of oxygen ( $P_{O_2(g)}$ ), the temperature of the oxygen ( $T_{O_2(g)}$ ), and the density of the N<sub>2</sub>O<sub>4</sub> at that same temperature ( $\rho_{N_2O_4}$ ).

Dalton’s law of partial pressures states that the total pressure exerted by a mixture of non-reacting gases is equal to the sum of the partial pressures of the individual gasses. This law is used to find the partial pressure of oxygen in the headspace,  $P_{O_2(g)}$ .

The liquid in the sample vessel after the oxidation process is entirely N<sub>2</sub>O<sub>4</sub>, while the gas in the sample vessel is a mixture of oxygen and N<sub>2</sub>O<sub>4</sub>. Thus, the total pressure in the vessel is equal to the sum of the partial pressures of oxygen and N<sub>2</sub>O<sub>4</sub>, respectively, and so the partial pressure of the oxygen can be found by subtracting the pressure of the N<sub>2</sub>O<sub>4</sub> from the total pressure in the vessel.

The total pressure in the vessel was measured as 44.7 psia, while literature states that the vapor pressure of N<sub>2</sub>O<sub>4</sub> at 0°C is 5.079 psi.[109] Subtracting one from the other gives the partial pressure of oxygen in the headspace as 39.62 psi.

As for the temperature of the oxygen and the density of the N<sub>2</sub>O<sub>4</sub>, MIL-PRF-26539G requires that the N<sub>2</sub>O<sub>3</sub> oxidation method be conducted at 0°C, such that  $T_{O_2(g)}$  is equal to 0°C. The density of N<sub>2</sub>O<sub>4</sub> at 0°C ( $\rho_{N_2O_4}$ ) is 1.49 g/mL.[110]

Using the stated values produces  $b = 0.003859$ . This number is about 0.06% higher than the number in the MIL-SPEC equation, which is 0.003857. Since the discrepancy between the two values is nearly negligible, we will use the value of 0.003857 from the MIL-SPEC equation, to simplify the derivation process.

The value for  $b$  calculated here is contingent on the literature sources used to determine N<sub>2</sub>O<sub>4</sub> vapor pressure but, unfortunately, not documented in the MIL-SPEC document. Varying sources could cause this discrepancy.

Now, nearly all of the sections of the equation have been accounted for. They will be combined in the next section.

### 5.3.6 Final Compilation of Results

The next step is to combine the previous results and create the MIL-SPEC equation. Recall that Eq. (45) was the last expression derived for NO weight percent:

$$NO \text{ wt. } \% = \frac{m_{O_2,2} - m_{O_2(g),3}}{m_{MON,2}} \cdot 187.5 - 187.5 \cdot \frac{m_{O_2(d),3}}{m_{MON,2}} \quad (45)$$

Substituting Eq. (65) for  $m_{O_2(g),3}$ , with  $b = 0.003857$  and  $\rho_{N_2O_4} = 1.49$ , into Eq. (45) produces:

$$NO \text{ wt. } \% = \frac{[m_{O_2,2} - 0.003857 \cdot (V_{vessel} \cdot \frac{m_{MON,2} + m_{O_2,2}}{1.49})] \cdot 187.5}{m_{MON,2}} - 187.5 \cdot \frac{m_{O_2(d),3}}{m_{MON,2}} \quad (67)$$

Thus, the NO weight percent equation continues to further resemble the MIL-SPEC equation in Eq. (33):

$$NO \text{ wt. } \% = \frac{\left[ m_{O_2,2} - 0.003857 \left( V_{\text{vessel}} - \frac{m_{MON,2} + m_{O_2,2}}{1.49} \right) \right] \cdot 187.5}{m_{MON,2}} - 0.15 \quad (33)$$

The left section of the equation is complete. Now, the 0.15 value needs to be derived.

#### 5.4 Solubility Factor Derivation

Now, an attempt will be made to derive and verify the 0.15 value based on the fundamental properties of the  $N_2O_3$  oxidation method. This will be called the “solubility factor”, and have the nomenclature of  $S$ :

$$S = 187.5 \cdot \frac{m_{O_2(d),3}}{m_{MON,2}} \quad (68)$$

Henry’s law states that the amount of dissolved gas in a liquid is proportional to its partial pressure above the liquid. In equation form, it is expressed as:

$$K = \frac{x}{P} \quad (69)$$

Where  $K$  is the Henry solubility constant,  $x$  is the molar mixing ratio of the particular species in the liquid, and  $P$  is the partial pressure of that species in the gas above the liquid under equilibrium conditions. Thus, the molar mixing ratio is:

$$x = K \cdot P \quad (70)$$

By definition, the molar mixing ratio of liquid  $O_2$  dissolved in the liquid portion of the  $N_2O_3$  oxidation sample is:

$$x_{O_2(d)} = \frac{n_{O_2(d),3}}{n_{oxid(l),3}} = \frac{m_{O_2(d),3} / M_{O_2}}{m_{oxid(l),3} / M_{oxid(l)}} \quad (71)$$

Where  $n_{oxid(l),3}$ ,  $m_{oxid(l),3}$ , and  $M_{oxid(l)}$  are the moles, mass, and average molar mass of the liquid sample after the  $N_2O_3$  oxidation method. This excludes any gases in the headspace of the vessel.

Solving for  $m_{O_2(d),3}$  in Eq. (71) produces:

$$m_{O_2(d),3} = x_{O_2(d)} \cdot \frac{M_{O_2}}{M_{oxid(l)}} \cdot m_{oxid(l),3} \quad (72)$$

And substituting the expression for  $x_{O_2(d)}$  from Eq. (70) into Eq. (72) produces:

$$m_{O_2(d),3} = K_{O_2 \text{ in } N_2O_4} \cdot P_{O_2,3} \cdot \frac{M_{O_2}}{M_{oxid(l)}} \cdot m_{oxid(l),3} \quad (73)$$

Entering  $m_{O_2(d),3}$  from Eq. (73) into Eq. (68) produces the final equation for the solubility factor:

$$S = 187.5 \cdot K_{O_2 \text{ in } N_2O_4} \cdot P_{O_2,3} \cdot \frac{M_{O_2}}{M_{oxid(l)}} \cdot \frac{m_{oxid(l),3}}{m_{MON,2}} \quad (74)$$

Given that the specified temperature for the  $N_2O_3$  oxidation method is  $0^\circ\text{C}$ , then literature states that the Henry solubility constant for  $O_2$  dissolving in  $N_2O_4$  at  $0^\circ\text{C}$  is  $9.2198\text{E-}4 \text{ atm}^{-1}$ . (Chang, 1965)

As stated before, the partial pressure of  $O_2$  in the headspace,  $P_{O_2,3}$  (also previously called  $P_{O_2(g)}$ ), was calculated by subtracting the partial pressure of  $N_2O_4$  at  $0^\circ\text{C}$  from the total pressure in the vessel. It was determined to equal 39.62 psi, or 2.696 atm.

The next step is to solve for the value of  $M_{oxid(l)}$ .

$M_{oxid(l)}$  is the average molar mass of the liquid portion of the sample produced by the  $N_2O_3$  oxidation method. Since the liquid portion of the sample is a mixture of liquid  $N_2O_4$  and dissolved  $O_2$ , then the average molar mass of the liquid sample can be derived as:

$$M_{oxid(l)} = M_{N_2O_4} \cdot \left( \frac{n_{N_2O_4(l),3}}{n_{oxid(l),3}} \right) + M_{O_2} \cdot \left( \frac{n_{O_2(d),3}}{n_{oxid(l),3}} \right) \quad (75)$$

Where  $\frac{n_{O_2(d),3}}{n_{oxid(l),3}}$  is the molar mixing ratio of  $O_2$  dissolved in the liquid  $N_2O_3$  oxidation sample, and is therefore:

$$\frac{n_{O_2(d),3}}{n_{oxid(l),3}} = x_{O_2(d)} = K_{O_2 \text{ in } N_2O_4} \cdot P_{O_2,3} \quad (76)$$

Since liquid  $N_2O_4$  and dissolved  $O_2$  are the only two species in the liquid:

$$\frac{n_{N_2O_4(l),3}}{n_{oxid(l),3}} = 1 - \frac{n_{O_2(d),3}}{n_{oxid(l),3}} = 1 - K_{O_2 in N_2O_4} \cdot P_{O_2,3} \quad (77)$$

Entering  $\frac{n_{O_2(d),3}}{n_{oxid(l),3}}$  and  $\frac{n_{N_2O_4(l),3}}{n_{oxid(l),3}}$  from Eq. (76) and (77) into Eq. (75) produces:

$$M_{oxid(l)} = M_{N_2O_4} \cdot (1 - K_{O_2 in N_2O_4} \cdot P_{O_2,3}) + M_{O_2} \cdot (K_{O_2 in N_2O_4} \cdot P_{O_2,3}) \quad (78)$$

All of these values are known, and they are all constants. As stated earlier, the Henry solubility constant,  $K_{O_2 in N_2O_4}$ , at 0°C is  $9.2198E-4 \text{ atm}^{-1}$ . [111] The partial pressure of  $O_2$  in the headspace,  $P_{O_2,3}$  (and previously called  $P_{O_2(g)}$ ), is 39.62 psi, or 2.696 atm.

Thus, the average molar mass of the liquid portion of every  $N_2O_3$  oxidation sample is the same, and can be calculated as:

$$M_{oxid(l)} = \left(92 \frac{g}{mol}\right) (1 - (9.2198E - 4)(2.696)) + \left(32 \frac{g}{mol}\right) ((9.2198E - 4)(2.696)) \quad (79)$$

$$M_{oxid(l)} = 91.851 \frac{g}{mol} \quad (80)$$

This is just slightly below the molar mass of  $N_2O_4$  of 92 g/mol, due to it being a mixture of mostly  $N_2O_4$  and a very small amount of  $O_2$  which has a lower molecular mass.

Entering all of the known values into Eq. (74) for the solubility factor produces:

$$S = (187.5)(9.2198E - 4)(2.696) \left(\frac{32 \frac{g}{mol}}{91.857 \frac{g}{mol}}\right) \cdot \frac{m_{oxid(l),3}}{m_{MON,2}} \quad (81)$$

$$S = 0.1624 \cdot \frac{m_{oxid(l),3}}{m_{MON,2}} \quad (82)$$

As stated in Eq. (56),  $m_{oxid(l),3}$  can be expressed as:

$$m_{oxid(l),3} = m_{MON(l),2} + m_{O_2,react(l),2} + m_{O_2(d),3} = m_{N_2O_4(l),3} + m_{O_2(d),3}$$

$m_{oxid(l),3}$  is the mass of the liquid portion of the sample, after the oxidation method. It comprises of three separate quantities:  $m_{MON(l),2}$ ,  $m_{O_2,react(l),2}$ , and  $m_{O_2(d),3}$ .

$m_{MON(l),2}$  is the mass of the liquid portion of the MON sample after MON synthesis.  $m_{O_2,react(l),2}$  is the mass of the O<sub>2</sub> that reacts during the oxidation method to create liquid N<sub>2</sub>O<sub>4</sub> (which has a mass of  $m_{N_2O_4(l),3}$ ).  $m_{O_2(d),3}$  is the mass of the O<sub>2</sub> that has dissolved into the liquid N<sub>2</sub>O<sub>4</sub> during the oxidation method. These quantities, combined, create the liquid portion of the sample, after the oxidation method, hence why the sum of their masses equals  $m_{oxid(l),3}$ . And, as stated before, the liquid N<sub>2</sub>O<sub>4</sub> ( $m_{N_2O_4(l),3}$ ) that exists after the oxidation method is created when the liquid MON ( $m_{MON(l),2}$ ) reacts with the reacted oxygen ( $m_{O_2,react(l),2}$ ), which explains the final portion of the equation.

This equation shows that, for a given initial liquid MON mass ( $m_{MON(l),2}$ ), the higher the NO weight percent, the more O<sub>2</sub> ( $m_{O_2,react(l),2}$ ) will react during the N<sub>2</sub>O<sub>3</sub> oxidation method, and thus the more liquid N<sub>2</sub>O<sub>4</sub> will exist in the sample after the N<sub>2</sub>O<sub>3</sub> oxidation method ( $m_{N_2O_4(l),3}$ ). This will result in a larger liquid portion of the N<sub>2</sub>O<sub>3</sub> oxidation sample mass ( $m_{oxid(l),3}$ ), and a larger  $\frac{m_{oxid(l),3}}{m_{MON,2}}$  ratio. Therefore, the solubility factor is not a constant value, and changes slightly depending on the MON composition of the sample.

(Indeed, later analytical analysis performed in Section 7 showed that the  $\frac{m_{oxid(l),3}}{m_{MON,2}}$  ratio ranges from unity for a sample of MON-0 (i.e. pure N<sub>2</sub>O<sub>4</sub>) to approximately 1.2 for a sample of MON-40. This would change the solubility factor from 0.1557 for a sample of MON-0 to 0.1868 for a sample of MON-40. However, this method of analytical analysis is far more complex than that in the MIL-SPEC equation, and should be viewed as a validation of other methods of calculation, rather than the preferred method of calculation.)

Despite the apparent derivation of the solubility factor in Eq. (82), the value of the solubility factor is still not attainable because the value of  $m_{oxid(l),3}$  cannot be calculated. It should also be noted that the MIL-SPEC equation (see Eq. (4)) designates the value of the solubility factor as a constant 0.15. At this point in the derivation, this value has yet to be verified or rebuked. The next chapter provides three different assumptions that can be made in order to estimate the value of the solubility factor, with the goal of finding the most optimal calculation method that fits the needs of the N<sub>2</sub>O<sub>3</sub> oxidation method MON composition analysis, and the goal of determining if the 0.15 value of the solubility factor is sufficient. A fourth option is also included, which does not rely on

any assumptions and is therefore closest to reality, in order to analytically check the validity of the other three estimation methods.

.

## 6. SOLUBILITY FACTOR DETERMINATION

As stated in the previous section, the solubility factor can be expressed as the following:

$$S = 0.1624 \cdot \frac{m_{oxid(l),3}}{m_{MON,2}} \quad (83)$$

The mass of the MON sample,  $m_{MON,2}$ , is known. Although the total mass of the N<sub>2</sub>O<sub>3</sub> oxidation method sample ( $m_{oxid,3}$ ) is known, the mass of the liquid portion ( $m_{oxid(l),3}$ ) is not. As a result, the solubility factor cannot be precisely calculated at this point, and the previous derivation of the solubility factor is not sufficient from an application-based perspective. As a reminder, the goal is to determine the accuracy and usefulness of the MIL-SPEC equation, which provides a solubility factor of 0.15. At this point in the derivation, this has yet to be verified. As a part of that verification process, several different derivations were explored in this chapter, to observe if any of them would converge on or near the 0.15 value or provide a more accurate non-constant approach to solubility.

The goal of this section is to use various assumptions to calculate the solubility factor in several ways. Each method has its own strength, application, and level of accuracy. They are listed in order of increasing accuracy and complexity.

### 6.1 MIL-SPEC Solubility Factor

The MIL-SPEC solubility factor is 0.15. It is unknown as to whether this number was calculated or measured empirically.

### 6.2 Option 1: $m_{oxid(l),3} = m_{MON,2}$

Eq. (82) states that the solubility factor can be expressed as:

$$S = 0.1624 \cdot \frac{m_{oxid(l),3}}{m_{MON,2}} \quad (82)$$

The simplest assumption is to state that the mass of the liquid portion of the N<sub>2</sub>O<sub>3</sub> oxidation method sample is equal to the total mass of the MON sample:

$$m_{oxid(l),3} = m_{MON,2} \quad (84)$$

Or:

$$\frac{m_{oxid(l),3}}{m_{MON,2}} = 1 \quad (85)$$

This assumption is relatively accurate, since the amount of O<sub>2</sub> added to the MON sample during the N<sub>2</sub>O<sub>3</sub> oxidation method is relatively small compared to the MON sample, meaning that the difference between the N<sub>2</sub>O<sub>3</sub> oxidation method sample and the MON sample is relatively small.

Unfortunately, the process of determining what quantities are assumed to equal zero is neither straightforward nor very helpful. Combining Eq. (56) and Eq. (84) produces:

$$m_{MON,2} = m_{MON(l),2} + m_{O_2,react(l),2} + m_{O_2(d),3} \quad (86)$$

Rearranging the variables produces:

$$m_{MON,2} - m_{MON(l),2} = m_{MON(g),2} = m_{O_2,react(l),2} + m_{O_2(d),3} \quad (87)$$

The concept that the mass of the gas in the headspace of the MON sample equals the mass of the reacted O<sub>2</sub> plus the dissolved O<sub>2</sub> after the oxidation method does not make much sense, nor provide any insight into the assumption made. In fact, many further attempts were made to identify what specific variables were deemed negligible, and those attempts did not yield helpful results. Due to the differences in substance phases ( $m_{MON,2}$  is a liquid-gas mixture, while  $m_{oxid(l),3}$  is a pure liquid), as well as in stages of the procedure ( $m_{MON,2}$  exists during the second stage, after the MON synthesis, while  $m_{oxid(l),3}$  exists during the third stage, after the oxidation method), these two variables do not share enough commonalities to provide much additional insight.

As stated earlier, analytical analysis showed that the  $\frac{m_{oxid(l),3}}{m_{MON,2}}$  ratio actually ranges from 1 for a sample of MON-0 (i.e. pure N<sub>2</sub>O<sub>4</sub>) to 1.2 for a sample of MON-40, meaning that this assumption is most valid at lower MON compositions.

Under this particular assumption, the solubility factor is a constant:

$$S = 0.1624 \quad (88)$$

This is the most similar option to the solubility factor present in the MIL-SPEC equation of 0.15, in that it is a constant value across a range of MON compositions. However, 0.1624 is still 8.2% larger than the 0.15 value seen in the MIL-SPEC equation.

Assuming that this method of derivation was used, then based on Eq. (74) there are only three values that could have caused this discrepancy (the rest of the values are well-known physical properties such as the molecular weight of oxygen).

The first value is  $K_{O_2 \text{ in } N_2O_4}$ , the solubility of  $O_2$  in  $N_2O_4$ . The value used in this report was found in a report by Chang, dated May 1965.[111] However, the first version of the MIL-SPEC document for MON debuted in July of 1964.[27] Efforts to obtain this report have not been successful thus far, so it is unclear whether or not the MIL-SPEC equation first appeared in that report, or the subsequent revision which was released in October of 1971.[40] If the equation was in the 1964 report, then its authors would not have had access to the values of  $O_2$  solubility in  $N_2O_4$  that were measured by Chang in 1965. Chang states that “*a literature search revealed that there were no data on the solubility of  $O_2$  in liquid  $N_2O_4$* ”.[111] Therefore, the authors of the original 1964 MIL-SPEC report did not have a value for the  $O_2$  solubility. If they were to have devised the MIL-SPEC equation, then it is likely that they did so empirically. That would certainly be a source of discrepancy between their results and ours.

The second value is  $P_{O_2,3}$ , the  $O_2$  partial pressure. This value is the difference between the measured pressure in the vessel and the  $N_2O_4$  vapor pressure from literature. Although there may be initial concerns that the measured vessel pressure can vary depending on the conditions and equipment of each laboratory, those concerns can be quelled by the fact that  $O_2$  partial pressure was used in the calculation of the  $b$  value (see Eq. (66)) which only had a 0.006% discrepancy from the  $b$  value found in the MIL-SPEC equation. Therefore, it can be inferred that those authors used a very similar  $O_2$  partial pressure.

The third value is  $M_{oxid(l)}$ , the average molar mass of the liquid portion of the sample produced by the  $N_2O_3$  oxidation method. However, Eq. (78) shows that  $M_{oxid(l)}$  is a function of  $K_{O_2 \text{ in } N_2O_4}$  and  $P_{O_2,3}$ , which are accounted for above.

Based on these observations, it is likely that the authors of the MIL-SPEC equation either did not have access to data on O<sub>2</sub> solubility in N<sub>2</sub>O<sub>4</sub>, determined the solubility factor 0.15 empirically, or both.

Another possibility is that the authors of the MIL-SPEC found that the ratio  $\frac{m_{oxid(l),3}}{m_{MON,2}}$  had a value of 0.924, resulting in a solubility factor of 0.15. However, as noted earlier, our best calculation showed that the  $\frac{m_{oxid(l),3}}{m_{MON,2}}$  ratio actually ranged from 1 to 1.2. Also, intuitively, it makes more sense for the numerator, the liquid portion of the oxidation sample, to have a larger mass than the total MON sample, due to the addition of oxygen during the oxidation method and the negligible mass of gas relative to the mass of the liquid. Finally, the mass of the liquid portion of the oxidation method sample will vary depending on MON composition, so this ratio should not be a constant. Therefore the value of 0.924 is likely to be inaccurate.

For the intended accuracy of the N<sub>2</sub>O<sub>3</sub> oxidation method, a difference of 0.0124 in the solubility factor, between our calculated value of 0.1624 and the MIL-SPEC value of 0.15, is negligible. For example, a sample that the MIL-SPEC equation would conclude as being MON-11.03 would instead be shown as MON-11.0424, based on this solubility factor option. However, due to the limitations of significant figures, our calculation is limited to three significant figures such that this would be considered as MON-11.0.

### 6.3 Option 2: $m_{oxid(l),3} = m_{oxid,3}$

The next simplest assumption is to state that the mass of the liquid portion of the N<sub>2</sub>O<sub>3</sub> oxidation method sample is equal to the total mass of the N<sub>2</sub>O<sub>3</sub> oxidation method sample:

$$m_{oxid(l),3} = m_{oxid,3} \quad (89)$$

Or:

$$\frac{m_{oxid(l),3}}{m_{MON,2}} = \frac{m_{oxid,3}}{m_{MON,2}} \quad (90)$$

This assumption is relatively accurate, because the mass of the vapor in the sample vessel after the N<sub>2</sub>O<sub>3</sub> oxidation method is small relative to the mass of the liquid, such that the liquid portion comprises of the vast majority of the total N<sub>2</sub>O<sub>3</sub> oxidation method sample.

Under this particular assumption, the solubility factor can be expressed as:

$$S = 0.1624 \cdot \frac{m_{oxid,3}}{m_{MON,2}} \quad (91)$$

This equation is advantageous to the previous version because the mass of the N<sub>2</sub>O<sub>3</sub> oxidation method sample,  $m_{oxid,3}$ , is measured and readily available. Therefore, this solubility factor is easily calculated while taking into account the growth of the N<sub>2</sub>O<sub>3</sub> oxidation method sample with increasing MON composition. (As stated in Section 5.4, for a given initial liquid MON mass ( $m_{MON(l),2}$ ), the higher the NO weight percent, the more O<sub>2</sub> ( $m_{O_2,react(l),2}$ ) will react during the N<sub>2</sub>O<sub>3</sub> oxidation method, and thus the more liquid N<sub>2</sub>O<sub>4</sub> will exist in the sample after the N<sub>2</sub>O<sub>3</sub> oxidation method ( $m_{N_2O_4(l),3}$ ). This will result in a larger liquid portion of the N<sub>2</sub>O<sub>3</sub> oxidation sample mass ( $m_{oxid(l),3}$ ), and a larger  $\frac{m_{oxid(l),3}}{m_{MON,2}}$  ratio. Therefore, the solubility factor is not a constant value, and changes slightly depending on the MON composition of the sample.)

For example, a sample of MON-11.03 had a calculated solubility factor of 0.1726, which was 15.1% larger than the 0.15 value seen in the MIL-SPEC equation.

#### 6.4 Option 3: $m_{N_2O_4(l),3} = m_{N_2O_4,3}$

The next most accurate assumption is that the gaseous component of N<sub>2</sub>O<sub>4</sub> in the sample vessel after the N<sub>2</sub>O<sub>3</sub> oxidation method is negligible compared to the liquid component of N<sub>2</sub>O<sub>4</sub> in the sample vessel, such that the liquid component of the N<sub>2</sub>O<sub>4</sub> can be considered as equivalent to the total mass of N<sub>2</sub>O<sub>4</sub>. Note that this assumption was already made early on in the derivation of the MIL-SPEC equation, in Eq. (54):

$$m_{N_2O_4(l),3} = m_{N_2O_4,3} \quad (54)$$

Based on this assumption, as stated in Eq. (56),  $m_{oxid(l),3}$  can be expressed as:

$$m_{oxid(l),3} = m_{N_2O_4,3} + m_{O_2(d),3} = m_{MON,2} + m_{O_2,react,2} + m_{O_2(d),3} \quad (56)$$

Entering  $m_{oxid(l),3}$  from Eq. (56) into a  $\frac{m_{oxid(l),3}}{m_{MON,2}}$  ratio as seen in and Eq. (82) will produce:

$$\frac{m_{oxid(l),3}}{m_{MON,2}} = \frac{m_{MON,2} + m_{O_2,react,2} + m_{O_2(d),3}}{m_{MON,2}} = 1 + \frac{m_{O_2,react,2}}{m_{MON,2}} + \frac{m_{O_2(d),3}}{m_{MON,2}} \quad (92)$$

This can be further simplified by expressing  $\frac{m_{O_2(d),3}}{m_{MON,2}}$  in terms of  $\frac{m_{O_2,react,2}}{m_{MON,2}}$ . Combining Eq. (68) and

Eq. (82) produces:

$$S = 187.5 \cdot \frac{m_{O_2(d),3}}{m_{MON,2}} = 0.1624 \cdot \frac{m_{oxid(l),3}}{m_{MON,2}} \quad (93)$$

Substituting  $\frac{m_{oxid(l),3}}{m_{MON,2}}$  from Eq. (92) into Eq. (93), and then solving for  $\frac{m_{O_2(d),3}}{m_{MON,2}}$ , produces:

$$\frac{m_{O_2(d),3}}{m_{MON,2}} = (8.667E - 4) + (8.667E - 4) \frac{m_{O_2,react,2}}{m_{MON,2}} \quad (94)$$

Entering  $\frac{m_{O_2(d),3}}{m_{MON,2}}$  from Eq. (94) into Eq. (92), and simplifying, produces:

$$\frac{m_{oxid(l),3}}{m_{MON,2}} = 1.0009 + 1.0009 \frac{m_{O_2,react,2}}{m_{MON,2}} \quad (95)$$

Recall Eq. (3838), which relates the mass of the reacted NO to the mass of the reacted O<sub>2</sub>:

$$m_{NO} = a \cdot m_{O_2,react} = 1.875 \cdot m_{O_2,react} \quad (3838)$$

Solving for  $m_{O_2,react}$ , and applying the standard convention for the variable subscripts produces:

$$m_{O_2,react,2} = \frac{m_{NO,1}}{1.875} \quad (96)$$

Entering  $m_{O_2,react,2}$  from Eq. (96) into Eq. (95) produces:

$$\frac{m_{oxid(l),3}}{m_{MON,2}} = 1.0009 + \frac{1.0009}{1.875} \frac{m_{NO,1}}{m_{MON,2}} \quad (97)$$

$$\frac{m_{oxid(l),3}}{m_{MON,2}} = 1.0009 + 0.5338 \frac{m_{NO,1}}{m_{MON,2}} \quad (98)$$

Or in other words:

$$\frac{m_{oxid(l),3}}{m_{MON,2}} = 1.0009 + 0.005338 \cdot (NO \text{ wt } \%) \quad (99)$$

This shows that as the NO weight percentage (i.e. the MON composition) of the sample increases, the  $\frac{m_{oxid(l),3}}{m_{MON,2}}$  ratio also increases, at a rate of 0.005338 (dimensionless) per 1% of NO increase.

Entering  $\frac{m_{oxid(l),3}}{m_{MON,2}}$  from Eq. (99) back into Eq. (82) produces:

$$S = 0.1624 \cdot (1.0009 + 0.005338 \cdot (NO \text{ wt } \%)) \quad (100)$$

$$S = 0.1625 + 0.000867 \cdot (NO \text{ wt } \%) \quad (101)$$

Thus, the solubility factor is linearly related to the NO weight percentage of the MON sample (i.e. the MON composition). Similar to the result in Option 2, the solubility factor is not a constant value, and ranges from 0.1625 for MON-0 to 0.197 for MON-40. This differs from the MIL-SPEC equation, in which the solubility factor remains constant at 0.15.

For example, a sample of MON-11.03 had a calculated solubility factor of 0.172, which was 14.7% larger than the 0.15 value seen in the MIL-SPEC equation.

## 6.5 Option 4: Solving the Oxidation Method System

In order to check the validity of the assumptions made in the previous derivations, all of the values listed as relatively negligible should be solved for and shown to truly be negligible. This is done by identifying a system of equations that dictate the relations between the many variables in the N<sub>2</sub>O<sub>3</sub> oxidation method and MON synthesis.

The additional objective is to calculate the mass of the liquid portion of the N<sub>2</sub>O<sub>3</sub> oxidation sample ( $m_{grav(l),3}$ ) without needing to make any assumptions and neglect any variables. This will provide the most accurate calculation of the solubility factor, based on Eq. (82).

### 6.5.1 Stoichiometric Relations

In this section, the stoichiometric equations of MON synthesis and the  $N_2O_3$  oxidation method are used to produce equations for several unknown quantities.

First, some of the relevant known variables that we have measured are the masses of the  $N_2O_4$  initially added during MON synthesis ( $m_{N_2O_4,1}$ ), the MON produced ( $m_{MON,2}$ ), and the  $O_2$  added during the  $N_2O_3$  oxidation method ( $m_{O_2,2}$ ). These values mean that we also have the numbers of moles of the  $N_2O_4$  initially added during MON synthesis ( $n_{N_2O_4,1}$ ) and the  $O_2$  added during the  $N_2O_3$  oxidation method ( $n_{O_2,2}$ ).

We do not know the number of moles of MON because MON is a mixture of  $N_2O_3$  and  $N_2O_4$ . We do not know the MON composition of the sample prior to analysis and therefore do not know the average molar mass of the mixture required to find the number of moles. Also, although we have measured the mass of NO initially added during MON synthesis ( $m_{NO,1}$ ), the goal of this section is to calculate that value independently, similar to the  $N_2O_3$  oxidation method, so it is treated as an unknown quantity.

The unknown variables that we wish to quantify are the numbers of moles of NO initially added during MON synthesis ( $n_{NO,1}$ ), unreacted  $N_2O_4$  after the MON synthesis ( $n_{N_2O_4,2}$ ), MON created by the MON synthesis ( $n_{MON,2}$ ),  $N_2O_4$  remaining after the  $N_2O_3$  oxidation method ( $n_{N_2O_4,3}$ ), and  $O_2$  remaining after the  $N_2O_3$  oxidation method ( $n_{O_2,3}$ ). These variables will be expressed as functions of each other and the known variables listed above.

As stated at the beginning of the MIL-SPEC equation derivation, the dominant stoichiometric equation for MON synthesis is:



And the stoichiometric equation for the  $N_2O_3$  oxidation method is:



Multiple relationships were determined between all of the listed numbers of moles across the two processes. Note that these are the number of moles that react with each other in a complete reaction,

driven to the products side by the addition of an oxygen excess. Refer to Figure 38 for the justification of this equation.

$$n_{NO,1} = 2 \cdot n_{N_2O_4,reacted,1} = n_{N_2O_3,2} = 2 \cdot n_{O_2,reacted,2} = n_{N_2O_4,created,3} \quad (32)$$

As stated earlier, it is important to note that  $n_{N_2O_4,reacted,1}$  is the moles of  $N_2O_4$  that reacted with the NO, which is different from  $n_{N_2O_4,1}$ , the total  $N_2O_4$  used during synthesis. Likewise, it should be noted that  $n_{O_2,reacted,2}$  is the moles of  $O_2$  that reacted with the  $N_2O_3$  during the oxidation method, which is different from  $n_{O_2,2}$ , the total  $O_2$  that was added to the sample vessel during the oxidation method. Also,  $n_{N_2O_4,created,3}$  is the moles of  $N_2O_4$  that was created by the addition of  $O_2$  during the oxidation method, which is different from  $n_{N_2O_4,3}$ , the total  $N_2O_4$  in the sample vessel after the oxidation method. Because the all of NO added during synthesis is completely consumed, and because all of the  $N_2O_3$  created during synthesis is completely consumed during the oxidation method, there is no need for that distinction with these two variables.

Next, we will use these relationships to express the number of moles of certain components in terms of other components that we have measured.

First, we express the number of moles of MON after the MON synthesis as the sum of the  $N_2O_3$  created by the NO addition, plus the remaining, unreacted  $N_2O_4$ . Based on Eq. (32),  $N_2O_3$  and NO addition have a 1-to-1 mole ratio such that:

$$n_{MON,2} = n_{N_2O_3,2} + n_{N_2O_4,2} = n_{NO,1} + n_{N_2O_4,2} \quad (102)$$

Remaining, unreacted  $N_2O_4$  after the MON synthesis can be expressed as the number of initial moles of  $N_2O_4$  minus the moles of  $N_2O_4$  that have reacted to the NO addition. Based on Eq. (32), reacted  $N_2O_4$  and NO addition have a 2-to-1 mole ratio such that:

$$n_{N_2O_4,2} = n_{N_2O_4,1} - n_{N_2O_4,reacted,1} = n_{N_2O_4,1} - \frac{1}{2}n_{NO,1} \quad (103)$$

Entering  $n_{N_2O_4,2}$  from Eq. (103) into Eq. (102) produces an equation for the number of moles of MON after MON synthesis as:

$$n_{MON,2} = n_{NO,1} + (n_{N_2O_4,1} - \frac{1}{2}n_{NO,1}) = \frac{1}{2}n_{NO,1} + n_{N_2O_4,1} \quad (104)$$

Eq. (104) can then be used to express the moles of NO added during MON synthesis as:

$$n_{NO,1} = 2 \cdot n_{MON,2} - 2 \cdot n_{N_2O_4,1} \quad (105)$$

Next, we can enter  $n_{NO,1}$  from Eq. (105) into Eq. (103) to express the moles of remaining, unreacted  $N_2O_4$  after the MON synthesis as:

$$n_{N_2O_4,2} = n_{N_2O_4,1} - \frac{1}{2}(2 \cdot n_{MON,2} - 2 \cdot n_{N_2O_4,1}) = 2 \cdot n_{N_2O_4,1} - n_{MON,2} \quad (106)$$

Next, we can express the average molar mass of MON as the sum of the molar masses of  $N_2O_4$  and  $N_2O_3$  multiplied by their respective mole fractions, under the assumption that they are the two only components in the MON mixture:

$$M_{MON,2} = M_{N_2O_4} \cdot x_{N_2O_4,2} + M_{N_2O_3} \cdot x_{N_2O_3,2} \quad (107)$$

$$M_{MON,2} = M_{N_2O_4} \left( \frac{n_{N_2O_4,2}}{n_{MON,2}} \right) + M_{N_2O_3} \left( 1 - \frac{n_{N_2O_4,2}}{n_{MON,2}} \right) \quad (108)$$

Entering  $n_{N_2O_4,2}$  from Eq. (106) into Eq. (108) produces:

$$M_{MON,2} = M_{N_2O_4} \left( 2 \frac{n_{N_2O_4,1}}{n_{MON,2}} - 1 \right) + M_{N_2O_3} \left( 2 - 2 \frac{n_{N_2O_4,1}}{n_{MON,2}} \right) \quad (109)$$

Next, we can enter  $M_{MON,2}$  from Eq. (109) into the equation for the moles of MON after MON synthesis to produce:

$$n_{MON,2} = \frac{m_{MON,2}}{M_{MON,2}} = \frac{m_{MON,2}}{M_{N_2O_4} \left( 2 \frac{n_{N_2O_4,1}}{n_{MON,2}} - 1 \right) + M_{N_2O_3} \left( 2 - 2 \frac{n_{N_2O_4,1}}{n_{MON,2}} \right)} \quad (110)$$

Simplifying the equation for  $n_{MON,2}$  produces:

$$n_{MON,2} = \frac{m_{MON,2} + n_{N_2O_4,1} (2 \cdot M_{N_2O_3} - 2 \cdot M_{N_2O_4})}{(2 \cdot M_{N_2O_3} - M_{N_2O_4})} \quad (111)$$

Next, we can express the moles of  $N_2O_4$  remaining after the  $N_2O_3$  oxidation method as the sum of the  $N_2O_4$  in the MON plus the  $N_2O_4$  produced by the  $O_2$  addition during the  $N_2O_3$  oxidation method. Based on Eq. (32),  $N_2O_4$  produced and the NO added during the MON synthesis have a 1-to-1 ratio such that:

$$n_{N_2O_4,3} = n_{N_2O_4,2} + n_{N_2O_4,created,3} = n_{N_2O_4,2} + n_{NO,1} \quad (112)$$

$n_{NO,1}$  from Eq. (105) can be entered into Eq. (112) to produce:

$$n_{N_2O_4,3} = n_{N_2O_4,2} + 2 \cdot n_{MON,2} - 2 \cdot n_{N_2O_4,1} \quad (113)$$

Finally, we can express the moles of  $O_2$  remaining after the  $N_2O_3$  oxidation method as the  $O_2$  added at the start of the  $N_2O_3$  oxidation method minus the  $O_2$  that is consumed by the  $N_2O_3$  oxidation method reaction between  $O_2$  and  $N_2O_3$ . Based on Eq. (32), reacted  $O_2$  and NO addition have a 2-to-1 mole ratio such that:

$$n_{O_2,3} = n_{O_2,2} - n_{O_2,reacted,2} = n_{O_2,2} - \frac{1}{2}n_{NO,1} \quad (114)$$

$n_{NO,1}$  from Eq. (105) can be entered into Eq. (114) to produce:

$$n_{O_2,3} = n_{O_2,2} - \frac{1}{2}(2 \cdot n_{MON,2} - 2 \cdot n_{N_2O_4,1}) = n_{O_2,2} - n_{MON,2} + n_{N_2O_4,1} \quad (115)$$

Now, we have expressed the numbers of moles of NO initially added during MON synthesis ( $n_{NO,1}$ ), unreacted  $N_2O_4$  after the MON synthesis ( $n_{N_2O_4,2}$ ), MON created by the MON synthesis ( $n_{MON,2}$ ),  $N_2O_4$  remaining after the  $N_2O_3$  oxidation method ( $n_{N_2O_4,3}$ ), and  $O_2$  remaining after the  $N_2O_3$  oxidation method ( $n_{O_2,3}$ ) as functions of each other and the known variables:  $N_2O_4$  initially added during MON synthesis ( $n_{N_2O_4,1}$ ),  $O_2$  added during the  $N_2O_3$  oxidation method ( $n_{O_2,2}$ ), and MON created ( $n_{MON,2}$ ).

Using these equations, we can first calculate the number of moles of MON created by the MON synthesis ( $n_{MON,2}$ ) by using Eq. (111), then the number of moles of unreacted  $N_2O_4$  after the MON synthesis ( $n_{N_2O_4,2}$ ) by using Eq. (106), then the number of moles of  $N_2O_4$  remaining after the  $N_2O_3$  oxidation method ( $n_{N_2O_4,3}$ ) by using Eq. (113), and finally the number of moles of  $O_2$  remaining

after the  $N_2O_3$  oxidation method ( $n_{O_2,3}$ ) by using Eq. (115). The final two values ( $n_{N_2O_4,3}$  and  $n_{O_2,3}$ ) will be used in the final calculations.

### 6.5.2 Phase Relations

In this section, the phase relations between the components in the sample after the  $N_2O_3$  oxidation method are used to produce equations for several unknown quantities.

First, some of the relevant known variables that we have measured are the total volume of the vessel ( $V_{total}$ ), the pressure of the  $O_2$  gas in the vessel ( $P_{O_2(g)}$ ), the pressure of the  $N_2O_4$  gas in the vessel ( $P_{N_2O_4(g)}$ ), the vessel temperature ( $T$ ), and the density of  $N_2O_4$  at this temperature ( $\rho_{N_2O_4}$ ). As previously stated, the number of moles of  $N_2O_4$  remaining after the  $N_2O_3$  oxidation method ( $n_{N_2O_4,3}$ ) and the number of moles of  $O_2$  remaining after the  $N_2O_3$  oxidation method ( $n_{O_2,3}$ ) were calculated in the previous section, and are thus considered as known variables to be used in the final calculations.

The unknown variables that we wish to quantify are the number of moles of liquid  $N_2O_4$  remaining after the  $N_2O_3$  oxidation method ( $n_{N_2O_4(l),3}$ ), the volume of liquid in the vessel after the  $N_2O_3$  oxidation method ( $V_{(l),3}$ ), the volume of gas in the vessel after the  $N_2O_3$  oxidation method ( $V_{(g),3}$ ), the number of moles of gaseous  $O_2$  remaining in the headspace after the  $N_2O_3$  oxidation method ( $n_{O_2(g),3}$ ), the number of moles of  $O_2$  dissolved in the liquid  $N_2O_4$  after the  $N_2O_3$  oxidation method ( $n_{O_2(d),3}$ ), and the mass of liquid in the vessel after the  $N_2O_3$  oxidation method ( $m_{oxid(l),3}$ ).

First, consider the diagram below:

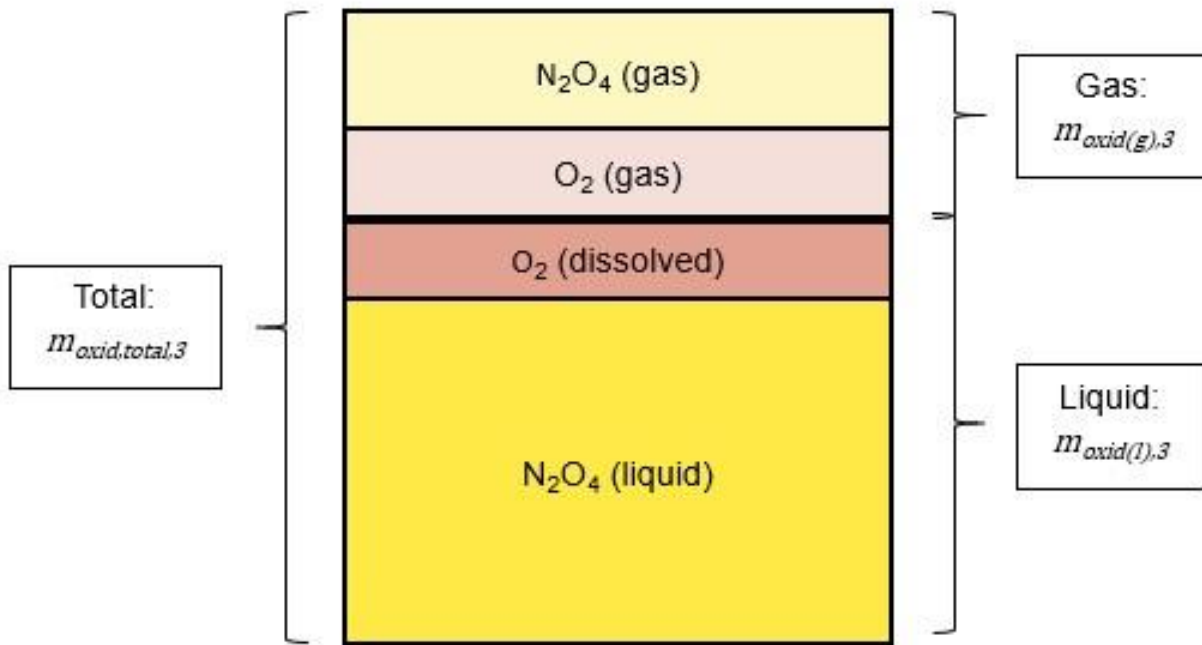


Figure 39. Phase Relations in  $N_2O_3$  Oxidation Method Sample

The diagram shows the components in the  $N_2O_3$  oxidation method sample. The total sample ( $m_{oxid,total,3}$ ) comprises of a gaseous ( $m_{oxid(g),3}$ ) and liquid ( $m_{oxid(l),3}$ ) portion. The gaseous portion comprises of a gaseous  $N_2O_4$  ( $m_{N_2O_4(g),3}$ ) and a gaseous  $O_2$  ( $m_{O_2(g),3}$ ) component, while the liquid portion comprises of a liquid  $N_2O_4$  ( $m_{N_2O_4(l),3}$ ) and dissolved  $O_2$  ( $m_{O_2(d),3}$ ) component.

First, we can express the total volume of the vessel as the sum of the gas volume and liquid volume:

$$V_{total} = V_{(g),3} + V_{(l),3} \quad (116)$$

The gas volume can be expressed using the ideal gas law:

$$V_{(g),3} = \frac{n_{O_2(g),3} \cdot R \cdot T}{P_{O_2(g)}} = \frac{n_{N_2O_4(g),3} \cdot R \cdot T}{P_{N_2O_4(g)}} \quad (117)$$

The liquid volume can be expressed using the density of  $N_2O_4$ :

$$V_{(l),3} = \frac{n_{N_2O_4(l),3} \cdot M_{N_2O_4}}{\rho_{N_2O_4}} \quad (118)$$

Entering  $V_{(g),3}$  and  $V_{(l),3}$  from Eq. (117) and (118) into Eq. (116) produces:

$$V_{total} = \frac{n_{N_2O_4(g),3} \cdot R \cdot T}{P_{N_2O_4(g)}} + \frac{n_{N_2O_4(l),3} \cdot M_{N_2O_4}}{\rho_{N_2O_4}} \quad (119)$$

The total number of moles of  $N_2O_4$  in the sample can be expressed as the sum of the liquid and gaseous numbers of moles of  $N_2O_4$ :

$$n_{N_2O_4,3} = n_{N_2O_4(l),3} + n_{N_2O_4(g),3} \quad (120)$$

$$n_{N_2O_4(g),3} = n_{N_2O_4,3} - n_{N_2O_4(l),3} \quad (121)$$

Entering  $n_{N_2O_4(g),3}$  from Eq. (121) into Eq. (119) and solving for  $n_{N_2O_4(l),3}$  produces:

$$V_{total} = \frac{(n_{N_2O_4,3} - n_{N_2O_4(l),3}) \cdot R \cdot T}{P_{N_2O_4(g)}} + \frac{n_{N_2O_4(l),3} \cdot M_{N_2O_4}}{\rho_{N_2O_4}} \quad (122)$$

$$n_{N_2O_4(l),3} = \frac{V_{total} - \frac{n_{N_2O_4,3} \cdot R \cdot T}{P_{N_2O_4(g)}}}{\frac{M_{N_2O_4}}{\rho_{N_2O_4}} - \frac{R \cdot T}{P_{N_2O_4(g)}}} \quad (123)$$

This equation for  $n_{N_2O_4(l),3}$  is solvable, given that all of the variables in the equation are known, including  $n_{N_2O_4,3}$  which was determined in the previous section via stoichiometric relations.

Next, by working backwards, much of the unknown variables can be calculated. Now that  $n_{N_2O_4(l),3}$  is known, we can use Eq. (118) to solve for the liquid volume in the  $N_2O_3$  oxidation sample ( $V_{(l),3}$ ). Then we can use a form of Eq. (116) to solve for the gas volume ( $V_{(g),3}$ ):

$$V_{(g),3} = V_{total} - V_{(l),3} = V_{total} - \frac{M_{N_2O_4}}{\rho_{N_2O_4}} \left( \frac{V_{total} - \frac{n_{N_2O_4,3} \cdot R \cdot T}{P_{N_2O_4(g)}}}{\frac{M_{N_2O_4}}{\rho_{N_2O_4}} - \frac{R \cdot T}{P_{N_2O_4(g)}}} \right) \quad (124)$$

Then we can use a form of Eq. (117) to solve for the number of moles of gaseous  $O_2$  remaining in the headspace after the  $N_2O_3$  oxidation method:

$$n_{O_2(g),3} = \frac{P_{O_2(g)}}{R \cdot T} \cdot V_{(g),3} = \frac{P_{O_2(g)}}{R \cdot T} \left[ V_{total} - \frac{M_{N_2O_4}}{\rho_{N_2O_4}} \left( \frac{V_{total} - \frac{n_{N_2O_4,3} \cdot R \cdot T}{P_{N_2O_4(g)}}}{\frac{M_{N_2O_4}}{\rho_{N_2O_4}} - \frac{R \cdot T}{P_{N_2O_4(g)}}} \right) \right] \quad (125)$$

Then we can solve for the number of moles of O<sub>2</sub> dissolved in the liquid N<sub>2</sub>O<sub>4</sub> after the N<sub>2</sub>O<sub>3</sub> oxidation method ( $n_{O_2(d),3}$ ), by using the relation between the dissolved O<sub>2</sub> and the gaseous O<sub>2</sub>:

$$n_{O_2,3} = n_{O_2(g),3} + n_{O_2(d),3} \quad (126)$$

$$n_{O_2(d),3} = n_{O_2,3} - n_{O_2(g),3} \quad (127)$$

Finally, the mass of liquid in the vessel after the N<sub>2</sub>O<sub>3</sub> oxidation method ( $m_{oxid(l),3}$ ) can be found as the sum of the liquid N<sub>2</sub>O<sub>4</sub> mass,  $n_{N_2O_4(l),3}$  (Eq. 123) and the dissolved O<sub>2</sub> mass (Eq. 127):

$$m_{oxid(l),3} = M_{N_2O_4} \cdot n_{N_2O_4(l),3} + M_{O_2} \cdot n_{O_2(d),3} \quad (128)$$

This  $m_{oxid(l),3}$  can then be used to find the actual solubility factor which affects the MON composition of the MON sample, via Eq. (82).

$$S = 0.1624 \cdot \frac{m_{oxid(l),3}}{m_{MON,2}} \quad (82)$$

Thus all of the components in the N<sub>2</sub>O<sub>3</sub> oxidation method have been or can be calculated using these equations, and a truly accurate solubility factor can be calculated.

The three variable numbers needed were the NO mass used during production, the N<sub>2</sub>O<sub>4</sub> mass used during production, and the O<sub>2</sub> mass adding during the oxidation method. Clearly, the first two values would not be available in the field, when trying to assess a batch of MON such as the MIL-SPEC equation does, but this calculation is more so to calculate the most accurate solubility factor possible to validate one (or several) of the options listed earlier in this report, and as a demonstration of the inner workings of the oxidation method.

In order to validate that this method is viable, an example calculation was done. The NO mass, N<sub>2</sub>O<sub>4</sub> mass, and O<sub>2</sub> mass values were taken from our final and most accurate test. Test data is necessary because, although the NO masses and N<sub>2</sub>O<sub>4</sub> masses can be set arbitrarily, such as with vectors across a range of values, the O<sub>2</sub> mass cannot be easily predicted. It could be calculated based on the first two numbers, but doing so would require a solubility factor. Thus, test data was used in this example.

For an example calculation of a sample with a NO weight percentage of 11.0288, this method back-calculated an NO weight percentage of 10.8812, resulting in an error of 1.33%. This was surprisingly low, given that it could be the result of a variety of reasons such as measurement and procedural inaccuracies rather than the calculation method itself. This indicated that the method was likely viable.

The final result of that calculation was a solubility factor of 0.1717. Compared to this value, the solubility factor in the MIL-SPEC equation has an error of 12.6% at MON-11, even though the difference between the two is only 0.0217%. Relative to the value of the NO weight percentage of 11%, this discrepancy only produces an error of 0.197%, demonstrating that it is rather negligible.

This value of 0.1717 is very similar to the solubility factors of option 3 (0.1721) and option 2 (0.1655).

## 7. EXPERIMENTAL DATA AND ANALYSIS

Five trials were conducted and recorded, to test the accuracy of the  $\text{N}_2\text{O}_3$  oxidation method for determining MON composition. The results of those tests are shown in Figure 40. The axes are the MON's actual composition as calculated via the weighing method during production, and the MON's measured composition as calculated via the oxidation method and MIL-SPEC equation. The diagonal line represents the theoretical case in which both values for a sample equal each other, meaning that the oxidation method is perfectly accurate. Datapoints above this line signify that the oxidation method produced too high of a NO content percentage, while datapoints below this line signify that the oxidation method produced too low of an NO content percentage.

A Matlab class called Uncertainty Propagation Class (UC) was used to allow error propagation through calculations.[112] The black lines surrounding each datapoint are their associated error bars.

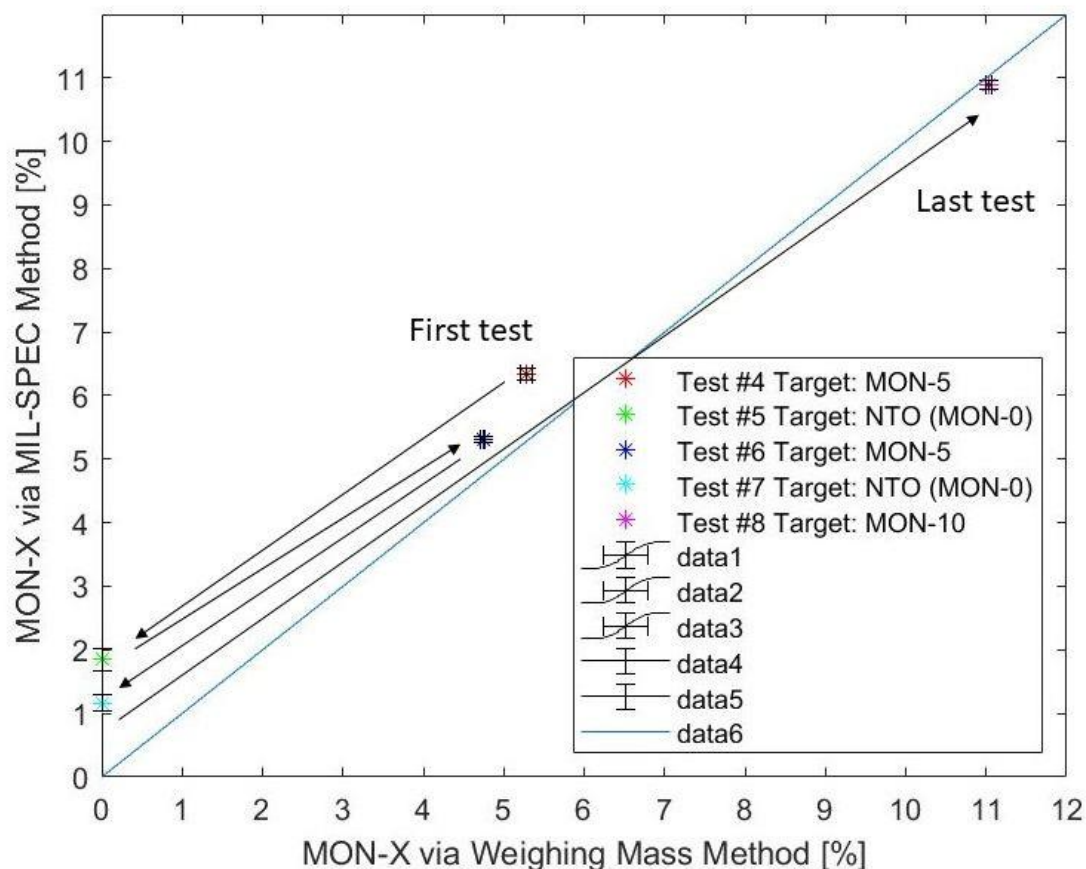


Figure 40. MON Composition via Mass Method vs. MON Composition via Oxidation Method

The plot implies that the accuracy of the oxidation method increases with higher NO content, although more data points are necessary to confirm this observation. Also, it should be noted that the accuracy of the oxidation method increased chronologically, from the first test to the last test. This was likely because the testing procedure was modified several times to increase the accuracy, as the team became more familiar with the process. However, despite the limited number of tests that we were able to conduct, a very accurate result was produced in the last test.

Ideally, the span of error bars would include the expected value for each data point. However, at no point did the error bars in Figure 40 span across the diagonal line which represents the expected value. This implies that, despite our attempts at accounting for uncertainty, there are other unknown phenomena at play that are causing the resulting data to miss the diagonal line. An example of a known phenomenon that was discovered to cause such error was water

contamination. Minimizing water contamination did result in improved accuracy. However, this likely means that there are other sources of error that have yet to be uncovered and mitigated. Further testing and scrutiny are needed to address the additional sources of error.

Next, the solubility factor was calculated for each of the tests, using the MIL-SPEC equation and four proposed alternatives. These values are shown in Figure 41. The MIL-SPEC solubility factor is labeled as “ $S_{MS}$ ”. The solubility factor from Section 6.2 (also referred to as “Option 1”) is labeled as “S1”. The solubility factor from Section 6.3 (also referred to as “Option 2”) is labeled as “S2”. The solubility factor from Section 6.4 (also referred to as “Option 3”) is labeled as “S3”. The solubility factor from Section 6.5 (also referred to as “Option 4”) is labeled as “S4”.

The plot shows that the current solubility factor of 0.15 is relatively adequate, although slight modifications can improve its accuracy. Calculating S3 and S4 would not be possible during the oxidation method, since the NO weight percentage and mass of the liquid in the gravimetric sample are not directly or easily measurable. S1 and S2, however, are simple alternatives to the current value of 0.15.

Also, it should be noted that different assumptions produced different results of varying increase in accuracy. For instance, the jump from  $S_{MS}$  to S1 produced more significant improvements than the jump from S2 to S3. Thus, the results may exhibit diminishing returns for increases in complexity.

Because these curves are expected to be linear, one can use the expected trends to estimate the solubility factors that are calculated for each method, for MON compositions up to MON 40. These values are plotted to further illustrate the varying validity of the calculation methods at different MON compositions, shown in Figure 42. Here it is more apparent that, at lower NO weight percentages, the discrepancies between the constant solubility factors and the changing solubility factors are smaller, but they increase as the NO weight percentage also increases.

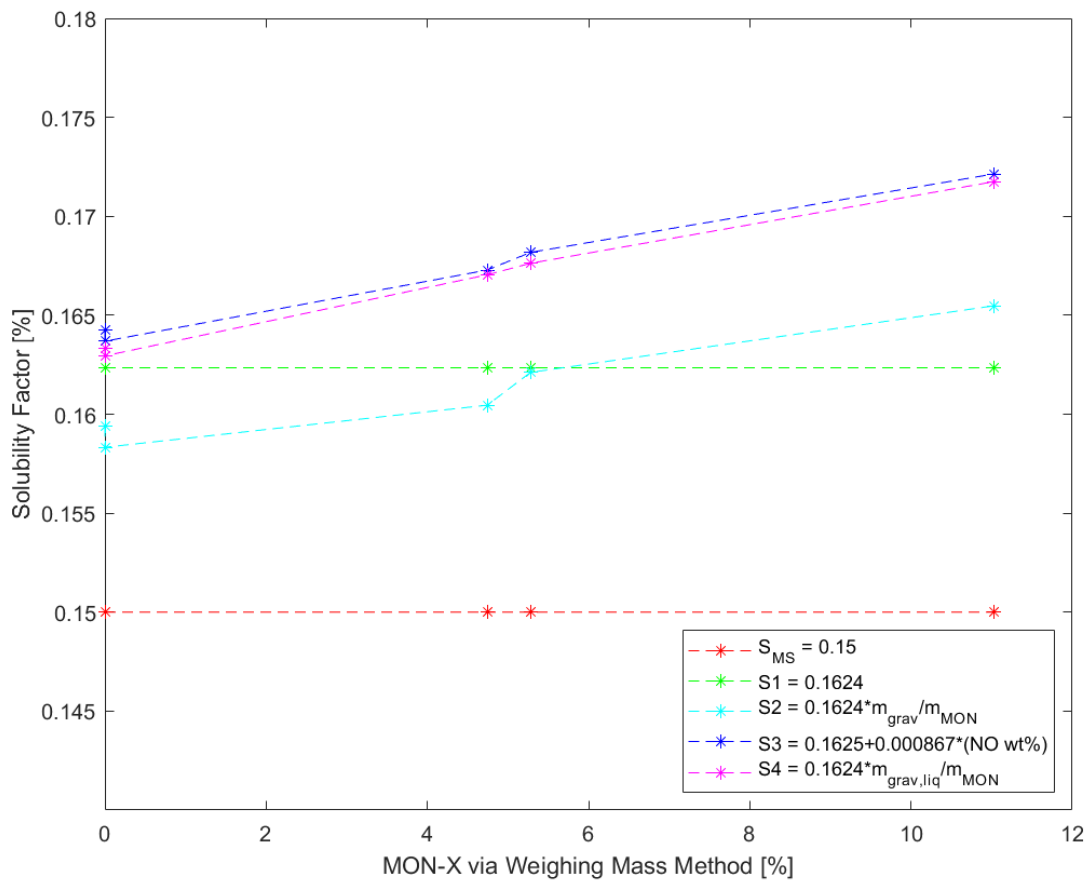


Figure 41. Solubility Factor vs. MON Composition

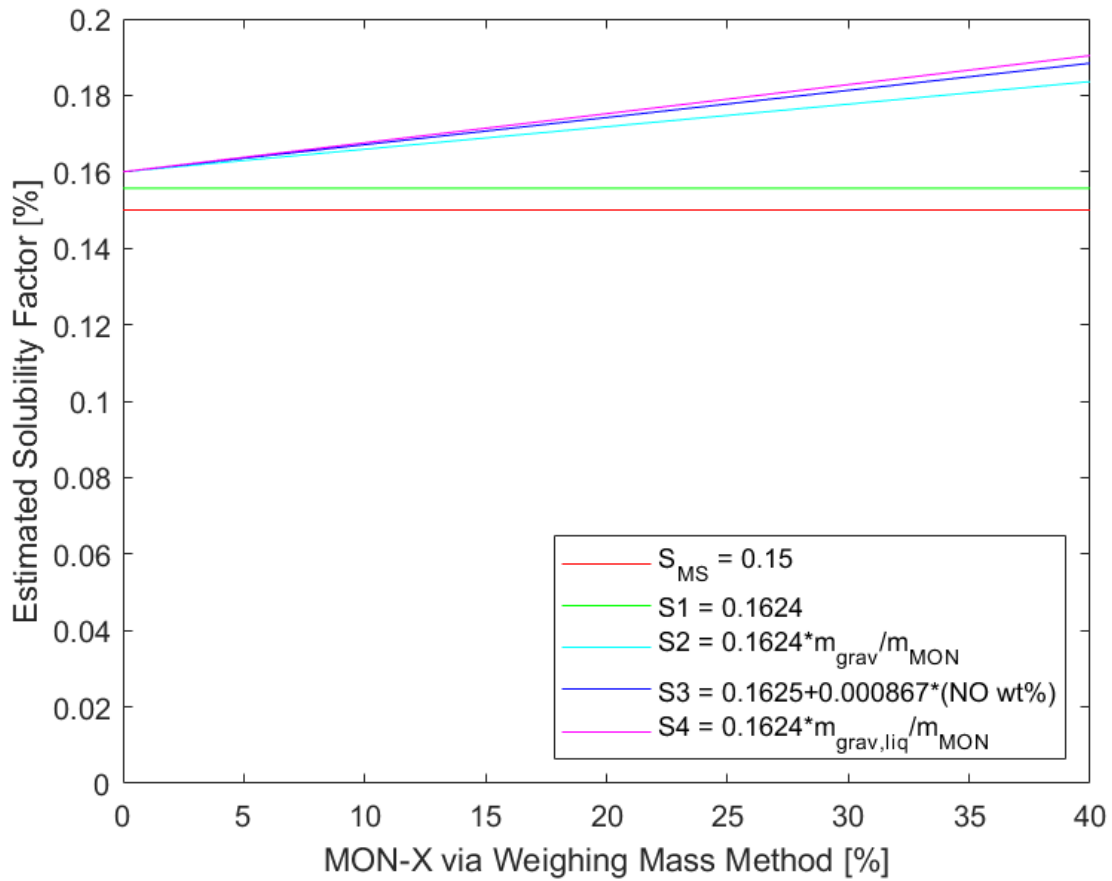


Figure 42. Expected Solubility Factor Trend Curves vs. MON Composition up to MON-40

## 8. DISCUSSION AND CONCLUSIONS

The results of this work accomplished several goals. First, the MIL-SPEC equation was derived, and the synthesis process and the oxidation method were studied and thoroughly understood. Next, several alterations of the equation were suggested. Finally, samples of MON were synthesized and analyzed by using the oxidation method. These trials demonstrated the capabilities of the test stand and provided an opportunity to analytically compare the alternatives of the MIL-SPEC equation. It was concluded that, although the MIL-SPEC equation is generally sufficient, some minor changes to the equation could produce more accurate results.

Based on the derivations listed in this report, the MIL-SPEC equation can be taken apart, and each layer of the equation can be understood separately. A diagram of this process is shown in Figure 43.

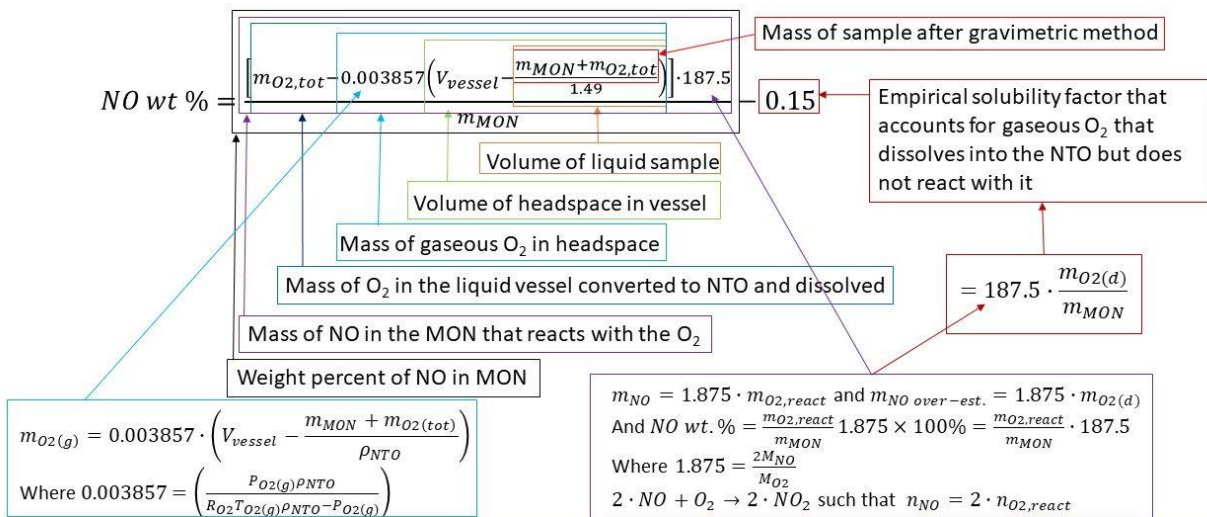


Figure 43. MIL-SPEC Equation Breakdown and Explanation

Beginning with the innermost portion of the equation and moving outwards:

- $m_{MON,2} + m_{O_2,2}$  is the sum of the MON sample mass and the added  $O_2$  mass, which gives the mass of the sample after the  $N_2O_3$  oxidation method is completed.

- $\frac{m_{MON,2}+m_{O_2,2}}{1.49}$  is the  $N_2O_3$  oxidation sample mass divided by the density of liquid  $N_2O_4$ , which gives an approximation of the volume of the liquid in the sample vessel, under the assumption that the vast majority of the mass in the sample vessel is liquid  $N_2O_4$ .
- $V_{vessel} - \frac{m_{MON,2}+m_{O_2,2}}{1.49}$  is the total vessel volume minus the volume of the liquid in the vessel subtracted, which gives the volume of the headspace in the vessel.
- 0.003857 is a value that converts a volume of headspace to the mass of gaseous  $O_2$  in that headspace
- $0.003857 \left( V_{vessel} - \frac{m_{MON,2}+m_{O_2,2}}{1.49} \right)$  is the previously mentioned conversion value multiplied by the volume of the headspace in the vessel, which gives the mass of gaseous  $O_2$  in the sample vessel.
- $m_{O_2,2} - 0.003857 \left( V_{vessel} - \frac{m_{MON,2}+m_{O_2,2}}{1.49} \right)$  is the total mass of  $O_2$  added during the  $N_2O_3$  oxidation method minus the mass of gaseous  $O_2$  in the sample vessel, which gives the mass of  $O_2$  in the liquid in the sample vessel. This includes  $O_2$  that was used to produce liquid  $N_2O_4$  and  $O_2$  that dissolved in the liquid  $N_2O_4$ .
- 187.5 is a value that converts a mass of reacted  $O_2$  to the corresponding mass of NO that created the  $N_2O_3$  in the MON sample that reacted with that  $O_2$ . It is multiplied by a factor of 100 to account for the final result of this equation being a percentage and in units of percent.
- $\left[ m_{O_2,2} - 0.003857 \left( V_{vessel} - \frac{m_{MON,2}+m_{O_2,2}}{1.49} \right) \right] \cdot 187.5$  is the previously mentioned conversion value multiplied by the mass of  $O_2$  in the liquid, which gives the corresponding mass of NO that created the  $N_2O_3$  in the MON sample that reacted with that  $O_2$ .
- $\frac{\left[ m_{O_2,2} - 0.003857 \left( V_{vessel} - \frac{m_{MON,2}+m_{O_2,2}}{1.49} \right) \right] \cdot 187.5}{m_{MON,2}}$  is the mass of NO that created the  $N_2O_3$  in the MON sample divided by the MON sample mass, which gives the weight percent of NO in the MON without accounting for the solubility of  $O_2$  in the liquid  $N_2O_4$  during the  $N_2O_3$  oxidation method.
- 0.15 is an empirical solubility factor which accounts for the gaseous  $O_2$  that dissolves in the liquid  $N_2O_4$  during the  $N_2O_3$  oxidation method but does not react with it. It can be

calculated as  $187.5 \cdot \frac{m_{O_2(d),3}}{m_{MON,2}}$  or  $0.1624 \cdot \frac{m_{oxid(l),3}}{m_{MON,2}}$ , both of which are equivalent functions of the NO weight percent of the MON sample.

This analysis sought to fully understand the mechanics and processes behind the MON synthesis and oxidation methods. A variety of methods and assumptions were explored, and an in-depth look was taken at the variety of equations that dictate the processes. By applying all of the relationships and solving them simultaneously, we were able to validate the other options for the solubility factor.

Based on the analysis of the experimental data and the results of the different methods for calculating the solubility factor, we concluded that the MIL-SPEC equation is sufficient for its purposes of providing a relatively accurate way of measuring the composition of a MON sample, while also being easy and quick to implement, both in measurements and in numerical calculation. However, some minor adjustments to the equation could produce consistently more accurate composition measurements without adding any more difficulty or complication. Options 1 and 2 for solubility factor are both viable alternatives that produce slightly more accurate results without much added complexity.

A thorough literature review resulted in a comprehensive depiction of the history of  $N_2O_4$  and MON development, starting with the important ability for  $N_2O_4$  to be storable in room temperature. Adding NO became necessary to reduce the freezing temperature and mitigate the corrosive tendencies of  $N_2O_4$ . A close examination of the current and upcoming uses of  $N_2O_4$ -based oxidizers showed that they are now being used almost extensively in highly refined propulsion systems, such as reaction control systems, liquid apogee engines, in-space primary propulsion systems, and lunar landing systems. These utilizations demand precise burns and delta-V's, such that the chemical composition and physical properties of MON propellant are especially important in order for the systems to produce the desired outcomes. Therefore, the ability to measure the MON composition via the oxidation method and the MIL-SPEC equation is of the utmost importance. Issues with water contamination can be especially troublesome because the presence of water can give the impression that there is more NO in the system than there may actually be, giving a false sense of security regarding freezing temperature reduction and corrosion mitigation. Finally, the date in which the MIL-SPEC equation was first published is unknown. If it had been

devised in 1964, with the first MIL-SPEC document on MON propellant, then it is possible that the authors did not have access to dependable data for the solubility of oxygen in  $N_2O_4$ . This lack of data could have affected the values of the constants in the MIL-SPEC equation.

There were several limitations to these findings. The main limitation was a low number of test samples. The synthesis and oxidation method research were part of a larger project to gather physical property data on MON, which required that the group move on to the next goals. Although synthesis and the oxidation method were understood to a satisfactory degree for the project, the lack of data points does make it difficult to draw meaningful conclusions. Each trial took an entire day, not including preparations taken the day before and analysis done the day after. Thus, these tests were very time-intensive. Only five trials are reported in this work (Tests #4-8), ranging from MON-0 ( $N_2O_4$ ) to MON-11. The changes of the processes at higher NO concentrations had to be extrapolated from the limited data that was available. Also, the synthesis and oxidation procedures were changing with each trial, to make improvements and increase accuracy. Thus, the conditions of each trial were not the same, making it difficult to accurately compare them.

Further research should include far more trials at a multitude of NO concentrations up to at least MON-25, with consistent procedures and conditions for each trial. More tests and scrutiny are needed to identify any other phenomena that are affecting the accuracy of the results (similar to water contamination). A reassessment of the uncertainties may be necessary to determine why the error bars do not span across the expected values in Figure 40. Another option would be to order different levels of MON propellant from manufacturers and then to conduct the oxidation method on samples of those propellants, to determine if the oxidation method results align with the propellant descriptions from the manufacturers. Finally, further research is needed to better understand which propellant transfer processes change the NO content of MON, and to what degree. Having a quantitative understanding of the effects of transferring MON in different ways can lead to better handling and loading practices within the space propulsion industry and academia.

## REFERENCES

- [1] J. Priestley, “Experiments and observations on different kinds of air,” vol. 3, 1777.
- [2] J. D. Clark, *Ignition!: an informal history of liquid rocket propellants*, Third. Rutgers University Press Classics, 2018.
- [3] C. Vaughan, “Apollo reaction control systems,” *Am. Inst. Aeronaut. Astronaut.*, 1968.
- [4] R. E. Johnson, G. F. Kappelt, and L. J. Korb, “A Case History of Titanium Stress Corrosion in Nitrogen Tetroxide,” Manned Spacecraft Center, Houston, Texas, N67-23277, Jan. 1966. [Online]. Available: <https://ntrs.nasa.gov/api/citations/19670013948/downloads/19670013948.pdf>
- [5] M. J. Mueller, “Vapor Pressure Fit for MON Oxidizer Blends Including Accuracy,” presented at the 51st AIAA/SAE/ASEE Joint Propulsion Conference, Orlando, FL, Jul. 2015. doi: 10.2514/6.2015-4159.
- [6] H. Martens, “MON-25 Low and High Temperature Monitor,” AFRPL TR-83-004, Mar. 1983.
- [7] “Performance Specification - Propellants, Dinitrogen Tetroxide,” Department of Defense, MIL-PRF-26539G, Apr. 2017.
- [8] D. B. Brice, “Some Physical Properties for the System Nitrogen Tetroxide-Nitric Oxide,” *ARS J.*, vol. 29, no. 5, pp. 354–357, May 1959, doi: 10.2514/8.4770.
- [9] *International Critical Tables of Numerical Data, Physics, Chemistry and Technology*, vol. IV. National Research Council, 1928. [Online]. Available: [http://reader.library.cornell.edu/docviewer/digital?id=chla2944761\\_2173#page/2/mode/1up](http://reader.library.cornell.edu/docviewer/digital?id=chla2944761_2173#page/2/mode/1up)
- [10] M. T. Constantine, “Engineering Property Determination of Rocket Propellants,” Rocketdyne, Division of North American Rockwell Corporation, AFRPL-TR-70-147, Nov. 1970.
- [11] A. G. Whittaker, R. W. Sprague, S. Skolnik, and G. B. L. Smith, “Vapor Pressures and Freezing Points of the System Nitrogen Tetroxide—Nitric Oxide,” *J. Am. Chem. Soc.*, vol. 74, no. 19, pp. 4794–4797, Oct. 1952, doi: 10.1021/ja01139a021.
- [12] I. R. Beattie and A. J. Vosper, “Dinitrogen trioxide. Part III. The vapour pressure of mixtures of nitrogen dioxide and nitric oxide,” *J. Chem. Soc.*, pp. 4799–4802, Jan. 1960, doi: 10.1039/JR9600004799.

- [13] C. Casci and C. Bruno, “Recent Advances in the Aerospace Sciences.” Plenum Press, 1985. [Online]. Available: <https://link.springer.com/content/pdf/bfm%3A978-1-4684-4298-4%2F1.pdf>
- [14] “ГЛУШКО ВАЛЕНТИН ПЕТРОВИЧ, Категория: Конструкторы (Valentin Petrovich Glushko).” Accessed: Apr. 16, 2021. [Online]. Available: <https://sovkos.ru/constructors/glushko-valentin-petrovich.html>
- [15] “Robert Esnault-Pelterie.” Hulton-Deutsch Collection/CORBIS/Corbis via Getty Images, Jan. 01, 1900. [Online]. Available: <https://www.gettyimages.com/detail/news-photo/robert-esnault-pelterie-news-photo/613465816>
- [16] A. Wright, *USAF Propellant Handbooks - Nitric Acid/Nitrogen Tetroxide Oxidizers*, vol. II. 1977. Accessed: Jan. 13, 2019. [Online]. Available: <https://apps.dtic.mil/dtic/tr/fulltext/u2/a036741.pdf>
- [17] “Titan Missile History,” *Strategic-Air-Command.com*. [http://www.strategic-air-command.com/missiles/Titan/Titan\\_Missile\\_History.htm](http://www.strategic-air-command.com/missiles/Titan/Titan_Missile_History.htm) (accessed May 13, 2021).
- [18] “Titan Missile,” *Strategic-Air-Command.com*. [http://www.strategic-air-command.com/missiles/Titan/Titan\\_Missile\\_Home\\_Page.htm](http://www.strategic-air-command.com/missiles/Titan/Titan_Missile_Home_Page.htm) (accessed May 13, 2021).
- [19] U.S. DoD - U.S. DefenseImagery photo, “Titan-II ICBM silo test launch, Vandenberg Air Force Base,” *Wikipedia*. [https://en.wikipedia.org/wiki/LGM-25C\\_Titan\\_II#/media/File:Titan\\_II\\_launch.jpg](https://en.wikipedia.org/wiki/LGM-25C_Titan_II#/media/File:Titan_II_launch.jpg) (accessed May 13, 2021).
- [20] E. Tao, “Titan II missile Engine, LR87-5, Stage-1.” Titan Missile Museum, Sahuarita, Arizona., Nov. 05, 2016. [Online]. Available: <https://www.flickr.com/photos/mactao/40098097840/in/photostream/>
- [21] J. M. F. Vickers and R. R. Garipay, “Thermal Design Evolution and Performance of the Surveyor Spacecraft,” Philadelphia, Pennsylvania, Oct. 1968, vol. No. 68-1029. Accessed: May 14, 2021. [Online]. Available: <https://arc-aiaa-org.ezproxy.lib.purdue.edu/doi/pdf/10.2514/6.1968-1029>
- [22] “TD-339 (SURVEYOR VERNIER) ROCKET ENGINE,” *HeroicRelics.org*. <http://heroicrelics.org/info/surveyor/surveyor-vernier.html> (accessed May 14, 2021).
- [23] “High Performance Target Drone,” AFRDQRA, Required Action Directive RAD 7-3-(1), Mar. 1967.
- [24] F. B. Mead and B. R. Bomborst, “Certification Tests of a Hybrid Propulsion System for the Sandpiper Target Missile,” Air Force Rocket Propulsion Laboratory, AFRPL-TR-69-73, Jun. 1969. Accessed: May 10, 2021. [Online]. Available: <https://apps.dtic.mil/sti/pdfs/AD0503586.pdf>

- [25] Navy Camera Operator: PH3 COLLEEN WHITE, “A view of an AQM-37A target...,” *Wikipedia*, Sep. 17, 1981. [https://en.wikipedia.org/wiki/Beechcraft\\_AQM-37\\_Jayhawk#/media/File:AQM-37A\\_target\\_on\\_an\\_A-6E\\_Intruder.jpg](https://en.wikipedia.org/wiki/Beechcraft_AQM-37_Jayhawk#/media/File:AQM-37A_target_on_an_A-6E_Intruder.jpg) (accessed May 13, 2021).
- [26] G. Story and J. Arves, “Chapter 14: Flight Testing of Hybrid Powered Vehicles,” NASA Marshall Space Flight Center, Feb. 2006. Accessed: May 13, 2021. [Online]. Available: <https://ntrs.nasa.gov/api/citations/20060048274/downloads/20060048274.pdf>
- [27] US Air Force, “Military Specification, Propellant, Mixed Oxides of Nitrogen,” MIL-P-27408, Jul. 1964.
- [28] US Air Force, “Military Specification, Propellant, Mixed Oxides of Nitrogen,” MIL-P-27408A, Oct. 15, 1971.
- [29] E. M. Jones and K. Glover, “Main Propulsion Quick Reference Data.” Accessed: May 17, 2021. [Online]. Available: [https://www.hq.nasa.gov/alsj/LM09\\_Main\\_Propulsion\\_ppMP1-22.pdf](https://www.hq.nasa.gov/alsj/LM09_Main_Propulsion_ppMP1-22.pdf)
- [30] Research Center, Hercules Incorporated, “A Study of the Mechanism of Chemical Reactivity of Nitrogen Tetroxide with Titanium Alloys,” Wilmington, Delaware, Quarterly Report HRC-67-3, Jan. 1968. Accessed: May 08, 2021. [Online]. Available: <https://ntrs.nasa.gov/api/citations/19680016724/downloads/19680016724.pdf>
- [31] “Missile, Surface-to-Surface, Minuteman III, LGM-30G,” *Smithsonian National Air and Space Museum*. [https://airandspace.si.edu/collection-objects/missile-surface-surface-minuteman-iii-lgm-30g/nasm\\_A19761115000](https://airandspace.si.edu/collection-objects/missile-surface-surface-minuteman-iii-lgm-30g/nasm_A19761115000) (accessed May 18, 2021).
- [32] “Minuteman Missile History,” *Strategic-Air-Command.com*. [http://www.strategic-air-command.com/missiles/Minuteman/Minuteman\\_Missile\\_History.htm](http://www.strategic-air-command.com/missiles/Minuteman/Minuteman_Missile_History.htm) (accessed May 08, 2021).
- [33] B. J. German, E. C. Branscome, A. P. Frits, N. C. Yiakas, and D. N. Mavris, “An Evaluation of Green Propellants for an ICBM Post-Boost Propulsion System,” Aerospace Systems Design Laboratory, RECON no. 20010029826, AD-A386589, 2000. [Online]. Available: <https://www.proquest.com/reports/evaluation-green-propellants-icbm-post-boost/docview/27636814/se-2?accountid=13360>
- [34] “ICBM POST BOOST VEHICLES,” *Aerojet Rocketdyne*, 2021. <https://www.rocket.com/defense/gbsd/icbm-post-boost-vehicles> (accessed May 18, 2021).
- [35] F. S. Forbes and P. A. Van Splinter, *Encyclopedia of Physical Science and Technology: Liquid Rocket Propellants*, Third. Academic Press, 2003. Accessed: May 18, 2021. [Online]. Available: <https://www.sciencedirect.com/topics/earth-and-planetary-sciences/nitrogen-tetroxide>

- [36] J. Dumoulin, “NSTS Shuttle Reference Manual: Orbital Maneuvering System,” *Web.Archive.org*, 1988. <https://web.archive.org/web/20110629115908/http://science.ksc.nasa.gov/shuttle/technology/sts-newsref/sts-oms.html> (accessed May 18, 2021).
- [37] J. Dumoulin, “NSTS Shuttle Reference Manual: Reaction Control System,” *Kennedy Space Center*, 1988. <https://science.ksc.nasa.gov/shuttle/technology/sts-newsref/sts-rcs.html#sts-rcs> (accessed May 18, 2021).
- [38] NASA, “RS-25 engines with the two Orbital Maneuvering System (OMS) pods,” *Wikipedia*, Feb. 26, 2011. [https://en.wikipedia.org/wiki/Space\\_Shuttle#/media/File:STS-133\\_Rendezvous\\_Pitch\\_Manuever\\_3.jpg](https://en.wikipedia.org/wiki/Space_Shuttle#/media/File:STS-133_Rendezvous_Pitch_Manuever_3.jpg) (accessed May 18, 2021).
- [39] NASA, “Diagram of OMS pod components,” *Wikipedia*, Sep. 10, 1995. [https://en.wikipedia.org/wiki/Space\\_Shuttle\\_Orbital\\_Manuevering\\_System#/media/File:OMS\\_Pod\\_schematic.png](https://en.wikipedia.org/wiki/Space_Shuttle_Orbital_Manuevering_System#/media/File:OMS_Pod_schematic.png) (accessed May 18, 2021).
- [40] US Air Force, “Military Specification, Propellant, Mixed Oxides of Nitrogen,” MIL-P-27408A, Oct. 1971.
- [41] US Air Force, “Military Specification, Propellant, Mixed Oxides of Nitrogen,” MIL-P-27408A (NOTICE 1), Aug. 1989.
- [42] “MIL-PRF-26539F Performance Specification Propellants, Dinitrogen Tetroxide,” Military Specification MIL-PRF-26539F, Apr. 2006.
- [43] “Liquid-propellant rocket,” *Wikipedia*, Apr. 10, 2021. [https://en.wikipedia.org/wiki/Liquid-propellant\\_rocket](https://en.wikipedia.org/wiki/Liquid-propellant_rocket) (accessed May 19, 2021).
- [44] M. Wade, “R-4D,” *Astronautix*, 2019. <http://www.astronautix.com/r/r-4d.html> (accessed May 20, 2021).
- [45] C. Stechman and S. Harper, “Performance Improvements in Small Earth Storable Rocket Engines,” presented at the 46th AIAA/ASME/SAE/ASEE Joint Propulsion Conferenc, Jul. 2010.
- [46] “Aerojet Rocketdyne’s R-4D Engine: From Apollo to Orion and Beyond,” *Aerojet Rocketdyne*, 2021. <https://www.rocket.com/media/news-features/aerojet-rocketdyne%E2%80%99s-r-4d-engine-apollo-orion-and-beyond> (accessed May 20, 2021).
- [47] “The Hangar/Orion,” *Spaceflight Insider*, 2021. <https://www.spaceflightinsider.com/hangar/orion/> (accessed May 20, 2021).
- [48] “File:LM RCS.jpg,” *Wikimedia*, Mar. 01, 2006. [https://commons.wikimedia.org/wiki/File:LM\\_RCS.jpg](https://commons.wikimedia.org/wiki/File:LM_RCS.jpg) (accessed May 20, 2021).

- [49] “200N Bipropellant Thruster,” *Orbital Propulsion Centre*, 2020. <https://www.space-propulsion.com/spacecraft-propulsion/bipropellant-thrusters/200n-bipropellant-thrusters.html> (accessed May 20, 2021).
- [50] “Automated Transfer Vehicle (ATV) Utilisation Relevant Data Rev. 1.2,” ESA ERASMUS User Centre, 2008. Accessed: May 20, 2021. [Online]. Available: [http://esamultimedia.esa.int/docs/ATV/FS003\\_12\\_ATV\\_updated\\_launch\\_2008.pdf](http://esamultimedia.esa.int/docs/ATV/FS003_12_ATV_updated_launch_2008.pdf)
- [51] “Dragon,” *SpaceX*, 2021. <https://www.spacex.com/vehicles/dragon/> (accessed May 19, 2021).
- [52] “Launch List,” *SpaceX Info*, 2021. <https://spacex-info.com/launch-list/> (accessed May 19, 2021).
- [53] A. Klamper, “SpaceX Says Dragon Prototype Will Fly on First Falcon 9,” *Space News*, Sep. 24, 2009. <https://spacenews.com/spacex-says-dragon-prototype-will-fly-first-falcon-9/> (accessed May 19, 2021).
- [54] E. Ralph, “SpaceX’s next Crew Dragon launch is delayed but that’s actually good news,” *Teslarati*, Dec. 18, 2019. <https://www.teslarati.com/spacex-next-crew-dragon-launch-delayed-good-news/> (accessed May 19, 2021).
- [55] M. Wade, “AJ10,” *Astronautix*, 2019. <http://www.astronautix.com/a/aj10.html> (accessed May 19, 2021).
- [56] J. Latrell, “Orion’s European Service Module Makes its Debut at Kennedy Space Center,” *Spaceflight Insider*, Oct. 27, 2018. <https://www.spaceflightinsider.com/organizations/lockheed-martin-organizations/orions-european-service-module-makes-its-debut-at-kennedy-space-center/> (accessed May 19, 2021).
- [57] “Orion Spacecraft Overview,” *Spaceflight 101*, 2021. <https://spaceflight101.com/spacecraft/orion/> (accessed May 19, 2021).
- [58] J. Foust, “NASA requesting proposals for Orion engine,” *Space News*, Mar. 27, 2020. <https://spacenews.com/nasa-requesting-proposals-for-orion-engine/> (accessed May 19, 2021).
- [59] P. Sloss, “NASA Launch Services Program outlines the alternative launcher review for EM-1,” *NASA Spaceflight*, Apr. 19, 2019. <https://www.nasaspaceflight.com/2019/04/nasa-lsp-studies-alternate-orion-options/3/> (accessed May 19, 2021).
- [60] N. Brügge, “Spacecraft-propulsion blocks (KDU) from Isayev’s design bureau (now Khimmash),” *B14643.de*, Jun. 02, 2015. [https://web.archive.org/web/20150602231608/http://www.b14643.de/Spacerockets/Diverse/KB-Isayev\\_KDUs/index.htm](https://web.archive.org/web/20150602231608/http://www.b14643.de/Spacerockets/Diverse/KB-Isayev_KDUs/index.htm) (accessed May 19, 2021).

- [61] M. Wade, “KTDU-80,” *Astronautix*, 2019. <http://www.astronautix.com/k/ktdu-80.html> (accessed May 19, 2021).
- [62] A. Zak, “Propulsion system for the Soyuz MS spacecraft,” *Russian Space Web*, Apr. 20, 2020. <http://www.russianspaceweb.com/soyuz-ms-kdu.html> (accessed May 19, 2021).
- [63] B. Chertok, *Rockets and People Vol. 3 — Hot Days of the Cold War*, “Chapter 18 — Birth of the Soyuzes.” NASA, 2009. Accessed: May 19, 2021. [Online]. Available: <https://history.nasa.gov/SP-4110/vol3.pdf>
- [64] “Soyuz: Motorization,” *Kosmonavtika*, Jan. 14, 2018. <https://www.kosmonavtika.com/vaisseaux/soyouz/tech/kdu/kdu.html> (accessed May 19, 2021).
- [65] “Bipropellant Thrusters.” IHI Aerospace, December 2014. Accessed: May 20, 2021. [Online]. Available: <https://web.archive.org/web/20160829161933/https://www.ihico.jp/ia/en/catalog/Bipropellant.pdf>
- [66] G. D. Krebs, “Cygnus-PCM,” *Gunter’s Space Page*, Apr. 17, 2016. [https://space.skyrocket.de/doc\\_sdat/cygnus-pcm.htm](https://space.skyrocket.de/doc_sdat/cygnus-pcm.htm) (accessed May 20, 2021).
- [67] G. D. Krebs, “HTV 1, ..., 9 (Kounotori 1, ..., 9),” *Gunter’s Space Page*, Aug. 24, 2016. [https://space.skyrocket.de/doc\\_sdat/htv.htm](https://space.skyrocket.de/doc_sdat/htv.htm) (accessed May 20, 2021).
- [68] G. D. Krebs, “Antares (Taurus-2),” *Gunter’s Space Page*, Aug. 12, 2016. [https://space.skyrocket.de/doc\\_lau/antares\\_osc.htm](https://space.skyrocket.de/doc_lau/antares_osc.htm) (accessed May 20, 2021).
- [69] “IHI Aerospace Manufactured Engines Selected for AEHF-4, MUOS-4, MUOS-5, and Vinasat-2 Satellites by Lockheed Martin Space Systems Company.,” *IHI*, Nov. 29, 2010. [https://web.archive.org/web/20160829162033/http://www.ihico.jp/en/all\\_news/2010/press/2010-11-30/index.html](https://web.archive.org/web/20160829162033/http://www.ihico.jp/en/all_news/2010/press/2010-11-30/index.html) (accessed May 20, 2021).
- [70] NASA, “The Cygnus space freighter from Northrop Grumman is pictured moments before its capture with the Canadarm2 robotic arm.,” *Wikipedia*, Feb. 22, 2021. [https://en.wikipedia.org/wiki/Cygnus\\_NG-15#/media/File:ISS-64\\_The\\_Cygnus\\_space\\_freighter\\_moments\\_before\\_its\\_capture.jpg](https://en.wikipedia.org/wiki/Cygnus_NG-15#/media/File:ISS-64_The_Cygnus_space_freighter_moments_before_its_capture.jpg) (accessed May 20, 2021).
- [71] “Nammo acquires Moog’s European In-Space Propulsion businesses,” *MyNewsDesk*, Jun. 12, 2017. <http://www.mynewsdesk.com/no/nammo/pressreleases/nammo-acquires-moogs-european-in-space-propulsion-businesses-2010740> (accessed May 19, 2021).

- [72] American Pacific Corporation, “LEROS Engine Propels the Juno Spacecraft on Its Historic Voyage to Jupiter,” *Cision PR Newswire*, Nov. 08, 2011. <https://www.prnewswire.com/news-releases/leros-engine-propels-the-juno-spacecraft-on-its-historic-voyage-to-jupiter-133466283.html> (accessed May 19, 2021).
- [73] “NASA Juno Spacecraft to remain in Elongated Capture Orbit around Jupiter,” Feb. 18, 2017. <https://spaceflight101.com/juno/juno-to-remain-in-elongated-capture-orbit/> (accessed May 19, 2021).
- [74] “400N Bipropellant Apogee Motors,” *Orbital Propulsion Centre*, 2020. <https://www.space-propulsion.com/spacecraft-propulsion/apogee-motors/index.html> (accessed May 19, 2021).
- [75] J. Daley, “Mission to Find Life on Mars Blasts Off,” Mar. 14, 2016. <https://www.smithsonianmag.com/smart-news/mission-find-life-mars-blasts-180958404/> (accessed May 19, 2021).
- [76] “PHOTO-REPORT FROM LAVOCHKIN SCIENTIFIC AND PRODUCTION ASSOCIATION, ONE DAY AT FREGAT UPPER STAGE MANUFACTURING FACILITY,” *GK Launch Services*, Jan. 27, 2020. <http://gklaunch.ru/en/news/photo-report-from-lavochkin-scientific-and-production-association-one-day-at-fregat-upper-stage-manufacturing-facility/> (accessed May 19, 2021).
- [77] “Fregat upper stage deploying Cluster,” *The European Space Agency*, Feb. 28, 1999. [http://www.esa.int/ESA\\_Multimedia/Images/2003/07/Fregat\\_upper\\_stage\\_deploying\\_Cluster](http://www.esa.int/ESA_Multimedia/Images/2003/07/Fregat_upper_stage_deploying_Cluster) (accessed May 19, 2021).
- [78] M. Wade, “Proton,” *Astronautix*, 2019. <http://www.astronautix.com/p/proton.html> (accessed May 20, 2021).
- [79] “Proton Heritage,” *ILS Launch*, 2021. <http://www.ilslaunch.com/launch-services/ils-proton-breeze-m-launch-vehicle/proton-heritage> (accessed May 20, 2021).
- [80] *Journal of the British Interplanetary Society*, vol. 51. British Interplanetary Society, 1998. [Online]. Available: <https://books.google.com/books?id=iThWAAAAMAAJ>
- [81] “Arctic weather satellite launch postponed (Russian),” *meteovesti.ru*, Oct. 05, 2020. <https://www.meteovesti.ru/news/63737588800-zapusk-meteosputnika-monitoringa-arktiki-otlozhen> (accessed May 20, 2021).
- [82] “Russia Reviews Proton Breeze M Reliability,” *Aviation Week*, Mar. 19, 2013. <https://aviationweek.com/defense-space/space/russia-reviews-proton-breeze-m-reliability>
- [83] T. Malik, “Russian Proton rocket launches Express communications satellites in stunning nighttime liftoff (video, photos),” *Space.com*, Jul. 2020. <https://www.space.com/russia-proton-rocket-launches-express-80-103-satellites.html> (accessed May 20, 2021).

- [84] “Space Launch Report: Ariane 5 Data Sheet,” *Space Launch Report*, Aug. 15, 2020. <http://www.spacelaunchreport.com/ariane5.html#components> (accessed May 21, 2021).
- [85] E. Kyle, “Ariane 6,” *Space Launch Report*, Jul. 28, 2018. <https://www.spacelaunchreport.com/ariane6.html> (accessed May 21, 2021).
- [86] D. MacKenzie, *Inventing Accuracy: A Historical Sociology of Nuclear Missile Guidance*, 1st ed. MIT Press, 1990. Accessed: May 21, 2021. [Online]. Available: <https://books.google.com/books?id=QymEXZIWEe8C&pg=PP1#v=onepage&q&f=false>
- [87] “Final Refurbished Titan II Missile Launches Defense Weather Bird,” *Space Daily*, Oct. 19, 2003. <https://www.spacedaily.com/news/milspace-comms-03zj.html> (accessed May 21, 2021).
- [88] E. Kyle, “HERITAGE ATLAS/TITAN/DELTA UPDATE,” *Space Launch Report*, Apr. 27, 2008. <https://www.spacelaunchreport.com/heritag.html> (accessed May 21, 2021).
- [89] “Atlas 5 Data Sheet,” *Space Launch Report*, May 18, 2021. <http://spacelaunchreport.com/atlas5.html> (accessed May 21, 2021).
- [90] “Space Launch Report: Delta IV Data Sheet,” *Space Launch Report*, Apr. 26, 2021. <http://www.spacelaunchreport.com/delta4.html> (accessed May 21, 2021).
- [91] “Frontier Aerospace Delected for NASA Award to Develop Deep Space Thruster using MON-25/MMH Propellant,” *Astrobotic*, Aug. 16, 2018. <https://www.astrobotic.com/2018/8/16/frontier-aerospace-selected-for-nasa-award-to-develop-deep-space-thruster-using-mon-25-mmh-propellant> (accessed May 21, 2021).
- [92] “Astrobotic - Payload User Guide.” Astrobotic Technology, 2018. Accessed: May 21, 2021. [Online]. Available: <https://www.astrobotic.com/payload-user-guide>
- [93] “Astrobotic Selects United Launch Alliance Vulcan Centaur Rocket to Launch its First Mission to the Moon,” *ULA Launch*, Aug. 19, 2019. <https://www.ulalaunch.com/about/news/2019/08/19/astrobotic-selects-united-launch-alliance-vulcan-centaur-rocket-to-launch-its-first-mission-to-the-moon> (accessed May 21, 2021).
- [94] “Astrobotic Awarded \$79.5 Million Contract to Deliver 14 NASA Payloads to the Moon,” *Astrobotic*, Mar. 31, 2019. <https://www.astrobotic.com/2019/5/31/astrobotic-awarded-79-5-million-contract-to-deliver-14-nasa-payloads-to-the-moon> (accessed May 21, 2021).
- [95] L. Grush, “This tiny rover will test how well small mobile robots can survive on the Moon,” *The Verge*, Jun. 05, 2019. <https://www.theverge.com/2019/6/5/18654253/carnegie-mellon-lunar-rover-astrobotic-nasa-peregrine-moon-lander> (accessed May 21, 2021).

- [96] “Astrobotic Technology,” *Wikipedia*, May 12, 2021. [https://en.wikipedia.org/wiki/Astrobotic\\_Technology](https://en.wikipedia.org/wiki/Astrobotic_Technology) (accessed May 21, 2021).
- [97] D. Hendrickson, “A Manifest of Delivery Missions to Make the Moon Accessible to the World.” *Astrobotic Technology*, Jul. 2020. Accessed: May 21, 2021. [Online]. Available: [http://fiso.spiritastro.net/telecon/Hendrickson\\_7-15-20/Hendrickson\\_7-15-20.pdf](http://fiso.spiritastro.net/telecon/Hendrickson_7-15-20/Hendrickson_7-15-20.pdf)
- [98] “Peregrine Lander,” *Astrobotic*, 2021. <https://www.astrobotic.com/peregrine> (accessed May 22, 2021).
- [99] “Astrobotic Awarded \$5.6 Million NASA Contract to Deliver Autonomous Moon Rover,” *Astrobotic*, Jul. 01, 2019. <https://www.astrobotic.com/2019/7/1/astrobotic-awarded-5-6-million-nasa-contract-to-deliver-autonomous-moon-rover> (accessed May 21, 2021).
- [100] B. Sprice, “CMU’s MoonRanger Will Search for Water at Moon’s South Pole,” *Carnegie Mellon University*, Sep. 20, 2020. <https://www.cmu.edu/news/stories/archives/2020/september/moonranger-to-search-for-water.html> (accessed May 21, 2021).
- [101] “What is the MXP-351 storable bipropellant?,” *Stack Exchange: Space Exploration Beta*, 2020. <https://space.stackexchange.com/questions/43363/what-is-the-mxp-351-storable-bipropellant> (accessed May 21, 2021).
- [102] “XL1/XL1T,” *Masten*. <https://stingray-flounder-2ly8.squarespace.com/xl1> (accessed May 22, 2021).
- [103] J. Foust, “Astrobotic wins NASA contract to deliver VIPER lunar rover,” *Space News*, Jun. 11, 2020. <https://spacenews.com/astrobotic-wins-nasa-contract-to-deliver-viper-lunar-rover/> (accessed May 21, 2021).
- [104] “Astrobotic Selects Lander Engines & More for Griffin/VIPER Mission,” *satnews*, Mar. 02, 2021. <https://news.satnews.com/2021/03/02/astrobotic-selects-lander-engines-more-for-griffin-viper-mission/> (accessed May 21, 2021).
- [105] “Griffin Figure.” <https://forum.nasaspaceflight.com/index.php?PHPSESSID=b12iaah9r732advtgq7qo7bncq&action=dlattach;topic=51174.0;attach=1938385;image> (accessed May 21, 2021).
- [106] “Griffin Lander,” *Astrobotic*. <https://www.astrobotic.com/griffin> (accessed May 21, 2021).
- [107] Eframgoldberg, “Nitrogen dioxide at different temperatures,” *Wikipedia*, Jul. 16, 2013. [https://en.wikipedia.org/wiki/Dinitrogen\\_tetroxide#/media/File:Nitrogen\\_dioxide\\_at\\_different\\_temperatures.jpg](https://en.wikipedia.org/wiki/Dinitrogen_tetroxide#/media/File:Nitrogen_dioxide_at_different_temperatures.jpg) (accessed May 24, 2021).
- [108] “Cloud Droplets and Rain Drops,” *Space Math @ NASA*. <https://spacemath.gsfc.nasa.gov/weekly/84Clouds8.pdf> (accessed Jun. 02, 2021).

- [109] R. D. McCarty, “The thermodynamic properties of nitrogen tetroxide,” p. 112.
- [110] M. J. Mueller, “Density Fit for MON Oxidizer Blends Including Accuracy,” presented at the 51st AIAA/SAE/ASEE Joint Propulsion Conference, Orlando, FL, Jul. 2015. doi: 10.2514/6.2015-4158.
- [111] E. T. Chang, N. A. Gokcen, and C. D. Robison, “Solubilities of O<sub>2</sub>, NO, and N<sub>2</sub>O<sub>3</sub> in Liquid N<sub>2</sub>O<sub>4</sub>,” Aerospace Corporation, TDR-469(5210-10)-6, May 1965.
- [112] T. V, “Uncertainty Propagation Class (UC),” *MathWorks*, Aug. 17, 2015. <https://www.mathworks.com/matlabcentral/fileexchange/46357-uncertainty-propagation-class-uc> (accessed Jun. 13, 2021).